Motion accumulates while movement disappears: spatial interactions in visual motion

Peter B. Meilstrup

A dissertation submitted
in partial fulfillment of the
requirements for the degree of

Doctor of Philosophy

University of Washington
2014

Reading Committee:
Michael N. Shadlen, chair
Farrel R. Robinson
John C. Palmer

Program Authorized to Offer Degree:
Neurobiology and Behavior

University of Washington

Abstract

Motion accumulates while movement disappears: spatial interactions in visual motion

Peter B. Meilstrup

Chair of the Supervisory Committee:
Professor Michael N. Shadlen
Department of Physiology and Biophysics

When objects move, they change position over time. However, the mechanisms in human vision that could be capable of tracking these changes in position are not well understood. I constructed stimuli that combined a first-order carrier motion with a position-defined envelope movement. When viewed in the periphery, the appearance of motion was very sensitive to changes in position of its envelope, regardless the amount of carrier motion. However, when multiple motion elements were placed close together, the appearance of the stimulus came to be dominated by its carrier motion. When elements were added, sensitivity to position-defined motion decreased at the same time as the sensitivity to first-order motion increased; visual clutter thus favors first-order motion over position-defined motion. These effects are modeled in terms of two mechanisms that each contribute to motion appearance. The first-order mechanism sums motion over larger areas of space without regard to their position; in the presence of clutter, it sums all signals together. The position-defined mechanism tracks the change in location of isolated features; it cannot pool signals over space and works best with salient, uncluttered objects. This mechanism suffers crowding when flankers are introduced. While first-order motion is understood in terms of spatiotemporal filtering, position-defined motion might be viewed as a feature integration problem, involving the comparison of successive positions over time. These systems have a subtractive interaction that may serve to locate objects that are moving differently from their background. Complementary characteristics and limitations of the two systems each play roles in the perception of moving objects.

1 Introduction

Accurate motion perception is essential for visually guided movement; complex behaviors such as chasing prey, escaping predators, avoiding obstacles, or catching a thrown ball require that an organism be able to rapidly determine the position and velocity of a moving object, and to anticipate its trajectory through space. Psychological research on motion perception has established that motion can be processed by separate mechanisms, an idea that dates back to Wertheimer's phenomenological distinction between the "phi" sensation elicited by faster motion and the "beta" sensation elicited by slower motion (Wertheimer 1912, 2012; Steinman et al., 2000). The goal of this thesis is to examine how separate mechanisms contribute to a unified perception of motion.

It is generally believed that there are multiple classes of motion mechanisms. One of these, the first-order motion mechanism, seems to respond to local spatiotemporal correlations in luminance contrast, at relatively short timescales and in small regions of space. It is generally agreed that the first-order motion mechanism originates with the direction selective response of cells in cortical area V1. Classic models of first-order motion detection use linear filters tuned to certain combinations of spatial and temporal frequencies, with the outputs of several such filters being combined nonlinearly (Adelson and Bergen, 1985; Watson and Ahumada, 1985). With some embellishments, the responses observed from cells in area V1 are largely compatible with this model (Movshon et al., 1978; Rust et al., 2005; Touryan et al., 2005; Chen et al., 2007), and models of higher order processing can be built atop this basis (Graham, 2011). Moreover, the size and bandwidth of motion sensing channels inferred from psychophysical measurements are similar to those observed of V1 neurons (Anderson and Burr, 1987, 1989; Banks et al., 1991; Anderson et al., 1991; Watson and Turano, 1995).

However, these first-order mechanisms cannot by themselves fully explain human motion perception. For example, perceiving visual motion does not necessarily require moving features to differ in mean luminance from the background, and does not require motion energy in the Fourier domain. Many forms of higher-order motion stimuli have been constructed that would not be

consistently detectable to first-order mechanisms, but these stimuli still elicit strong sensations of movement (Derrington and Badcock, 1985; Chubb and Sperling, 1988; Zanker, 1990). These stimuli have been used to provide evidence for and characterize motion sensing systems separate from the first-order mechanisms. They have been constructed variously by modulations in contrast, texture, or other stimulus features, but generally involve the change in position, over time, of some feature in the image (Lu and Sperling, 1995).

One possible reason for having multiple motion systems is that first-order motion signals are not always a reliable indication of the veridical motion of an object. In a complicated visual world, motion can come from many sources, and accurate perception of the movement of objects requires disambiguating motion signals attributable to the object from irrelevant motions in the background or of other objects. Consider the task of trying to track the movement of a zebra among a background of waving grass. One challenge this task presents is that a motion energy sensor with a limited receptive field size will report the component of the zebra's motion orthogonal to its stripes, rather than the veridical motion of the zebra, an instance of the so-called "aperture problem" (Ilildreth and Ullman, 1982; Adelson and Movshon, 1982). Combining the component motion signals from V1 cells sensing different orientations might allow disambiguation of the true velocity. This extraction of pattern motion from component motion appears to be one of the roles of visual area MT (Movshon et al., 1985; Simoncelli and Heeger, 1998; Rust et al., 2006). However, this computation of pattern motion cannot completely explain motion perception either, as combining different motion signals allows the object's motion to be mixed with irrelevant background motion. If motion information is pooled over larger areas, the motion of the background grass will create a subset of the pooled signals that are substantially incorrect; an MT cell analyzing the motion of the zebra will mix together signals from the zebra's stripes with signals from the grassy background.

A related problem is that computing the velocity of a pattern discards information about its location, because receptive fields must be larger to collect pattern motion. The computation in

MT resolves pattern motion but appears to lose information about where the motion is occurring within the large MT receptive fields (Majaj et al., 2007). This is puzzling because the ostensible purpose of motion perception is often to track and anticipate the change in position of a physical object. Consider tracking an animal moving through obscuring tall grass, or watching waves pass over choppy water. The stalks of grass, or the foam and texture on the water, do not progressively change position; they only oscillate in place as the movement passes under them. A computation based on pattern motion would generally track the oscillation of the surface texture rather than that of the underlying movement. However it is the underlying movement that is more relevant, and often dominates the perception of motion.

Literature on visual motion processing has drawn many different demarcations between types of motion. Various papers have discussed first-order versus second-order, short-range versus long-range, local vs. global, textural versus figural, and so on, based on particular demarcations drawn among stimulus properties or proposed mechanisms (Nishida, 2011). For the purposes of this thesis I will also have to pick a demarcation. The examples of animals in the grass and waves on the water draw a contrast between the first-order motion produced by an object, and the fact that the object changes position over time. The latter is what I will be referring to as position-defined motion. A moving object generally produces both first-order and position-defined motion. To track the zebra might require integrating first-order motion signals over space and time as the zebra changes position, while discarding adjacent signals that are inconsistent with its trajectory. However most proposed first-order motion mechanisms do not detect changes in position. For first-order motion processing we are reasonably confident of the mechanisms involved, but mechanisms that detect changes in position are less well understood.

Note that selecting any demarcation involves some reinterpretation when reading the literature. There is an extensive literature on second-order motion but not all of it is applicable to position-defined motion. A typical model for second-order motion processing functions analogously to first-order motion but with a rectifying input nonlinearity. The position-defined stimuli I will use

in this thesis might be detectable as second-order in this sense, but will be outside the temporal frequency range thought to apply to this type of mechanism (Lu and Sperling, 2001). Some papers on second-order motion stimuli use stimuli that are not position-defined, but others use second-order stimuli that also happen to involve the movement of salient features. I consider the latter results to be potentially informative of position-defined motion processing.

There is evidence that perception of position-defined motion stimuli may have a separate neural substrate from first-order motion. For example, adding position-defined motion noise to a display does not appear to change the threshold of detection for first-order motion, and it is unclear whether adding first-order motion noise interferes with detecting position-defined motion (Edwards and Badcock, 1995; Nishida et al., 1997; Cassanello et al., 2011, but see Hedges et al., 2011). When differing first-order and position-defined components are present in a stimulus, the motion after-effect is always determined by the first-order component, whereas appearance of the stimulus is often determined by the position-defined motion (Derrington and Badcock, 1985; Chubb and Sperling, 1989; Nishida and Sato, 1992). Neuropsychological evidence suggests a double dissociation between first-order and position-defined motion processing deficits in a number of patients (Vaina and Cowey, 1996; Vaina and Soloviev, 2004), suggesting that different motion mechanisms may have anatomically distinct pathways. Another difference between first-order and position-defined stimuli that suggests different mechanisms is that the latter seems to be capable of tracking objects through over distances larger than what can be achieved through individual local filters. "Long-range" apparent motion stimuli span a distance greater than the classical receptive field size in V1, eliciting sensations of motion without explicit direction selective activity in V1.

Interestingly, the physiological substrate of position-defined motion processing is still unclear. Cortical area MT (or somewhere downstream) has been proposed as a locus of integration between motion and position information (Nishida and Johnston, 1999; McGraw et al., 2004; Mather and Pavan, 2009). While the receptive fields of cells in cortical areas MT and MST are large enough that they might be able to integrate information about objects that change position, recordings of

these cells find their responses dominated by first-order motion and showing little to no selectivity to position-defined motion, even when the latter corresponds better to the experience of viewing these stimuli (Livingstone et al., 2001; Ilg and Churan, 2004; Hedges et al., 2011). So while signals present in MT have an influence on perceived position, MT does not itself appear to track perceived position. Despite the fact that these two motion systems clearly both contribute to determining the appearance of the moving world, the question of whether and how they interact to produce a single coherent percept of motion remains open (Nishida, 2011). In this thesis I examine the combination of these two types of motion using a display that contains first-order and position-defined components whose direction of motion can be independently manipulated.

Figure 1.1 provides examples of first order and higher order motion. The elements are Gabor-like stimuli that can be understood as a carrier grating windowed by a spatial envelope. The envelope moves independently of the carrier, so that the *carrier* provides *first order motion* while the *envelope* produces *position-defined motion*. Figure 1.1A illustrates the difference between first-order and position-defined motion. On the left is a single element with carrier motion but no envelope motion. On the right side, the element has envelope motion but its no carrier motion (only an equivalent amount of flicker). The motion on the right is seen as a clear progressive change in position, while the motion on the left has an appearance more like a flicker that has a direction to it. (The position of the element on the left does appear to shift slightly, in an example of motion-induced position shift; De Valois and De Valois, 1991; Ramachandran and Anstis, 1990).

In Figure 1.1B, elements have both carrier and envelope motion. On the left, the carrier and envelope components move in the same direction; on the right the carrier and envelope motions are in opposite directions. Full details of the construction of this display are given in Section 3. Figure 1.1C is the same but with five elements around each fixation point.

When elements with combined envelope and carrier motions are viewed in isolation, as in Figure 1.1B, the appearance of the direction of motion follows the motion of the envelope, and not strongly affected by the direction of the carrier. The carrier motion does cause a change in the sense

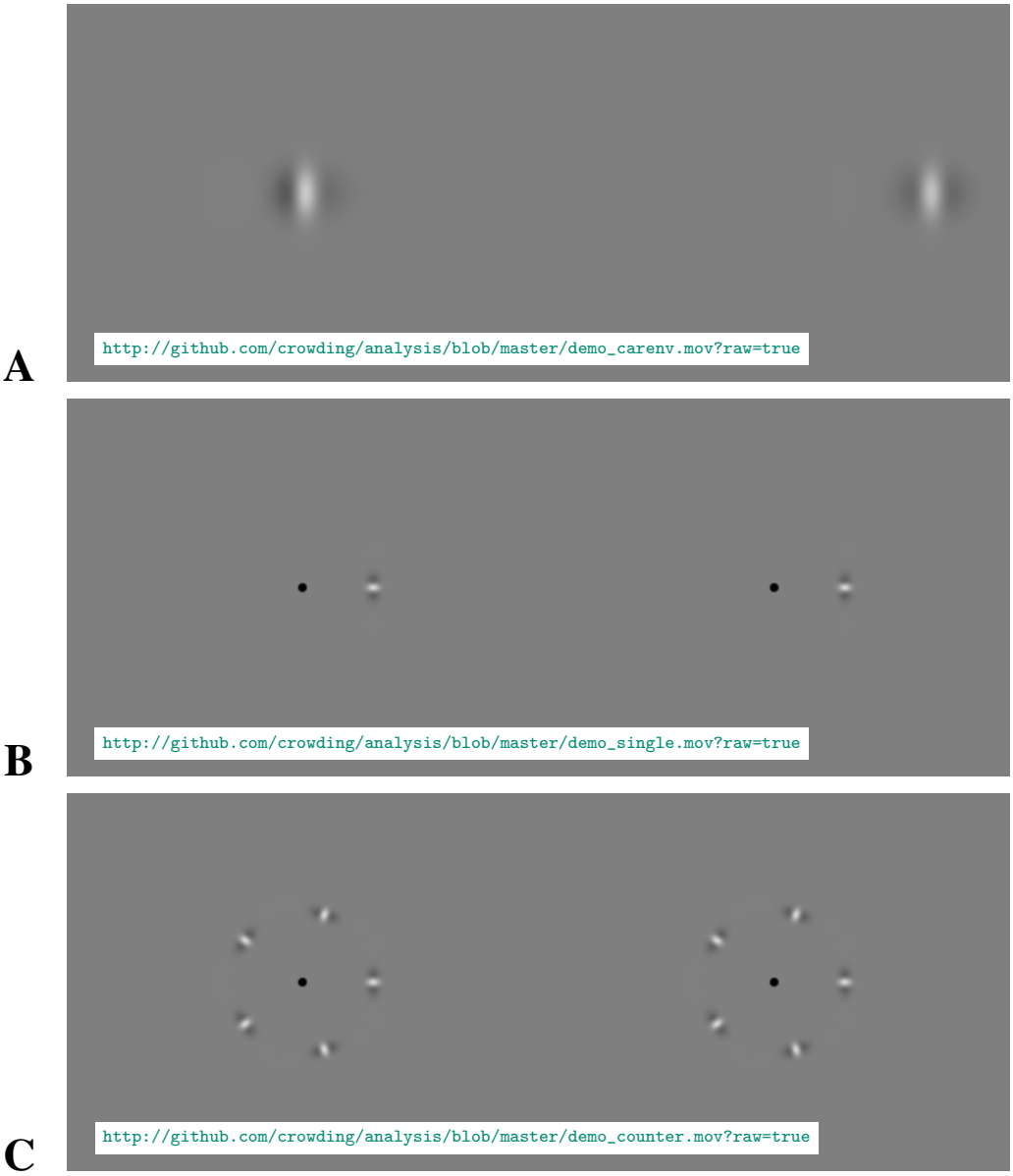

Figure 1.1: Examples of carrier/envelope stimuli. **A.** (`demo_carenv.mov`) At left, an element contains carrier (first-order) motion in the absence of higher order motion. At right, an element whose carrier motion is balanced, but the envelope moves (higher order motion.) **B.** (`demo_single.mov`) Single motion elements, moving in circles. At left, the carrier motion is opposite the envelope motion. At right, the carrier motion is in the same direction as the envelope motion. **C.** (`demo_counter.mov`) Five elements, each identical to the single element in subfigure B, distributed around each fixation point. When elements are closely spaced, there is an eccentricity-dependent change in appearance. The appearance of the wheel on the left (with opposing carrier and envelope motions) changes depending on where the eyes fixate.

of "smoothness," with conflicting motion having a more jittery appearance , but does not strongly affect the apparent direction or even the apparent speed of the motion. However, in Figure 1.1C, when multiple elements are placed in proximity, but not overlapping, the apparent motion depends on whether the stimulus is viewed centrally or peripherally. When the five-element ring on the left is viewed centrally, the apparent direction of motion is consistent with the envelope. When the same element ring is viewed in the periphery, the apparent direction of rotation matches that of the carrier. If an observer maintains attention on the leftward ring, which has carrier and envelope in conflict, while moving their eyes so as to move the stimulus from central to peripheral vision, the apparent motion may appear to reverse in concert with the eye movement.

From this demonstration it appears that having more than one element in proximity affects how first-order and higher-order motion are combined. That the appearance changes with retinal eccentricity of the stimulus suggests that the range of spatial interaction scales with retinal eccentricity. A plausible explanation could be that the presence of flanking objects limits the ability to see movement of the envelope, thereby allowing the carrier motion to determine the percept; that is, crowding (Levi, 2008; Pelli, 2008) may be affecting how first-order and higher-order motion are combined.

In this thesis I examine how first-order and higher order mechanisms interact in forming an overall perception of motion. In Experiment 1 I quantify how element spacing determines the sensitivity to first-order and higher order motions and present a simple model to capture the results, wherein first-order and higher-order motion signals are processed separately and combined at a decision stage. In Experiment 2 we vary the number of elements independently of the spacing of targets and determine that first-order motion sums inputs over a large area, while higher order motion perception is sensitive to the spacing between elements and flankers.

2 Demonstrations and Subjective Observations

A model of visual processing of this class of stimuli responses will need to account for changes in the direction of apparent motion. When elements are isolated, the apparent direction of motion follows that of the envelopes; when multiple elements are placed in proximity, the direction of apparent motion changes to agree with that of the carrier. I will proceed to quantify this reversal effect in subsequent sections. In order to do so I asked naïve observers to make binary classifications of their impressions of the overall direction of motion (clockwise or counterclockwise.) However, binary responses collapse together a number of perceptual qualities, so that these simple direction judgments do not fully capture the appearance of these stimuli.

Below are three demonstrations that place the fixation point in the center of the screen and the moving elements on a circle of constant eccentricity. The motion of the individual elements is the same in each demo; only the spacing and number of elements changes. These movies are arranged to loop, however the psychophysics I will discuss in subsequent sections is based on brief (500ms) presentations of motion.

Figure 2.1 shows six elements, so the spacing between elements is $1.04e$ measured circumferentially. In this demonstration the carrier motion is clockwise and the envelope motion is counterclockwise. For all observers I have shown this stimulus to, the perceived direction of motion is counterclockwise, in agreement with the envelope motion. This illustrates that higher order motion can be clearly seen in the periphery, and that at these wide element spacings the envelope motion dominates the perception. Compared to other stimuli it is relatively difficult to tell the direction of motion of the carrier, so we could say that the envelope motion "captures" the carrier motion (Hedges et al., 2011). For the largest values of carrier strength, (for these demonstrations, the carrier strength C as defined in General Methods is 100%,) the carrier motion might appear as a "wind" which overlays the moving envelopes, somewhat similar to the appearance of a low-contrast moving grating superposed on a stationary pedestal grating (Lu and Sperling, 2001). Incidentally, when carrier motions are directed opposite to envelope motion, as can be seen in

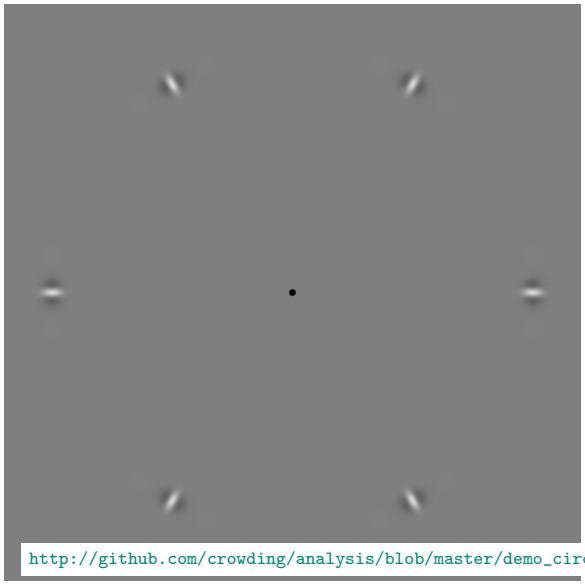

Figure 2.1: (`demo_circle_6.mov`) An example motion stimulus similar to those used in my experiments. There are six elements, with the carrier motion clockwise and the envelope counterclockwise. The envelope motion dominates the subjective appearance.

Figure 1.1, the elements appear to have more flicker, and the perceived motion, while agreeing in direction with the envelope, seems less smooth.

As the number of elements in the display increases and the spacing between elements decreases, the appearance of the motion changes. The demonstration in Figure 2.2 increases the number of elements to 16; the spacing between elements is $0.39e$, which seems close to the "critical spacing" for many observers. Generally the carrier motion becomes more visible and observers begin to equivocate in their reports of perceived motion direction. The perception is a mixture of both carrier and envelope motions, but the form of this mixture can take on several different appearances. Observers viewing stimuli near the critical spacing described a number of different qualitative impressions of the stimulus:

- Transparent motion, in which different layers seemed to slide over each other in opposite directions;
- Windowed motion, in which the elements appear to be rotating aperture through which a

moving background is seen.

- Motion that changes direction over time. In these cases the immediate perception was usually in agreement with the carrier motion while the later percept was in agreement with the envelope motion.

- A non-uniform appearance where one side of the wheel appears to move one direction and the other side in the other direction.

- A few isolated elements move in agreement with the envelope motion and can be attentively tracked, but non-attended regions of the wheel seem to move in the opposite direction.

The subjective speed of the motion can change as spacing is brought near critical; if carrier motion opposes envelope motion, the perceived speed of the stimulus reaches a minimum at a certain spacing, being faster in the direction of envelope motion when spacing is larger and faster in the direction of carrier motion when spacing is smaller.

Some observers saw motion directions in agreement with the carrier immediately after stimulus onset which then changes to be more in agreements with the envelope motion. For this reason I asked observers in Experiment 1 to respond within a restricted time window. Observers often reported the sensation of giving a mistaken response (i.e. they gave a response but their perception of motion changed after they had committed to the response.)

One perceptual phenomenon that did *not* seem to occur is bistability. Both the carrier and envelope motions are individually consistent with a global rotation of the display around the fixation point, so that we might have anticipated perceptions exclusively consistent one rigid movement or the other (Anstis and Kim, 2011). However, the appearances of critically spaced stimuli tended to reflect a mixture of two motions rather than one overriding motion, and there was never the spontaneous all-at-once switch that occurs for perceptually bistable stimuli.

The third demonstration in Figure 2.3 has 22 elements spaced at $0.29e$. For most observers it becomes difficult to see the envelope motion at this density especially at short viewing durations.

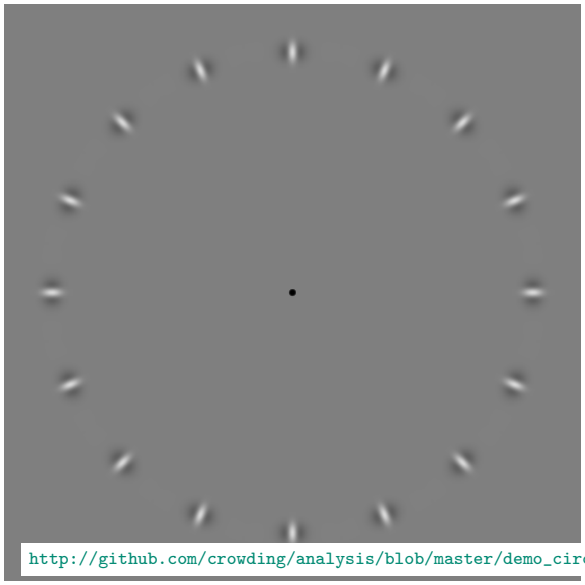

Figure 2.2: (`demo_circle_16.mov`) Same stimulus as Figure 2.1 with sixteen elements. The appearance may be a mixture of carrier and envelope motions.

When elements are this closely spaced the overall impression is of motion in the direction of the carrier. There is not as much of the appearance of two separate motions. However, the amount of subjective flicker does appear to increase when carrier motion is incongruent with envelope motion.

While I did not describe the stimulus construction in detail to naïve observers, all observers after having practiced at the task employed in Experiment 1 commented spontaneously on the two forms of motion being employed. More than one observer when commenting on the stimuli called the envelope morion "real" and the carrier motion "fake." However the two motions are not equally salient or distinguishable in all conditions; the carrier motion appears less salient when spacing is wide, with few elements on screen, and envelope motion is more difficult to discern in the contrary situation. Motion after-effects appear to always be directed opposite the carrier motion regardless the spacing or the envelope motion.

There seems to be some individual variation as to how relatively strong carrier and envelope motions are. For some observers I was able to find a configuration of carrier strength, envelope

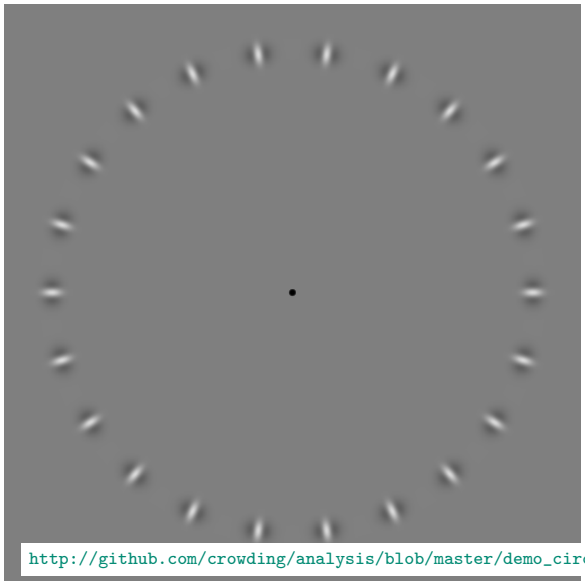

Figure 2.3: (`demo_circle_22.mov`) A stimulus with 22 identical elements. For most observers, carrier motion dominates the appearance.

motion, and spacing which I would perceive as clearly being clockwise but the observer would perceive as counterclockwise. While appearance was affected by carrier motion, it was not always affected in the *direction* of carrier motion; I sometimes found that adding carrier motion in one direction to a stimulus prompted a report that the stimulus was now moving in the opposite direction to the change. Sometimes I could even find a stimulus whose carrier and envelope motion were clockwise but whose appearance was counterclockwise to a particular observer. An effort at modeling the processes underlying this behavior will therefore have to capture this individual variation and the apparent nonlinearity in carrier motion perception.

There are too many stimulus parameters to explore the entire configuration space exhaustively, but I can report some impressions as to the robustness of the appearance of the stimulus. In particular I wondered whether the density-driven reversal of apparent motion was robust to changes in stimulus properties such as element size and eccentricity. A scaling of critical spacing with eccentricity and robustness of critical spacing against changes in target size target size have been proposed as two diagnostic tests of visual crowding (Pelli, 2008).

Adjusting the spacing from wide to narrow by adding more elements revealed a point at which the appearance of motion changed from envelope-dominated to carrier-dominated. I noted the spacing (or equivalently the number of elements) at which the appearance seemed to change, while varying other stimulus parameters. I found that I could vary the eccentricity, size, and velocity of the envelopes by a factor of 2 in either direction, while the critical spacing required to induce a change in motion appearance remained roughly the same. Similarly I could vary the spatial frequency and temporal frequency of the carrier by a factor of 2 in either direction without much affecting the critical spacing. At the extremes of the configuration space, the change in character of the motion was present among other percepts of motion, and could become hard to distinguish. The largest effect seemed to be for spatial frequency and element size, for which a change of a factor of four (going from 0.67 to 2.67 cycles per degree at 10 degrees eccentricity, the element size scaling inversely) only modestly increased the number of elements required for reversal, from 13 to 18. Scaling all spatial parameters (element size, eccentricity, envelope velocity, spatial frequency) at once did not affect the spacing at reversal; the critical spacing scaled with eccentricity.

The demonstrations shown in Figure 1.1 and in this section suggest that multiple motion elements placed in proximity in peripheral vision interact in such a way that the carrier motion becomes more perceptually salient and the envelope motion less so. When envelope and carrier motion are put into conflict, the inter-element spacing (depending on retinal eccentricity) appears to be the most reliable determinant of which component wins. In the following sections I report psychophysical experiments designed to capture and model the determining factors explaining perceived motion direction.

3 General Methods

3.1 Observers

Observers were the author (PBM) and 10 naïve observers (3 male, 7 female.) All had normal or corrected-to-normal vision. All observers provided informed written consent, and all procedures involved were approved by the Institutional Review Board at the University of Washington.

3.2 Equipment

Stimuli were presented on a flat CRT video monitor (ViewSonic PF790). Its resolution was set to 800×600 pixels with a display area of 35.5×25.8cm, spanning $33.0 \times 24.3^\circ$ of visual angle. The monitor used a refresh rate of 120Hz. Experiments were programmed in MATLAB using the Psychtoolbox (Brainard, 1997) and Eyelink toolbox extensions (Cornelissen et al., 2002), along with custom OpenGL code. All guns were fixed at the same voltage to show grayscale stimuli. The monitor was calibrated using a Tektronix J17 photometer. A gray background of $30.2\text{cd}/\text{m}^2$ was used; the black point and white point of the display measured against that background were $0.13\text{cd}/\text{m}^2$ and $60.97\text{cd}/\text{m}^2$. A hardware lookup table with 10-bit resolution was used to linearize the display response.

Observers sat behind a blackout curtain so that ambient illumination was mostly due to the monitor and viewed the screen binocularly using a chin and forehead rest with the eyes 60cm from the screen, aligned with the screen's center axis. Eye position was monitored using a video-based eye tracker (EyeLink 1000; SR Research) using a sample rate of 1000Hz. Observers gave responses by turning a knob (PowerMate; Griffin Technologies) with their preferred hand in the direction of the perceived motion.

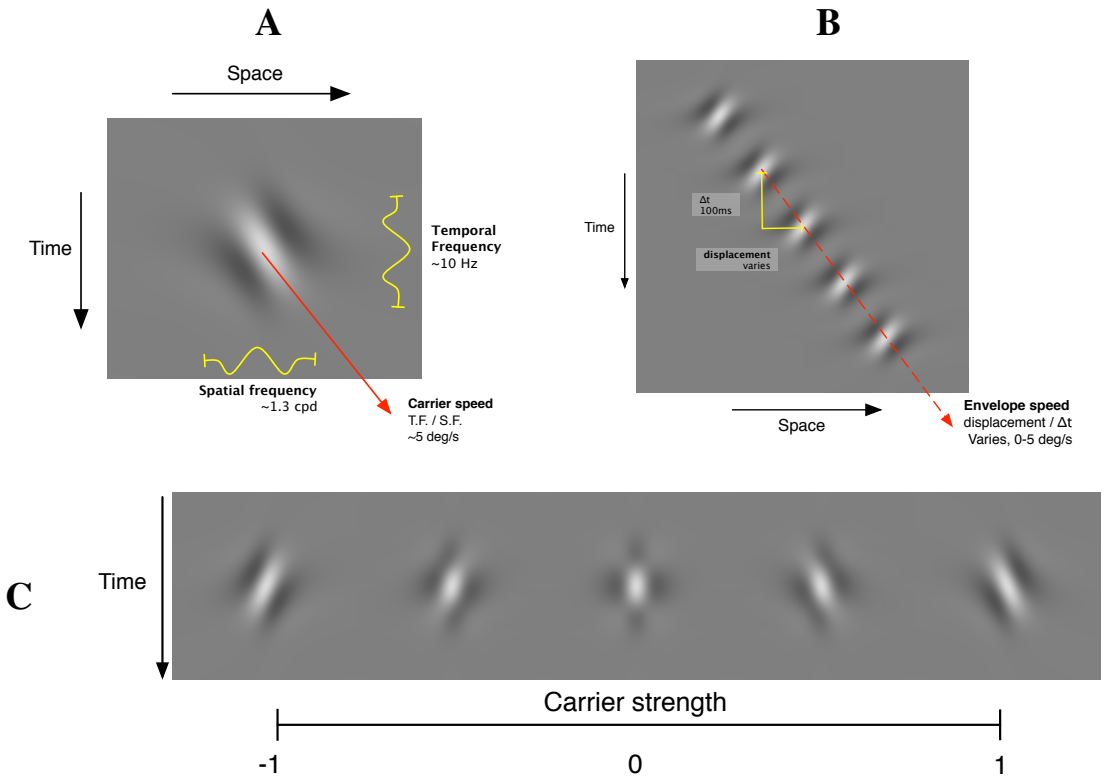

Figure 3.1: Construction of motion-direction stimuli. **A.** A single motion pulse, shown in a space-time diagram. Space is shown across the horizontal axis, and time is shown running down the vertical axis. Each pulse is Gabor-like with a moving carrier (visible as the local orientation in this diagram) and a fixed envelope. **B.** Motion elements were constructed of several motion pulses, offset by regular intervals in space and time. Displacement or Δx refers to the spatial displacement of the Gabor-like elements between pulses. **C.** We varied the direction of the carrier by mixing two carriers in opposite directions. A carrier strength of 0 is counterphase flicker, with equal energy along both directions of carrier motion. A carrier strength of 1 uses only the clockwise carrier.

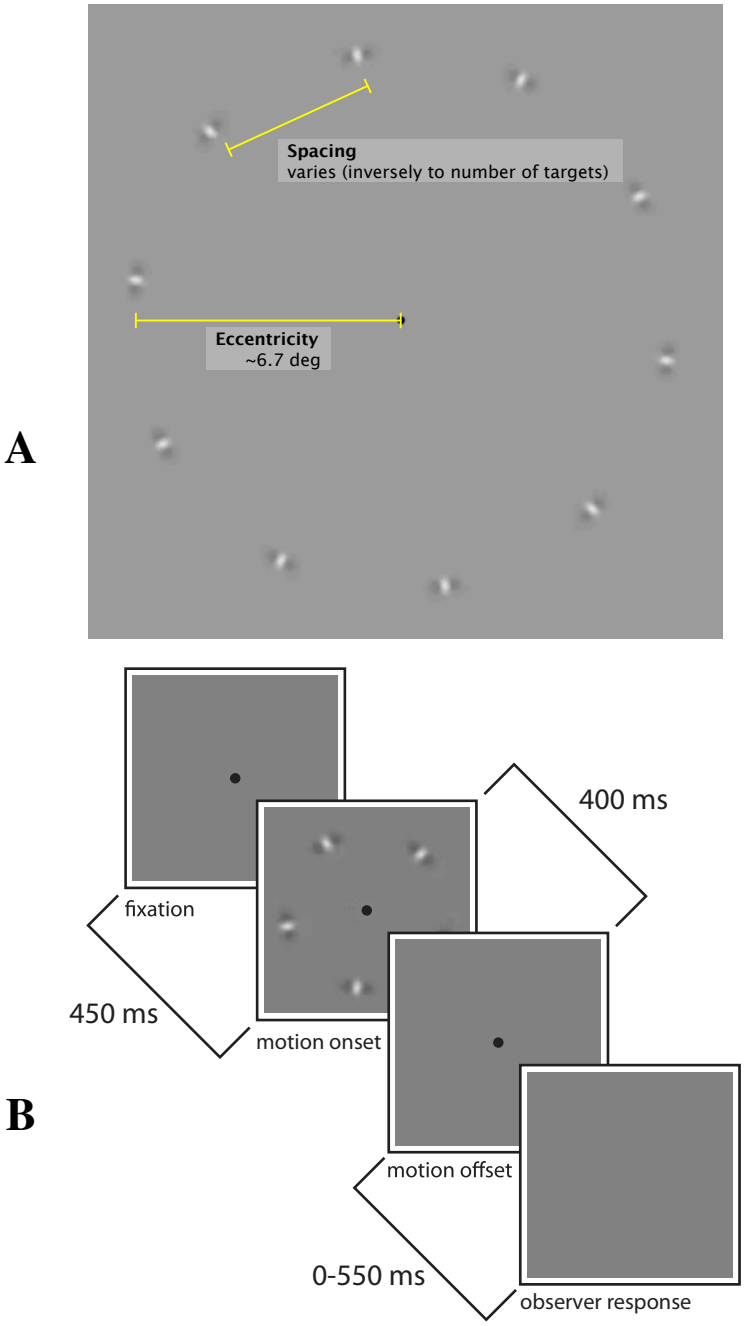

Figure 3.2: **A.** Stimuli comprised several motion elements arranged around a circle, with the directions of carrier and envelope motion along its circumference. **B.** Illustration of task. Observers fixated a central dot, viewed motion stimuli such as in Figure 2.1, and reported the apparent direction of motion within a prescribed time window.

3.3 Stimuli

This construction of the stimuli is illustrated in Figure 3.1 and Figure 3.2. The stimuli consisted of a number of identically moving elements arranged into a circle centered on the fixation point and moving circumferentially. Each element consisted of a series of 5 motion pulses separated by a regular spatial displacement Δx and temporal intervals Δt. Along the direction of motion, the luminance distribution of a pulse was given by a Cauchy filter function (Klein and Levi, 1985). At right angles to the direction of motion the pulses were windowed by a Gaussian envelope with standard deviation $w/2$, while the temporal onset and offset of each pulse had a Gaussian profile with standard deviation $d/2$. An equation describing the luminance profile of a single pulse, centered at $(x,y,t) = (0,0,0)$ with carrier motion along x is:

$$L(x,y,t) = \cos^n\left(\tan^{-1}(fx/n)\right)\cos\left(n\cdot\tan^{-1}(fx/n) + \omega t\right)e^{-(t/2d)^2-(y/2w)^2}$$

Here ω controls the temporal frequency and f the spatial frequency of the carrier, d, the duration of the pulse, w the radial width of the envelope and n the circumferential width of the envelope (relative to the spatial frequency.) At the moment of maximum contrast the carrier was always in cosine phase.

To control the direction and amount of carrier motion I overlaid two pulses with opposite directions of carrier motion, with varying amounts of relative contrast. This is parameterized by the carrier strength C,

$$C = \frac{C_{CW} - C_{CCW}}{C_{CW} + C_{CCW}}$$

where C_{CW} and C_{CCW} are the contrasts of clockwise and counterclockwise components. Thus C has a range of $[-1,1]$ and a value of 0 indicates a counterphase flicker with equal parts clockwise and counterclockwise motion energy. The total luminance contrast is held at $C_{CW} + C_{CCW} = 0.5$ for the experiments reported here.

The examples in Section 2 have the following settings, the same as used in Experiment 1 and

Experiment 2: 5 pulses at intervals of $\Delta t = 100$ms, carrier temporal frequency $\omega = 10$Hz, and (with an eccentricity of $e = 6.67^\circ$,) $w = 0.5^\circ$ and $f = 2$ cpd.

3.4 Task

The time course of a trial is illustrated in Figure 3.2B. A fixation point was presented. The computer then waited for the observer to fixate. 450ms after detecting fixation, the motion stimulus was shown for 400 ms (the initial pulse, then 4 steps of envelope displacement occurring at 100ms intervals.) After the motion stimulus concluded, the observer indicated the direction of perceived motion by turning the knob within a response window from 400 to 950ms measured from stimulus onset. If the observer blinked or broke fixation before the offset of the motion stimulus, the trial was aborted and reshuffled into the stimulus set, to be repeated later in the session. If the response was outside the window, the observer received visual feedback that their response was either too fast or too slow, and the trial was also reshuffled into the stimulus set. An audio click was played each time observers gave a response; this seemed to help observers establish a consistent rhythm through the experiment. No feedback was given as to the correctness of an observer's response, only whether they had responded within the time window. Observers were instructed to report the apparent direction of motion, and advised that there were no "correct" answers. In some conditions observers reported seeing conflicting or overlapping directions of motion. In those cases they were advised to choose whichever direction of motion appeared more salient.

Observers performed the task in sessions that lasted a maximum of 1 hour, divided into 4 to 6 blocks, and were prompted to take a break between blocks. They could also rest at any time by simply delaying fixation. At the beginning of each block, the eye tracking system was automatically recalibrated by asking the observer to make saccades to a sequence of targets at randomly chosen locations on the screen.

3.5 Staircase procedure

I used staircase procedures to collect data relating the proportion of clockwise responses as to the envelope displacement, Δx. For each psychometric function we used two staircases, one 2-up-1-down and the other 2-down-1-up, to bracket the particular displacement at which subjects were equivocal about perceived direction (the point of subjective equality or PSE.) In a typical session, 6-8 pairs of staircases, each with a different stimulus configuration, were run concurrently, with each staircase operating independently and trials from all staircases being randomly interleaved. Example data from this procedure is shown in Figure 5.1, with envelope displacement Δx plotted on the abscissa and the proportion of "clockwise" responses on the ordinate. In these graphs we scale the area of the data points to be proportionate to the number of trials collected at that displacement. Thus, the smaller a data point, the further it may acceptably lie from the model fit; some data drawn using the smallest dots may represent a single trial at a value of displacement that the staircase procedure did not revisit.

3.6 Data folding

When staircase procedures were used, they employed randomized folding; a staircase configured to use a carrier strength C of 0.2 would actually pseudorandomly present either clockwise (0.2) or counterclockwise (-0.2) carrier on each trial, with the staircase-controlled envelope motion reversing direction accordingly.

I similarly presume that an observer's responses to a stimulus and its mirror image are symmetric up to a constant bias. Therefore we will present and write about stimuli, without loss of generality, as though the carrier motion runs clockwise in all trials, even though the underlying data contains a balanced mixture of clockwise and counterclockwise trials. The mirror image of a trial reverses the sign of three properties: the carrier motion, the envelope motion, and the observer's response. So, a trial with carrier strength $C = -0.2$ and envelope motion $\Delta x = 0.1$, where the observer responded "clockwise," will be presented equivalently to a trial with carrier strength

$C = 0.2$ and envelope motion $\Delta x = -0.1$, where the observer responded "counterclockwise." I use the convention that carrier strength is always shown as positive. Note that the direction of envelope motion can differ from that of carrier strength, so that envelope motion will still take both positive and negative values when data is folded.

In some cases observers exhibit a bias toward clockwise or counterclockwise responses. I include a global bias term in our model to account for this - this is the only term in the model that is not symmetric. I fit the model using unfolded data. When drawing fitted curves to illustrate model predictions, I sum out the bias by averaging the model predictions for clockwise and counterclockwise conditions.

3.7 Data analysis

Data analysis was performed using the R language (R Core Team, 2013). Models in Experiment 1 were fit using the `gnm` package (Turner and Firth, 2012). Models in Experiment 2 were fit using the Stan modeling language (Stan Development Team, 2014). Graphics were prepared using the `ggplot2` (Wickham, 2009) and `rgl` (Adler and Murdoch, 2013) packages. Original datasets and analysis scripts for this manuscript will be published online at `https://github.com/crowding/thesis`.

4 Model details and motivation

A schematic explanation of our model is shown in Figure 4.1. The model combines two signals to produce decisions about motion direction (**Figure 1.1**A): M_Δ is an estimate of the change of position of a tracked target, corresponding to envelope motion in these stimuli, and is computed within a restricted region illustrated as the smaller, yellow dotted circle. The sensitivity to changes in position is a function of the spacing between elements (**Figure 1.1**B). M_S is a sum of first order motion energy (carrier motion in these stimuli) inside a larger region illustrated by the blue dashed outline. The sensitivity to first order motion depends on the number of elements falling within the region (**Figure 1.1**C). These two signals are compared by subtraction, producing a difference signal M_I (**Figure 1.1**D), then all signals are combined to produce a decision. The carrier motion input to the subtraction is normalized (it does not depend on the number of elements).

For M_S, we begin by assuming that the strength of the first order motion signal is linear with respect to carrier strength C. However, as spacing decreases and there are more elements within the summation region, we expect signals from multiple elements to sum, so that the local motion signal is proportionate to the direction content of individual elements. A model parameter β_S determines each observer's sensitivity to the first order component:

$$M_s = \beta_S CN$$

For M_Δ, assume that envelope motion is computed by taking the difference between successive noisy estimates of the position of a given element. The sensitivity to envelope motion β_Δ will then be inversely proportional to the uncertainty in element position. As flanking elements come closer to the tracked element, the visual system will be less able to isolate a single element to determine its position, so the sensitivity to changes in position will decline. We model this by making the sensitivity $\beta_\Delta(S)$ a sigmoid function of the spacing between elements:

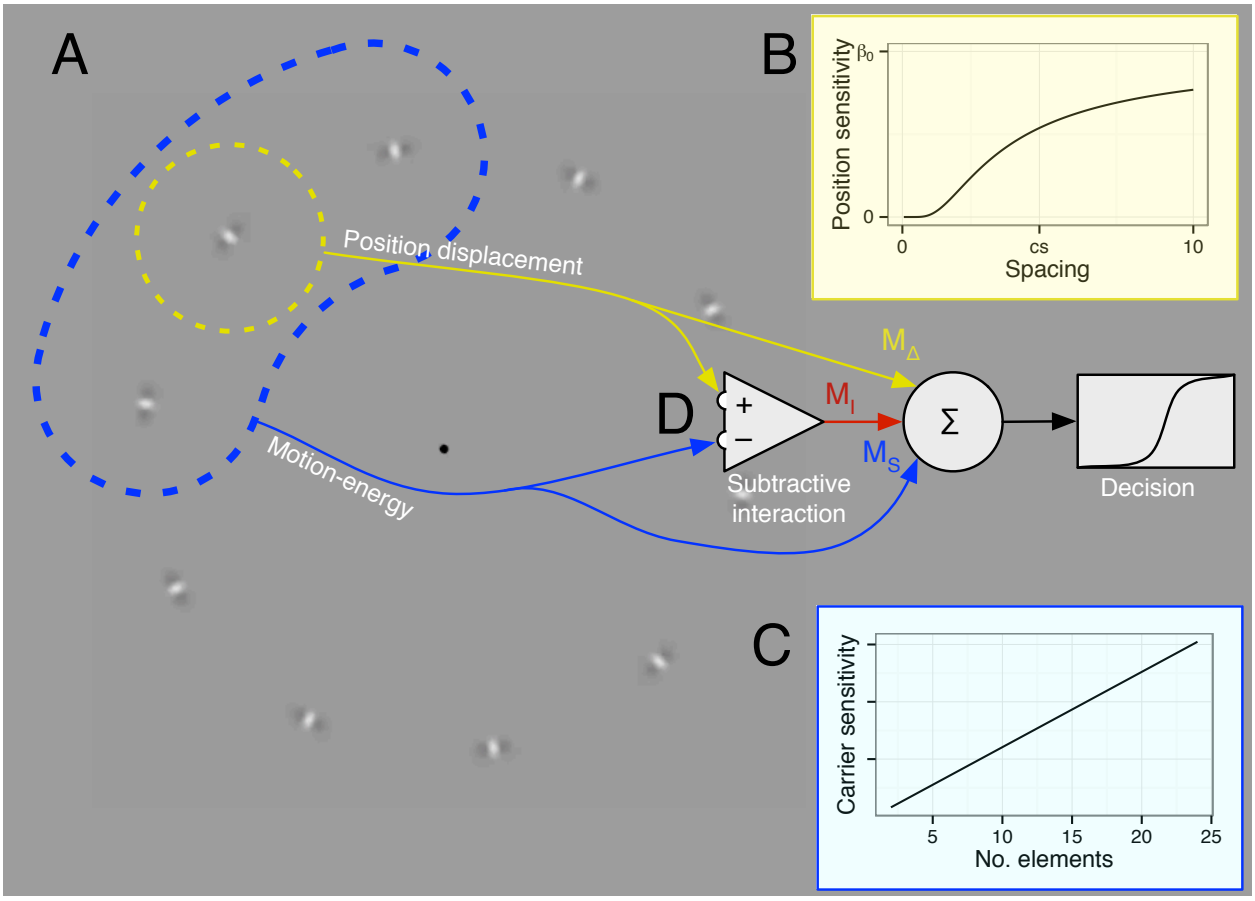

Figure 4.1: Schematic of motion model. **A.** The background shows a typical motion stimulus. The motion stimulus contains two sources of information. The positional displacement of an individual, attended element is computed within a limited region, as illustrated by the smaller, circle. First order motion energy is summed over a larger region. **B.** The sensitivity to displacements depends on the distance between elements. **C.** The sensitivity to carrier motion strength scales with the number of elements. **D.** If first-order velocity differs from position-defined velocity, the difference adds a third signal. All signals are weighted to produce a decision.

$$M_\Delta = \beta_\Delta(S)\,\Delta_X, \text{ where } \beta_\Delta(S) = \beta_0\left(2 - \frac{2}{1+e^{-\frac{S_C}{S}}}\right)$$

This function results in sensitivity that approaches β_0 at large spacings and approaches zero at small spacings, as plotted in Figure 4.1B. β_0 is the model parameter controlling sensitivity to envelope displacement for isolated, uncrowded targets; the parameter S_C describes the distance over which spatial interference between targets takes place. S_C has a natural interpretation as the spacing at which the threshold for discriminating a feature (in this case envelope motion) increases by a constant factor, which is often used as an empirical definition of the "critical distance" of crowding

(Levi et al., 2002; Pelli and Tillman, 2008; Whitney and Levi, 2011).

These two forms for M_S and $M_\Delta$capture the phenomenon that decreasing the spacing between elements has opposite effects on the first-order and position-defined motion mechanisms. For the carrier motion signal, cramming more elements into the summation region increases the strength of the signal, since it is a simple summation of motion energy within that region. For the envelope motion signal, cramming more elements into the summation region makes it difficult to estimate the position of any individual element, and thereby weakens the signal. Thus, decreasing the spacing results in carrier motion having a stronger influence on the perceived motion, and envelope motion having a weaker influence.

One addition to this basic model is required to account for a repulsion effect I observed when carrier motion velocity disagrees with envelope velocity. In Figure 1.1A, it might appear to some observers that the carrier motion leftward with a stationary envelope results in perceived motion rightward, and vice versa. I account for this by adding a comparison between carrier and envelope velocity, which generates a third component in the model M_I. Since carrier motion has a high temporal frequency for the stimuli I use, its effective speed is high, so I let this depend on the carrier strength per element only. It has a linear term controlled by a coefficient $\beta_{I_a}$and a second-

order, nonlinear term controlled by β_{I_b}:

$$M_I = \left(\beta_{I_a} C + \beta_{I_b} C|C|\right),$$

The nonlinear component was necessary to account for a nonmonotonic effect of carrier strength on observers' responses (see § 5.4.6.)

These three components contribute to the modeled subjects' responses according to a probabilistic rule;

$$\Pr\left(\text{clockwise} \mid \Delta x, C, s, n\right) = (1-\lambda)\,\text{logit}^{-1}\left(M_\Delta + M_S + M_I + k\right) + \frac{\lambda}{2}$$

where $\text{logit}^{-1}(r) = (1+e^{-r})^{-1}$ is the standard logistic cumulative distribution function. The free parameters of the model are β_0, S_C, β_S, β_{I_a}, β_{I_b}, and k. The bias term k accounts for an overall clockwise or counterclockwise bias, which some observers exhibit. The lapse rate λ is intended to improve the robustness of the fit (Wichmann and Hill, 2001); I constrained λ to lie between 0 and 0.05.

5 Experiment 1: Relation of first-order and position motion sensitivity to element spacing.

The movies shown in Section 2 seem to suggest that the perceived change in motion is a function not only of the properties of individual elements but of a spacing-dependent interaction between nearby elements. In this experiment I measured hoe the sensitivity to carrier and envelope motion changed as a function of the distance between elements.

5.1 Methods

Stimuli for this experiment consisted of a circle of evenly spaced elements presented at an eccentricity of 6.7°. As described above in § 3.5, I used an interleaved staircase procedure, with the staircase varying the speed of the envelope motion. Each staircase used a fixed carrier strength and spacing. The first training session used four values for spacing and two for carrier strength; I used data from this session to select values of spacing and carrier strength that were likely to provide good information about the effects of each variable. Subsequent sessions were in two types. One focused on the effect of spacing, and tested several spacings at a single chosen carrier strength. The other focused on the effect of carrier strength, and tested a fixed set of carrier strengths (0.1, 0.2, 0.4 and 1.0), at two chosen values of spacing. It is possible that observers adapted to the set of stimuli when a single carrier strength or limited sets of spacings was used for an entire session. However, I found that a single model fits all types of sessions adequately, so all data is pooled and presented together.

5.2 Results

I first show individual psychometric functions that illustrate the effects of spacing, carrier strength and envelope displacement. I found three effects relating envelope motion, carrier motion, and spacing. I will describe and show these effects qualitatively first, then show how they are accounted

for by the model described in Section 4 and quantify these effects.

5.2.1 Sensitivity to envelope displacement decreases as spacing decreases

First consider the effect of reducing spacing (and simultaneously increasing number) on the perception of envelope motion. There are two potential effects. A reduction in spacing may cause crowding, while an increased number of identical elements may allow summation or pooling of their identical envelope motions. These hypotheses would predict opposite effects on the sensitivity to envelope motion. Pooling would predict that more elements would lead to a greater sensitivity to envelope motion; crowding would predict that reduced spacing will reduce sensitivity to envelope motion. I found the latter; an example of this is shown in Figure 5.1, for a subset of the data collected. This figure plots the envelope displacement per step, Δx, on the horizontal axis and the probability of the observer responding "clockwise" to that stimulus on the vertical axis. For Figure 5.1 data for two values of spacing at the same carrier strength are shown, for three observers. In each case the psychometric function fit to data collected at the smaller spacing has a shallower slope, independently of any shifts it may have. Below in § 5.4.3 I will quantify and graph the relation of sensitivity to element spacing.

Even if crowding causes interference at smaller spacings, there might still be pooling of envelope motion between widely spaced elements. Therefore I tested whether there was a change in envelope motion sensitivity with element number at wider spacings, outside the range of spacings that might be subject to crowding, but I found no significant effect (§ 5.4.2). The values of Δx tested are smaller than half the inter-element spacing of the smallest spacings used, so that spatial aliasing (the wagon wheel illusion) should not explain why there is additional uncertainty in motion direction.

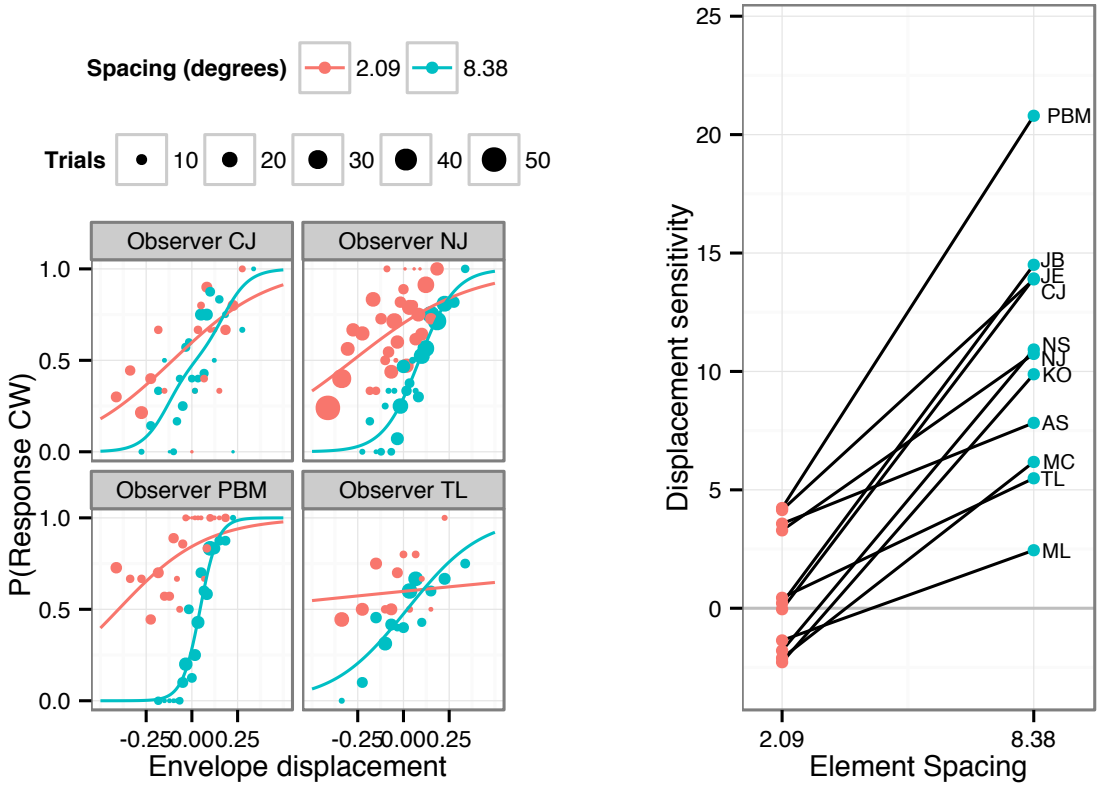

Figure 5.1: When spacing is reduced, sensitivity to envelope motion decreases. LEFT: Data from four observers is shown, each showing two spacings. Carrier strength was fixed at $C = 0.2$. The horizontal axis shows the envelope displacement per step Δx in degrees, and the vertical axis plots the proportion of trials answering "clockwise" to that stimulus. Curves show a psychometric function fit. RIGHT: Displacement sensitivities. Displacement sensitivities correspond to the slopes of the psychometric functions. Lower sensitivities are seen at narrow spacings and higher sensitivities are seen at wider spacings. NOTE: Points on the graph are scaled according to the number of trials made at those stimulus configurations. Therefore larger points are expected to lie closer to the model fit, while smaller points have more uncertainty and may be expected to lie farther from the model fit. In the extreme, a particular stimulus configuration might only be visited once or twice while the staircase moves past it; these smallest points would lie on either $\Pr(\text{clockwise}) = 1$ or 0.

5.2.2 Sensitivity to carrier strength increases as spacing increases; carrier motion is repulsive in sparse displays

Contrary to the results for envelope motion, the more elements on screen, the more effect carrier motion had on the appearance. That is, when there were few elements on screen, the effect of changing carrier motion strength was small; when there were more elements on screen, changes in carrier motion had more effect on motion appearance (Figure 5.2). This was complicated by a repulsive effect; when few elements were used on screen, carrier motion in one direction often caused observers to shift their reports of perceived motion in the opposite direction. Thus the response to carrier motion was nonmonotonic; adding elements to a blank display caused observers to report directions of motion opposite that of the carrier, but adding more closely-spaced elements caused apparent motion to shift in the direction of carrier motion. Figure 5.2 gives examples of both these effects, again using a subset of the data collected. This figure shows data using two different values of carrier strength, each at two different element spacings. The lower row shows data collected at the wider of the two spacings.

When more elements were added to the display, the sensitivity to carrier motion increased, indicating summation of carrier motion. The sensitivity to carrier motion corresponds to the change in responses associated with an increment of carrier strength. Figure 5.2 shows this measurement for an increment from carrier strength of 0.1 to 0.2, for sparse (5 elements) and dense (20 elements) displays. The sensitivity to carrier motion corresponds to the vertical shift in the y-intercept of the psychometric function, illustrated as black arrows in Figure 5.2.

Note that sensitivity being discussed is based on the shift in the *y*-intercept rather than a shift in the point of subjective equality (where the psychometric function intercepts $p = 0.5$.) The change in PSE corresponds to the sensitivity divided by the slope of the psychometric function. Therefore a change in slope without a change in sensitivity would still lead to a change in PSE. However, since the change in the y-axis intercept changes with spacing, there is an effect of element number on carrier motion as well as an effect of spacing on envelope motion. Both effects contribute to the

change of appearance seen in Section 2. As more elements are added to the display and packed closer together, the appearance is less determined by the envelope motion, while it is more determined by the carrier motion. The combination of both effects mean that carrier motion determines the appearance when the display is dense and envelope motion determines the appearance when the display is sparse.

Note that when fewer elements are displayed, incrementing carrier motion tends to bias the appearance in the opposite direction from the carrier motion. In other words carrier motion is repulsive in sparse displays. In the left column of Figure 5.2, the psychometric functions fitted to this data intercept the vertical axis at values of $\Pr(\text{clockwise})$ less than 0.5; furthermore, increasing the carrier strength from 0.1 to 0.2 increases the repulsion. So at wide spacings, observers were more likely to perceive a stimulus with stationary envelopes and clockwise carrier motion as actually moving counterclockwise. When more elements were added to the display, repulsion turned to assimilation; the same increment to carrier motion shifted the appearance of the stimulus in agreement with the motion added.

This repulsion means that there are some stimuli for which both envelope and carrier motion are slightly clockwise, but the perceived motion is still counterclockwise; this is the case when the curves pass through the lower right quadrants in Figure 5.2 ($\Delta x > 0$ and $\Pr < 0.5$.) In these conditions the observer will respond "counterclockwise" to a stimulus whose carrier and envelope motions are both slightly clockwise.

Figure 5.2 presents folded data, i.e., values shown here with a single value for carrier strength, which I nonetheless refer to as "clockwise," represent data collected from both that stimulus and its mirror image, and envelope motions and responses are mirrored correspondingly. So a point appearing below $P < 0.5$ in this graph can be read as indicating that the observer chose "counterclockwise" to a particular stimulus more often than they chose "counterclockwise" to that stimulus's mirror image. Thus the presentation of folded data here averages out any static biases toward one direction.

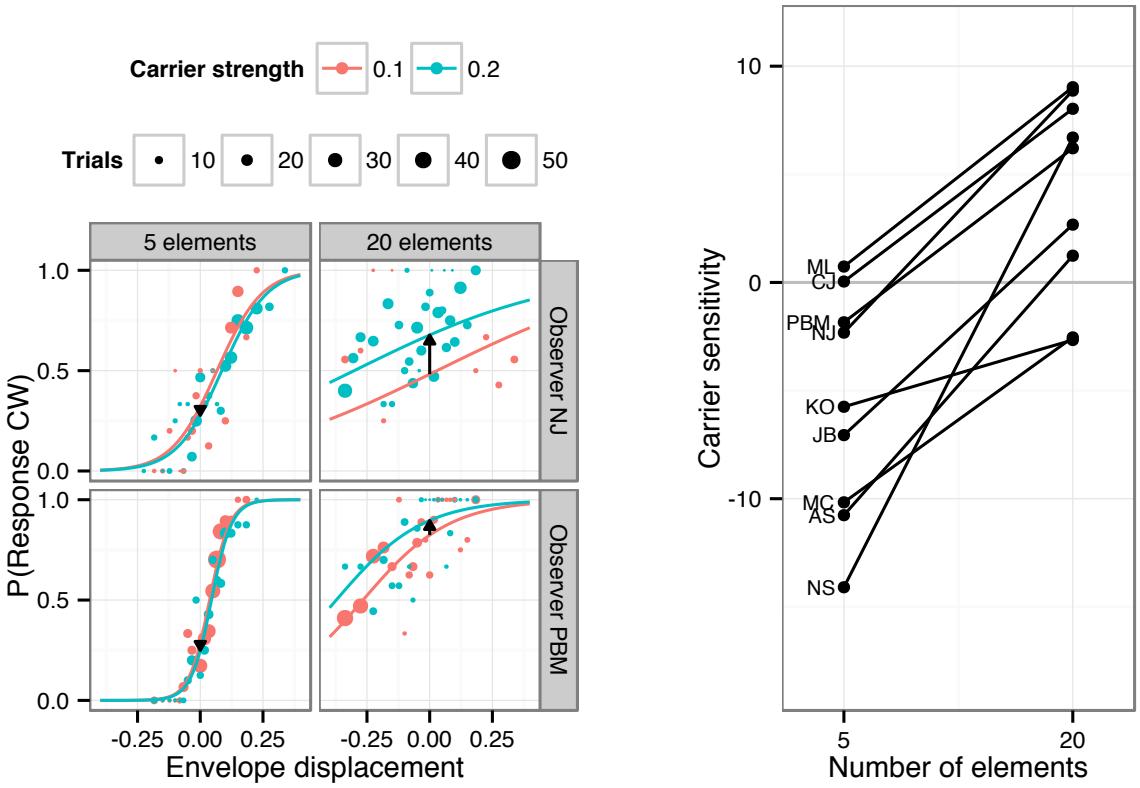

Figure 5.2: Adding more elements increases the sensitivity to carrier motion. LEFT: An example subset of the data from Experiment 1 is plotted, showing two observers' responses at two values of carrier strength and two spacings. The horizontal axis plots envelope displacement, while the vertical axis plots the proportion of responses clockwise. Colors indicate two strengths of carrier motion. Psychometric functions are fit using equal slopes at equal spacings. Changing the carrier motion shifts the psychometric function: the sensitivity to carrier motion corresponds to the vertical separation between psychometric functions, indicated by black arrows. When more elements are added, the sensitivity to carrier motion increases (arrows extend upwards.) RIGHT: Carrier sensitivity is measured, for 5 and 20 elements, using an increment of carrier strength from 0.1 to 0.2. Increasing the number of elements increases carrier sensitivity for each observer. Note that most observers have negative carrier sensitivity when fewer elements are on screen, indicating a tendency to respond in opposition to the carrier motion.

In the previous section I illustrated that the sensitivity to envelope motion, visible as the slope of the psychometric function, decreased when element spacing decreased. In this section I illustrated that carrier motion has the opposite change in sensitivity; carrier motion has a stronger influence on perceived motion for narrowly spaced stimuli. In this experiment the spacing between elements covaries with the number of elements, so that it is indeterminate whether either effect should be considered an effect of the reduced spacing or of the increased number (this will be explored in Section 6. However, in either case, this contrast identifies a way in which position-defined motion is processed differently from first-order motion; it appears that envelope motion signals from separate objects are not pooled in this task, while carrier motion does appear to pool between adjacent objects.

5.3 Model and data visualizations

Having given examples illustrating some of the effects that a model should capture, this section attempts to present an overview both of the entire dataset, and how the model specified in Section 4 fits that data. In the subsequent section I will examine particular features of the model and evaluate their fit to the data.

This experiment related three parameters – carrier strength, envelope motion and spacing – to a fourth variable, the motion perceived by the observer. One can visualize those variables as forming a three-dimensional space illustrated in Figure 5.3. The combination of these three variables determines the likelihood with which the observer will respond "clockwise" or "counterclockwise" to the given stimulus. The model's prediction of the proportion of responses clockwise visualized as a density coloring each point in the space. Four planar sections are shown through this space to highlight model features of interest. In Figure 5.4 these same planar sections are pulled out and shown in relation to the observed data.

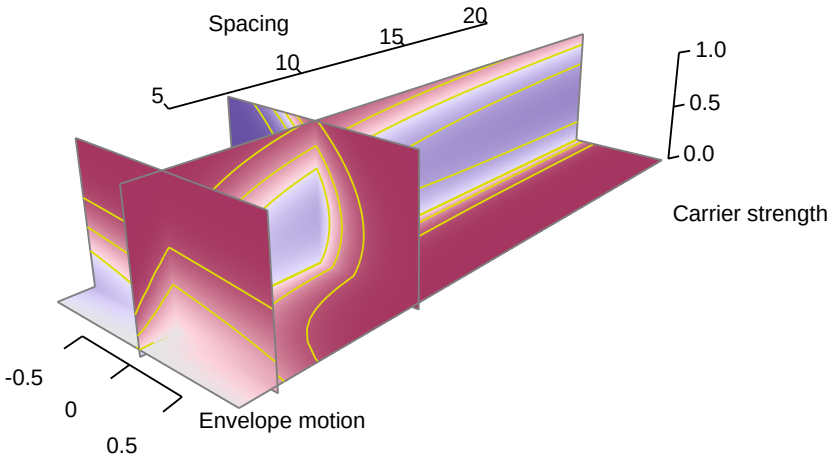

Figure 5.3: A three-dimensional representation of the model fit for one observer (NJ). Axes correspond to the three stimulus parameters varied in this experiment: inter-element spacing S in degrees of visual angle, envelope motion Δx, in degrees per step, and carrier strength C. Four planar sections through the three-dimensional space are shown, and correspond to the four panels in Figure 5.4. The color scale indicates the probability of responding clockwise according to the model fit. Red shades indicate stimuli for which the model predicts clockwise responses (i.e. $P > 0.5$) and blue indicates predicted counterclockwise responses. In both cases the luminance depends the difference between the response probability and 0.5, with response probabilities further from 0.5 colored darker and more saturated. Yellow contour lines are placed at response probabilities of 0.1, 0.3, 0.5, 0.7 and 0.9.

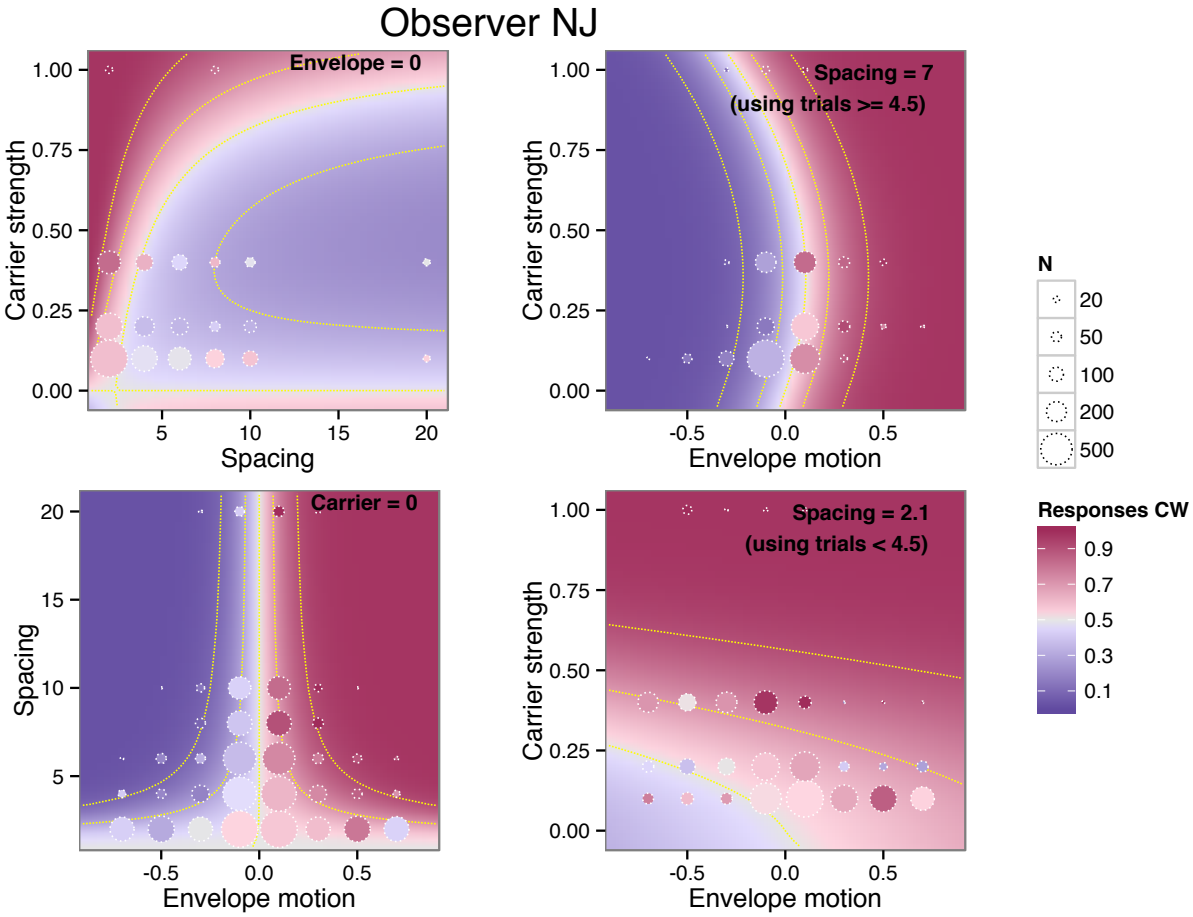

Figure 5.4: Data and model responses for observer NJ. The four plots shown correspond to the four planes shown in Figure 5.3; color scale and contour line placement are the same. Circles represent observers' recorded responses for trials whose parameter are binned near that stimulus. The shading of each circle depends on the residual between the recorded responses and the model prediction for that set of stimuli; an identical shade inside the circle as outside indicates no residual, and the shading should be interpretable on the same scale as the probability scale of the background. Each circle summarizes the subset of trials falling near that point in the two dimensions of its panel. UPPER LEFT: Response probability as a function of spacing and carrier strength, with envelope motion fixed to zero. Residuals collect trials across all envelope motions (see § 5.3.2.) LOWER LEFT: Response probability as a function of envelope motion and spacing, for stimuli with no carrier strength (i.e. counterphase flicker). Residuals collect trials across all carrier strengths. UPPER RIGHT and LOWER RIGHT: Fitted model response as a function of carrier spacing and strength, for two different values of spacing (indicated in the upper right). Residuals shown in the upper right are of trials with spacing from 4.7 to 21 degrees, while residuals shown in the lower right are of trials with spacing between 1.7 and 4.2 degrees.

5.3.1 Model figure construction

Figure 5.3 and Figure 5.4 show data from one observer; the complete set of illustrations for all observers is shown in an appendix. The background color scale depicts the probability of responding "clockwise", with high probabilities shaded red and low probabilities (i.e. tending counterclockwise) shaded blue; probabilities further from 0.5 in either direction are shown with darker and more saturated colors. The four subplots correspond to the four planes shown in Figure 5.3.

The colored background in Figure 5.4 shows the model's predictions as a function of two of the three variables, leaving the other fixed; the value of the fixed variable is noted in the upper right corner of each panel. The four panels show how model responses vary (UPPER LEFT) as a function of spacing and carrier strength, for stimuli with zero envelope motion, (LOWER LEFT) as a function of spacing and envelope movement, for stimuli with zero carrier strength, (UPPER RIGHT) as a function of envelope motion and carrier strength, for stimuli with a fixed, wide spacing, and (LOWER RIGHT) as a function of envelope motion and carrier strength (same slice direction as UPPER RIGHT), for stimuli with a fixed, narrow spacing.

Figure 5.4 also represents the observer's responses. Trials are sorted into bins according to stimulus parameters and a summary circle is plotted for each bin. The circles are drawn with area proportional to the number of trials they summarize. The shade within the circle is a weighted average of the observer's responses, as explained below. Any difference between the shading inside the circle and that of the background indicates a residual between the model and the subset of observed data summarized in that circle. Each plot uses a different binning, according to its axes. For example, a circle in the lower left figure summarizes a set of trials with a particular range of envelope motion and spacing, but any value of carrier strength.

5.3.2 Binning and color scaling

This section gives technical details of how responses are binned and averaged for display in Figure 5.4. The shading within each circle is not simply the arithmetic mean of observers' responses,

but is based on the difference between the data and model predictions. I based the plot on the residuals rather than the sample mean for reasons related to the three dimensional parameter space and the sampling of data throughout that space. First, each circle represents the subset of trials that lie closest to it in the two dimensions of the plot, but these trials may be located at any value in the third dimension. For example, in the UPPER LEFT panel, showing a slice across carrier strength and spacing, data are combined across all speeds of envelope motion. The response probability varies in the unseen dimension, so that one circle may combine stimuli for which the observer tends to respond clockwise with stimuli for which the observer tends to respond counterclockwise. Since I used a staircase procedure to choose envelope displacement, the the mean response probability in each bin clusters around 0.5, which would not be useful to display. Since the data are not uniformly sampled throughout the stimulus configuration space, adjacent bins collect trials with a different sampling in the unseen dimension, as determined by the staircase procedure. A simple arithmetic mean of each bin would not lead to a depiction of observed data that could be visually compared with either adjacent bins or the model on the 2-d slice.

Instead the shading within each circle is determined by computing the Pearson residual between model predictions and observations, then applying that residual at the location of the bin center to obtain a remapped response probability. Consider n trials, whose parameters are x_i, and binary responses $y_i \in \{0,1\}$, falling within a bin centered on a mean stimulus $\bar{x}$. Recall that the Pearson residual for a set of n binary observations y_i and corresponding predicted probabilities $\widehat{\mu}_i$ is defined as

$$R = \frac{\sum_i (y_i - \widehat{\mu}_i)}{\sqrt{\sum_i \widehat{\mu}_i \cdot \sum_i (1 - \widehat{\mu}_i)}}$$

which is the total difference between data and observation, scaled by the standard deviation of the predicted count (the predicted count being the sum over each Bernoulli$(\widehat{\mu}_i)$ random variable.) If the model is a function of the stimulus parameters x so that $\widehat{\mu}_i = \widehat{\mu}(x_i)$, I define a remapped response probability $\bar{y}(x)$ in terms of the Pearson residual,

$$\bar{y}(x) = \widehat{\mu}(x) + R\frac{1}{\sqrt{n}}\sqrt{\widehat{\mu}(x)(1-\widehat{\mu}(x))}$$

The shading of the circles in Figure 5.4 is chosen according to $\bar{y}(x)$, while the background is colored according to $\widehat{\mu}(x)$. This is designed so that the difference between background and observation drawn on the graph fairly depicts the difference between model fit and data: if the Pearson residual is zero for a bin of trials, then $\bar{y}(x) = \widehat{\mu}(x)$; if all the trial parameters coincide with the bin center so that all $x_i = x$, $\bar{y}$ collapses to the sample mean $\bar{y}(x) = \frac{1}{n}\sum_i y_i$; and for a given set of random observations y_i, $\bar{y}(x) - \widehat{\mu}(x)$ is proportional to R.

Figure 5.4 does not include a measure of standard error or significance. Below in § 6.2.1 I will consider model predictions and data one variable at a time, at which point I can display standard errors of observed and predicted data and obtain goodness of fit statistics. However, the areas of the plotted circles in Figure 5.4 are scaled to the number of observations, so that the error in each average corresponds inversely to the size of each circle; it is expected that smaller circles will have larger differences between observation and model.

5.3.3 Phenomena captured in the model

The four plots in Figure 5.4 illustrate effects associated with carrier strength, envelope motion, and spacing. The lower left panel shows how the observer's response varies for stimuli with no carrier motion (i.e. with all elements flickering in counterphase.) The horizontal axis measures the degree of carrier motion used in the stimulus, while the vertical axis measures the inter-element spacing. When there is no carrier motion, observers tend to report clockwise apparent motion for envelope motions that are clockwise, and vice versa. This is reflected by the right half of the graph taking values greater than 0.5 (in red) and the left half of the graph taking values less than 0.5 (in blue.)

The effect captured in the lower left panel is how the sensitivity to envelope displacement (which corresponds to the inverse of the horizontal distance between contour lines) changes as a function of spacing. In the model the spacing-dependent sensitivity is described by the function

$M_\Delta(S)$ and is controlled by the sensitivity parameter β_0 and the "critical spacing" parameter S_C. The sensitivity to envelope motion decreases at smaller spacing, causing contour lines to spread apart at the bottom of the graph. The data that is observed, whose residuals are plotted in circles, shows analogous behavior. Note that at smaller spacings, data has been collected over a wider range of envelope speeds than at the larger spacings. This is a result of using a staircase procedure which steps over a wider range when the sensitivity is lower. Even at the smallest spacings most data has been collected with envelope step sizes significantly smaller than half the spacing, so that the ambiguity of forming correspondences between element appearances (i.e. the wagon wheel illusion) should not contribute to the lessening of sensitivity.

The upper right panel of Figure 5.4 characterizes responses to envelope and carrier motion at a wide spacing. Consider starting at the point (0,0), where the response probability is 0.5. Traveling up the graph, corresponds to adding carrier motion to the stimulus; response probabilities at first drop below 0.5, exhibiting repulsion. Increasing the carrier motion further, the repulsion reverses and the observer now reports motion in the direction of the carrier. At any point, moving horizontally corresponds to a change in the envelope motion; at the large spacing captured in this graph, sensitivity to envelope motion is high.

The lower right panel has the same axes as the upper right but shows narrow spacings. Moving vertically in this graph gives a large change in response, reflecting a higher sensitivity to carrier motion than in the upper right panel. By comparison, moving horizontally shows much less sensitivity to envelope motion than in the upper right panel. The repulsion effect M_I that was evident in the upper graph is swamped by the higher sensitivity to carrier motion M_S.

Finally, the upper left panel shows the combined effects of both the nonlinear repulsion and spacing-dependent summation effects. Here the envelope motion is fixed to zero. At relatively wide spacings, moderate carrier strengths induce repulsion, indicated by mostly blue colors on the right side of the panel. Carrier strengths less than 0.4 generally cause repulsion but as the carrier strength approaches 1 again, carrier motion once again becomes positive in strength. The repulsion

effect also disappears at narrower spacings. Both the repulsion at weak carrier strengths and its reversal at at high carrier strengths occurred for most observers in the dataset.

The repulsion effect M_I is modeled as a function only of the carrier strength; it is independent of both the number of elements on the display and the spacing between them. I explored changing or adding similarly formulated terms that were dependent on element number and on spacing, but these did not result in better fits as assessed by the AIC measure (Akaike, 1974) That is to say, the same strength of repulsion appears to exist for spare displays as for dense displays; when very dense, repulsion is usually overwhelmed by the summation (M_S) term.

While sensitivity to envelope motion decreases when spacing is reduced, the sensitivity to carrier motion typically increases. The combination of the two effects can be seen in comparing the upper right and lower right panels of Figure 5.4. When spacing is relatively wide, as in the upper right panel, the gradient of the decision function is steeper along the axis of envelope motion, and the model is relatively insensitive to carrier strength. In the lower left graph, showing data at narrow spacings, the situation has reversed. Broadly speaking it appears that motion is driven by envelope motion at wider spacings but by the carrier motion when spacing is narrow.

Similar patterns of behavior are found for most observers. The set of plots for all observers who participated in this experiment is included in Section 8.

It is worth noting the areas where the model is not fully successful at reproducing observers' data. Often the repulsion measured at a carrier strength of 0.2 is stronger than the model fit, and the repulsion at 0.4 is weaker (see Figure 5.7 below.) This suggests that the functional form I have chosen for $M_I(C)$ might need to be improved, however the current data do not have the power that would select a better principled parameterization.

Another area where the model does not fully capture the observers' behavior is that their responses at smaller spacing are more variable than the model would predict. This is visible to some extent in the raw data plotted in Figure 5.1; the data collected at wider spacings trace out a psychometric function, but the data collected at narrower spacings have more dispersion than one would

expect from the model fit. This is also visible in the bottom row of circles in the lower left panel of Figure 5.4, where the differences between model and observed data are more apparent.

5.4 Model components, effect sizes, and goodness of fit

This model captures the effect of three factors - carrier strength, envelope motion and spacing - that each affect apparent motion. The model is phrased in terms of three effects: summation of carrier motion, crowding of envelope motion, and repulsion driven by carrier motion strength. This model potentially allows for variation in the appearance of these stimuli between observers. I have shown that it fits qualitatively, in so far as its fit appears to capture some of the variation in observed responses. But to justify each choice made in modeling the data I should try to justify the inclusion of each effect, by showing that including each effect produces a model that better captures each observers' data.

There is inter-subject variability; identical stimuli produce different appearances of motion in different observers. The model I have proposes that this variability is due to different proportions the same underlying effects. To check this, I will evaluate each effect separately and discuss how they apply to each observer. One of my goals is to show that despite this variability, the same qualitative effects appear in each observer; that is, effects should be present in each observer, though they may vary in proportion.

In the following sections I attempt to check the model's performance in describing behavior with reference to the three proposed effects. This will help evaluate and provide some justification for each component of the model, and will also show whether each effect is consistent across observers. The goal is to justify the inclusion of each of the three effects, and by looking at each effect to show that it whether it is consistent across each observer.

5.4.1 Statistical considerations for binary psychophysical data

Tests of goodness of fit such as residual deviance and Pearson χ^2 operate by comparing the predictions of the proposed model to those of a saturated model, one with as many parameters as observations, that captures all the variance, as well as to a null model, which only includes an intercept. However the idea of a saturated model does not have a perfect equivalent in the case of binary responses; since an observer will respond both "yes" and "no" to the same stimulus, one cannot capture all the variance, and for cases where the observer always gives the same answer, this leads to undefined likelihood values. Standard goodness-of-fit checks are also problematic when the sampling is not evenly grouped over the predictors (Collett, 2003), or when the observations sparsely sample the space spanned by multiple predictors (Hosmer et al., 2013). Both of these situations apply to this dataset.

Rather than an overall goodness of fit test, I wish to evaluate each effect separately. Applying an overall goodness of fit test to a model with multiple effects involving multiple predictors would not give a useful evaluation of how well each component effect is capturing behavior. To examine each effect I would like diagnostic model checks that focus on each effect in turn, that is, partial goodness of fit checks for each effect. Since I sampled a discrete set of spacings and of carrier strength, this can be done by expanding the proposed model m_P into model $m_{S,E}$ that is saturated over one predictor E; while the proposed model fits carrier sensitivity as a function of spacing (say,) the saturated model would fit a separate value of sensitivity at each spacing. This makes a "effect saturated" model $m_{S,E}$; refitting the model without the proposed effect builds a null or intercept model $m_{0,E}$. Then the success of each effect term can be characterized by nested comparisons between null, proposed (m_P) and saturated models (Tsiatis, 1980; Archer et al., 2007), and by the log-likelihood-based pseudo-R^2 measure

$$R^2_{L,E} = \frac{L(m_P) - L(m_{0,E})}{L(m_P) - L\left(m_{S,E}\right)}.$$

The $R^2_{L,E}$ statistic can be interpreted as the proportion of available likelihood that is captured by the proposed model, relative to a null model. Building effect-saturated models will allow for visual comparison of the saturated model to the proposed models.

5.4.2 Lack of pooling of envelope motion across large distances

I motivated the description of the model proposed in Section 4 by considering that the observer attends a single element of the display; other elements are not attended, may but exert an influence via crowding or summation. However, in our task the stimulus is composed of identical, identically moving elements. Therefore in principle, it is not necessary that an observer isolate any particular element to measure envelope motion; any element or combination of elements will do the job. When distinct objects move concurrently, one can perceive the motion as being of a larger element of which the distinct components are features, such as in Ternus displays (Boi et al., 2009) or as being components of a larger rigid body (Anstis and Kim, 2011). In the present stimuli, both envelope and carrier motion are, considered separately, consistent with that of a wheel rotating around the fixation point. Knowing this, an observer might pool multiple envelope position signals in order to improve sensitivity to envelope motion. If that is the case, then the sensitivity to envelope motion (i.e. the slope of the psychometric function relating envelope motion to response probability) should increase when additional, coherently-moving elements are added to the display, as long as targets remain widely separated enough to avoid crowding.

For 9 of the observers who participated in this experiment, I collected data with both 2 and 4 elements on the display (at an eccentricity of 6.67°, corresponding to spacings of 20.9° and 10.5° around the circle.) These spacings should be large enough to escape crowding effects. To assess the presence or absence of pooling at large distances I compared observers' sensitivities to envelope displacement at 2 and 4 elements using a logistic regression model formulated as

$$\Pr(\text{clockwise} \mid \Delta x, C, n) = \text{logit}^{-1}\left(\beta_n \Delta_X + k_{|C|,n} C + b_{|C|,n}\right)$$

where the slope of the psychometric function corresponds to β_n and separate proportionality constants k and b were used for each absolute value of direction content and element number. Using a treatment contrast for β_n, I asked how sensitivities changed as a function of element number. For 6 of the observers, the sensitivity coefficient decreased at 4 elements as compared to 2; for the remaining 3 it increased. However, any change only reached a significance level of $p < 0.05$ for only one observer (whose sensitivity decreased as element number changed from 2 to 4.) The subset of data considered here comprises 5561 trials. I conclude that there is not pooling of envelope motion data between separate objects in this experiment, which agrees with the choice of a form of $\beta_\Delta(S)$ which reaches an asymptote at large spacings.

5.4.3 At narrow element spacings, sensitivity to envelope motion declines.

A central feature of the proposed model as illustrated in Figure 4.1 is that it expects the sensitivity to envelope motion to decline as spacing between elements declines, i.e. there is a crowding effect on the detection of envelope motion. As described above, to assess whether the model captures an the effect of spacing on sensitivity in the presence of other effects, I compare this model to a null model without this effect and a saturated model formed by expanding the parameterization of $\beta_\Delta(S)$ into a set of dummy variables coded to capture a different value $\beta_{\Delta,S}$ for each distinct value of spacing tested. The null model uses a constant value of sensitivity at all spacings. All other aspects of the model are left as described in Section 4.

The proposed and saturated models are plotted in Figure 5.5 for three observers (the entire set is shown in Figure 8.23.) The measurement obtained in the saturated model is noisy, but the sensitivities do approach zero as spacing approaches zero. Also confirming the analysis in § 5.4.2, as spacings become large, sensitivity appears to reach an asymptote. So both general features chosen for the functional form of $\beta_\Delta(S)$, an asymptote at large spacings, and a collapse to zero at small spacings, are consistent with the data. Comparing the proposed to the null model, all observers show highly significant improvements, with the largest p-value being 10^{-5}. Further

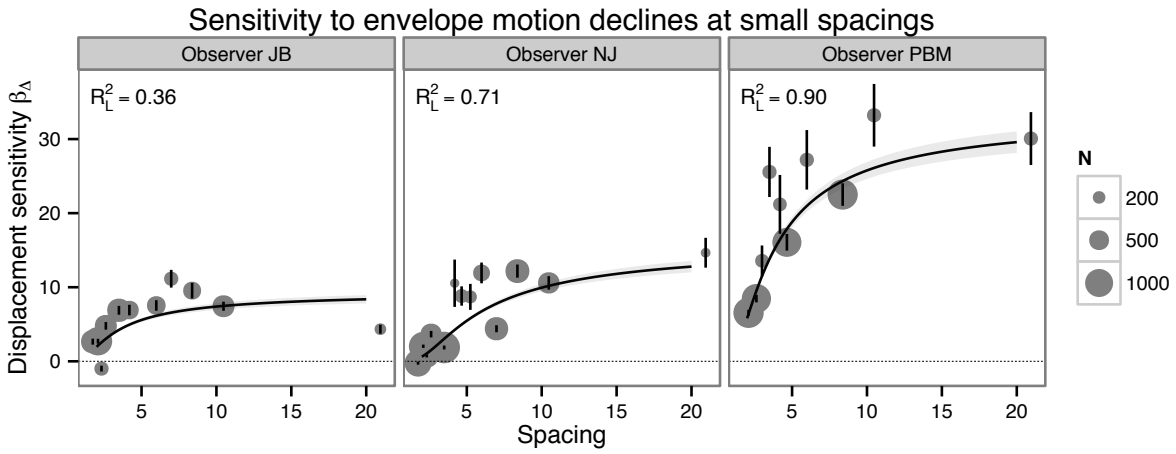

Figure 5.5: Sensitivity to displacement collapses at narrow spacing. In each subplot, the horizontal axis denotes spacing, while the vertical axis measures sensitivity to direction content (corresponding to the slopes of the psychometric functions shown in Figure 5.1.) Data points are obtained by re-fitting the model while allowing sensitivity to vary freely for each value of spacing, while other aspects of the model are unmodified. Vertical segments at each point indicate $\pm$ standard error and the size of each point indicates the number of underlying trials. The vertical axis is the sensitivity to envelope motion (corresponding to the the change in log-likelihood of answering "clockwise" to a stimulus when changing Δx by 1°.) Curves show the prediction of our model fitted to the same data $\beta_{\Delta x}(S)$, as a function of spacing S. Three observers are shown here; the complete set is shown in Figure 8.23.

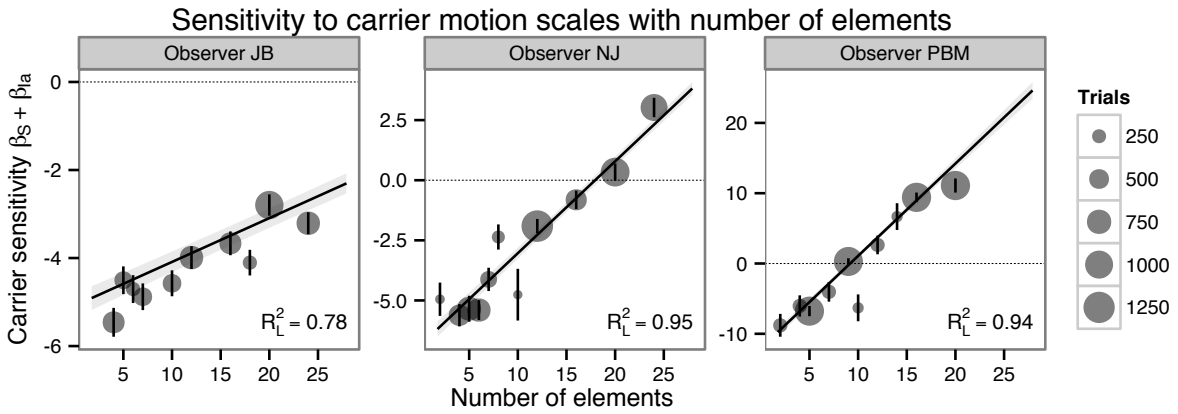

Figure 5.6: The sensitivity to carrier motion scales with the number of elements. The vertical axis measures the sensitivity to carrier motion $M_s(S)$ as a function of the number of elements used in the stimulus. Individually plotted points are obtained by letting this coefficient vary freely for each value of spacing; lines indicate model fits. Vertical segments at each point indicate $\pm$ standard error and the size of each point indicates the number of underlying trials. Because the sensitivity and amount of repulsion vary between observers, each panel has a different scale on the vertical axis; the dotted horizontal line indicates a sensitivity of 0, which marks the boundary between assimilation and repulsion. Data from three observers is shown here; the complete set is shown in Figure 8.24.

comparing the proposed to the saturated model, 3 out of 11 observers show a significant difference between proposed and saturated model.

Labels in each facet of the plot show the pseudo-R^2_L measure described above. Aggregating across all observers, I obtain a value of $R^2_L = 0.58$. Note that for observer PBM (the author) the sensitivities are much larger than for other observers, while still showing the same form of collapse at narrow spacings. The higher sensitivity might be attributed to overtraining relative to the naïve observers.

5.4.4 When more elements are added, carrier motion summates.

While the sensitivity to envelope motion decreases as flanking elements are brought closer, the sensitivity to carrier motion increases as more elements are added. I assessed this effect using the same technique as before, forming a saturated model by dropping the term $M_s(S)$ and including variables $\beta_S C$ for each distinct value of spacing. The saturated model drops the linear repulsion term $\beta_{I_a} C$ (as it is proportional to carrier strength and thus linearly dependent with the indicator terms.) The other components of the model remain, including the nonlinear component of repulsion $\beta_{I_b} C|C|$. The intercept model retains the term $\beta_{I_a} C$ (i.e. it has a constant sensitivity to carrier motion that does not vary with the number of elements.) For data at a few spacings tested at a carrier strength of 1, there are some all-clockwise or all-counterclockwise responses, which leads to undefined likelihoods for those data in the saturated model; those data are disregarded for purposes of model comparison (Collett, 2003).

The comparison of proposed and saturated models is shown in Figure 5.6. The units β_S are interpretable as the change in log-odds of responding "clockwise" in proportion to a small change in the carrier strength. Likelihood ratio tests show significant improvements from null to proposed models for all observers, with the largest p-value being $p < 10^{-4}$ for observer NS. 10 of 11 observers also showed significant differences between proposed and saturated models. In aggregate, the proposed model is successful, obtaining $R_L^2 = 0.7874$ with reference to null and saturated models. For several observers the proposed linear relation between number of elements and carrier sensitivity captures the response very well, obtaining $R_L^2 > 0.9$ for 3 observers. However, some observers are not as well fit (Figure 8.24.) Note that for some observers such as JB and MC the measurement of carrier sensitivity does not find assimilation even at the smallest spacings; small increments of carrier motion are repulsive for these observers even when the display is dense with elements. However the sensitivity measure here does not include the nonlinear repulsion term $\beta_{I_b} C|C|$ which can make increments of carrier motion assimilative for larger values of carrier motion.

5.4.5 Weak carrier motion repels direction judgments.

Note that the carrier sensitivity measured in the previous section, in addition to the inverse proportionality to spacing, has a constant generally negative offset. I have referred to this offset as "repulsion," since negative values of carrier sensitivity means that increments in carrier strength bias the observer's judgements in the opposite direction. Thus, in Figure 5.6 carrier sensitivity does not approach zero for sparse displays, but some usually negative value. Carrier motion generally become assimilative when there are more, closely packed elements in the display. The first is that the strength of repulsion seems to be determined by the carrier strength of an individual element, rather a sum over nearby elements. That is, after accounting for summation, which as we saw in § 5.4.4 can be well fit by a term proportional to the number of elements, there is a remainder that appears to be independent of the number of elements or their spacings. This repulsion effect is independent of element spacing, while the spacing-dependent component of carrier strength is directly proportional to the number of elements; this might indicate some element of carrier motion processing that is independent of the number of elements or their spacing.

5.4.6 Repulsion is nonlinear in carrier strength.

At carrier strengths approaching 1, the repulsion effect can weaken and even reverse. This effect is visible in the upper left panel of Figure 5.4, where moderate values of carrier strength at wider spacings are repulsive (blue shades) but become assimilative (red shades) as carrier strength is further increased. That corresponds to a situation in which, starting with a display with no envelope or carrier motion, a little clockwise carrier is added and the display appears to go counterclockwise, but adding more changes the appearance to clockwise. The summation effect contributes to this, but is not strong enough for sparse displays to account for the reversal of apparent motion. There are two notable characteristics of this repulsion. The first is that the degree of repulsion appears to be a nonlinear function of direction content. This repulsion is captured in the model in the function $M_I(C)$. This can be understood as a component of the observer's response that is a function of the

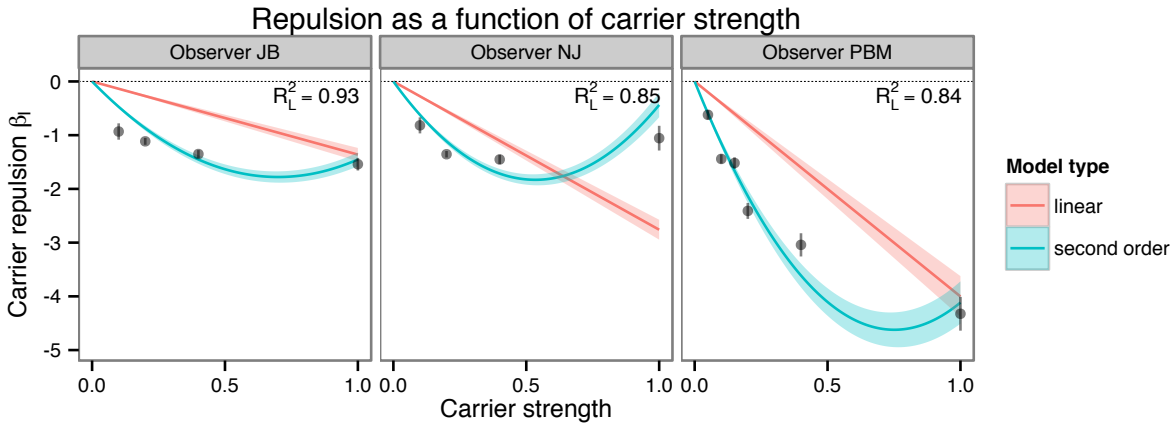

Figure 5.7: Effects of motion repulsion at wide spacing. The vertical axis shows the response rate to stimuli with zero envelope motion at a nominal spacing of 10° with the horizontal axis showing the carrier motion. Data points are obtained from a model whose repulsion term is saturated over carrier motion (see § 6.2.1.) Curves illustrate predictions from two alternative models, one where repulsion is a linear function of carrier strength, and another where there is a second-order nonlinearity. The second order model obtains a better fit (see § 5.4.6.) R^2_L values are computed with reference to a null model which has no repulsion. Under this model, all but one observer (the complete set is plotted in Figure 8.25) shows a negative slope of the curve where direction content crosses zero, indicating a repulsive effect for weak carrier strength, while the second order coefficient weakens or reverses this effect for stronger carriers.

carrier strength but is independent of the element spacing or number.

Similarly to previous sections, I analyze the presence of this nonlinearity by comparing nested models. The null model has no effect of carrier motion, i.e. $M_I = 0$, but is otherwise identical to the full model described above in Section 4. The second model is one in which the repulsion is linearly related to the carrier strength of the stimulus; $M_I = \beta_I C$. For the linear model, 9 out of 11 observers showed a significant ($p < 0.05$) improvement over the null model. However, the linear model does not capture the observation that while weak carrier strengths repel motion direction judgements, stronger carrier strengths do not. The proposed model adds a a second-order, odd-symmetric component to repulsion signal; $M_I = \beta_{I_a} C + \beta_{I_b} C|C|$. As compared to the linear model,

I found that for all 11 observers, the fit was significantly improved by adding the second-order component, the largest p-value being $p = 2.4 \times 10^{-7}$ for observer CJ.

Additionally, while the signs of β_I in the linear model are mixed, the second-order model is more consistent between observers. Every observer with the exception of CJ has a negative value of β_{I_a} and a positive value of β_{I_b}, indicating that small imbalances of motion energy at wide target spacings usually lead to repulsion, but that the repulsion is proportionately weaker, or even reverses, with stronger direction content.

Figure 5.7 plots the the strength of repulsion as a function of carrier strength. The figure shows fitted curves for the linear and second-order models, and data points corresponding to a saturated model. As mentioned above, for all observers except CJ, the slope of the linear component of the second order model is negative, indicating a repulsive effect of carrier motion; for the same observers the coefficient of the second-order component is positive, indicating that the repulsion proportionately weakens, or in some cases reverses, when direction content approaches $|C| = 1.0$. The computed values do not include the spacing-dependent summation effect, which is also proportional to carrier strength; when both effects are added together the model obtains the behavior of repulsion at moderate carrier strength but summation at high carrier strength that are observed in the data. Aggregated over all observers, the second order model obtains a score of $R^2_L = .66$ with reference to a saturated model.

6 Experiment 2: Changes in density versus number of elements

In Experiment 1 I reported that judgements of motion direction were more sensitive to envelope motion when spacing is large. In that experiment, because spacing was determined by changing the number of elements, the same results could equally well be described as sensitivity being higher when there are fewer elements. Similarly, in the case of carrier motion, I modeled the sensitivity to carrier motion as being proportional to the number of identical elements, but it could also be described as inversely proportional to the spacing between elements. Mathematically this would be expressed by substituting N for $\frac{2\pi r}{S}$ in the model formulation or vice versa. This leaves the question of which variable provides a better characterization of motion perception in this task.

Experiment 2 attempts to resolve the confounding of spacing and element number, to determine which provides a better characterization of motion perception in this task. The answer does not have to be the same for both types of motion; sensitivity to envelope motion may be determined by number while sensitive to number whereas sensitivity to carrier motion is determined by spacing, or vice versa. Another way to frame the question is to ask whether the changes in sensitivity to envelope and carrier motion are due to influences from nearby flankers, or due to effects at a larger scale. For both carrier and envelope motion, a dependency on element spacing (as opposed to number) would imply a LOCAL process, sensitive to the immediate context of each element but insensitive to elements farther away. Conversely a dependence on element number would indicate a GLOBAL process, which combines information across multiple elements even at large separations. To distinguish these alternatives, in Experiment 2 I used stimuli which decoupled the number of elements from the element spacing by creating a display where the elements cover only a portion of the scene. I did this by varying the *extent* of the stimulus, defined as the circumferential distance covered by the array of moving elements, as shown in Figure 6.1. That is, the elements form a partial instead of a full circle.

If the array of elements covers only a portion of the scene, spacing and number can be varied independently. This involves varying the *extent* of the stimulus, defined as the circumferential

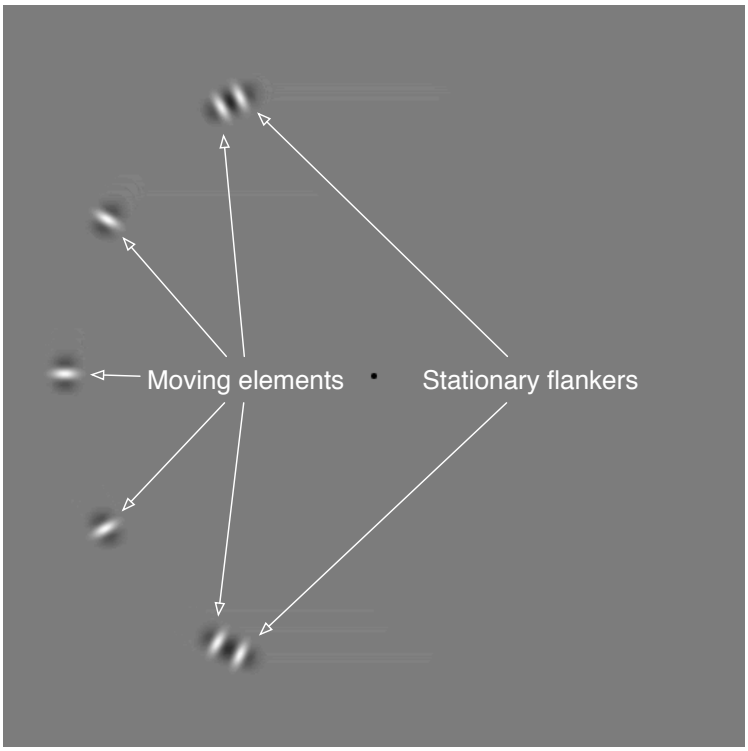

Figure 6.1: Example frame from a partial-circle stimulus. A number of moving elements are present on one side of the display. Two additional flanking elements are added, which always have carrier strength of 0 (i.e. they flicker in counterphase.) The flanking elements were positioned so as to be $0.5 to 1^\circ$ away from the nearest moving elements at their closest approach.

distance covered by the array of moving elements. Any two of these variables (spacing, number, and extent) determine the third, so I will somewhat arbitrarily focus on spacing and element number as the relevant variables.

6.1 Methods

The task was identical to that in Experiment 1. The motion elements were fixed at 6.67° eccentricity. The stimulus consisted of evenly spaced moving elements, identical to those in Experiment 1, but instead of being distributed around the entire circle, the elements were distributed along a partial-circle on either the left or right wide of the display. Stimuli were positioned either left or right of the fixation point. In pilot experiments observers found it difficult to judge the direction of

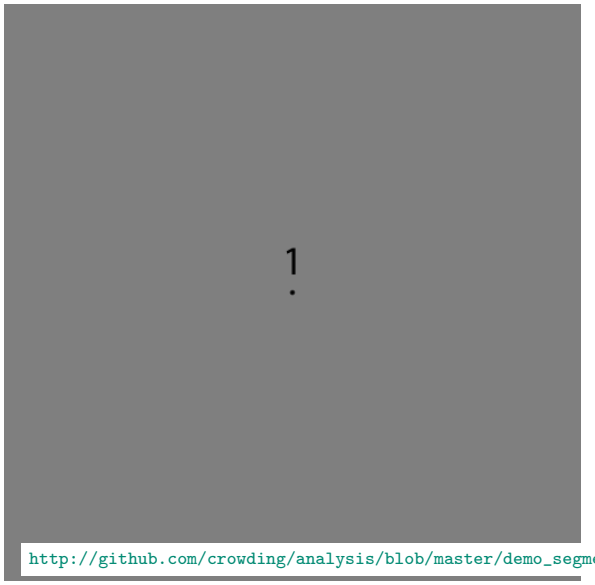

Figure 6.2: (`demo_segment.mov`) Example stimuli for Experiment 2. In this movie, the elements are shown in the left hemifield; in the experiment, stimuli alternated across hemifields, blockwise. Two stationary flankers with no carrier motion (showing counterphase flicker) are present at either end of the array of elements. Stimulus pairs 1-2 and 3-4 show stimuli with identical spacing, with different numbers of targets; pair 2-3 holds target number constant while reducing spacing. The numbers index the stimulus set given in Figure 6.3.

motion if the stimulus appeared in a random location on each trial, so stimuli alternated between hemifields in blocks. Each session used an equal number of stimuli positioned in the left and right hemifields, with the position alternating in blocks of 100 to 200 trials.

I varied both the spacing and the number of elements used; accordingly, the total spatial extent of the stimulus varied from trial to trial. The stimuli used are plotted in Figure 6.3. This stimulus set was constructed so that each value of spacing was tested using more than one value for the element number, and vice versa. I chose a set of stimuli that was symmetrically arranged in element number and spacing, spanning a similar range for both variables (covering a factor of 2.67 in element number and a factor of 2.78 in element spacing.)

In addition to the moving elements, the display included two stationary flanking elements, indicated in Figure 6.1. These served to hide the displacement of outermost moving elements, which would otherwise be easy to discern, as elements on the edge of an array suffer less crowding

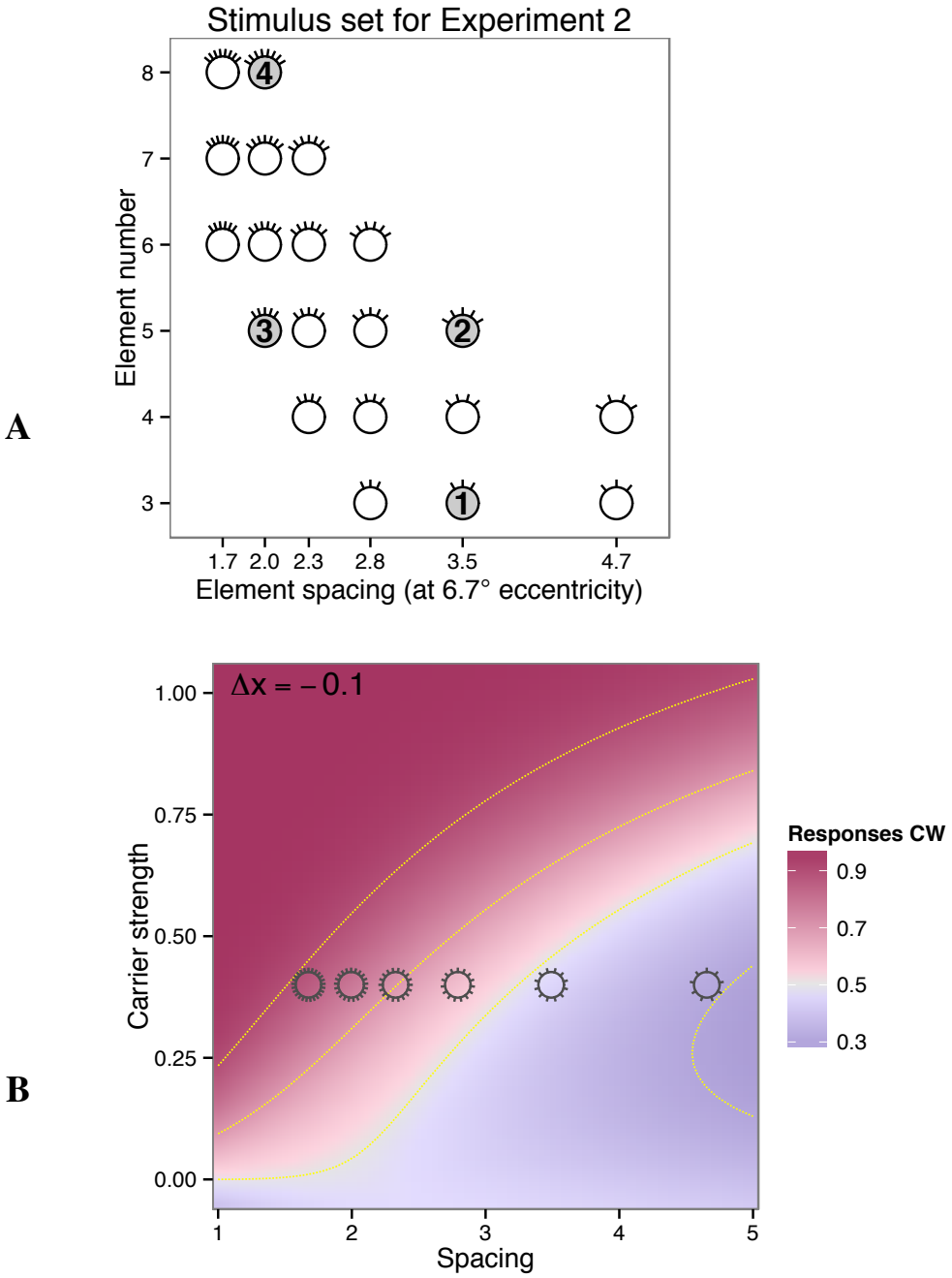

Figure 6.3: The combinations of element spacing and element number used in Experiment 2. **A.** Tick marks on symbols mimic variations in spacing and number of the motion elements (which are also shown on the two axes.) Numbered markers denote stimuli demonstrated in . **B.** The set of spacings and element counts was fixed for all experiments, but the carrier strength and displacement were selected by the experimenter for each observer. These parameters were chosen so that responses might span a useful range of response rates. Here example settings chosen for observer NJ are shown. Background color indicates model fit using data from Experiment 1, while symbols illustrate values of spacing that would be used in Experiment 2.

than elements within the array (Felisbert et al., 2005). The flankers had no envelope movement and zero carrier strength (i.e., they flickered in counterphase.) The space between the moving elements and the flankers changes over the course of the trial as the elements move; the flankers were positioned so that they were between 0.5° and 1° away from the adjacent moving element at its closest approach, which prevented conspicuous gaps opening or closing between the flankers and the moving elements during the brief motion stimulus. The flankers spanned a partial circle that was at least 56° and no more than 165° measured around the fixation point. The movie shown in demonstrates these stimuli for the four configurations indicated with numbers in Figure 6.3.

While element spacing and number varied across trials, carrier and envelope motion were held constant during each session. I selected values for direction content and envelope motion for each subject based on preliminary findings of Experiment 1; with the intent to find values such that that changes in spacing or number would produce a distinct change in response rate. Figure 6.5 illustrates the choice of stimulus parameters for one observer, with reference to the model fit from Experiment 1 shown as a heatmap as in Figure 5.4. Some observers were tested using more than one value of envelope displacement or carrier strength, but results were qualitatively similar in these cases, so they are aggregated in the graphs shown in this thesis; the original values were preserved in modeling. Table 1 shows the selections of carrier strength and envelope displacement used for each observer.

6.2 Results

Of the observers who had previously participated in Experiment 1, 8 participated in Experiment 2. Example data for three observers is shown in Figure 6.4. Each plot shows the rate at which subjects responded "clockwise" to a stimulus at a particular value of spacing and of element number, with the spacing values indicated on the horizontal axis and element numbers indicated by color and symbol. The response patterns of these two observers appear different. NJ's direction judgements change little with changes in element spacing, while being greatly affected by changes in

	Observer	Envelope displacement	Carrier strength
1	JB	-0.1 - 0.000	0.4
2	JE	0.0	0.4
3	MC	0.4	0.4
4	ML	-0.1	0.4
5	NJ	-0.2 - -0.044	0.4
6	NS	-0.2 - 0.000	0.2
7	PBM	-0.5	1.0
8	TL	-0.4	0.2 - 0.4

Table 1: Stimulus configurations used in Experiment 2. The envelope displacement and carrier strengths were chosen by the experimenter; spacing and element number were prescribed by the stimulus set in Figure 6.3A. For some observers, multiple values of stimulus parameters were tried, noted as ranges here.

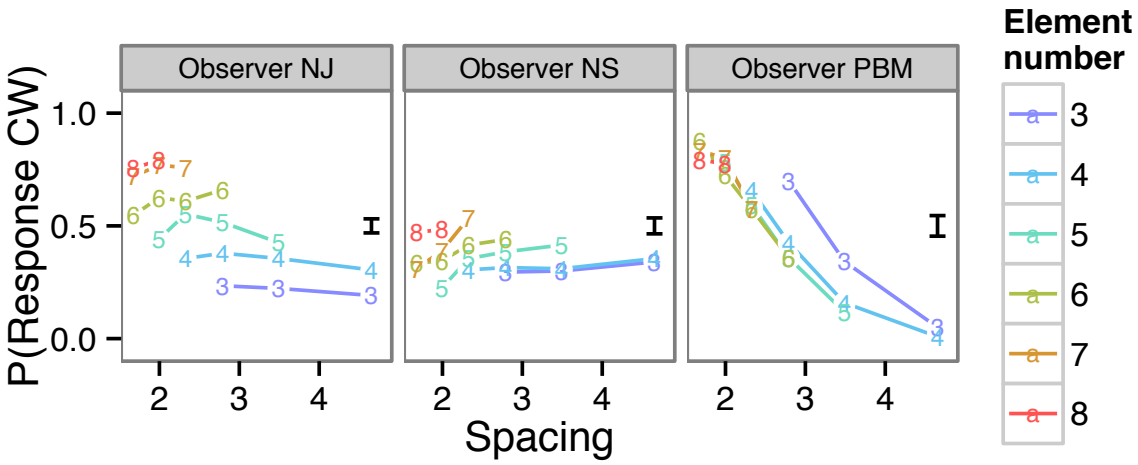

Figure 6.4: Example data from Experiment 2. Here data for three observers is shown. The vertical axis shows proportion of responses clockwise, while the horizontal axis measures the spacing between elements. Lines connect stimuli with the same number of elements, indexed by color and symbol. Lines show how the proportion of responses clockwise varies as a function of element spacing, with other parameters (envelope displacement, carrier strength and element number) held constant. The error bar at right spans twice the maximum standard error over all data points.

element number. In contrast, PBM's responses are sensitive to changes in spacing, while being little affected by changes in element number. NS shows a slight increase in proportion of responses clockwise with increasing spacing, while PBM shows a steep decrease. However, despite these differences, there are commonalities in these data sets. For none of the observers does there appear to be much interaction between spacing and element number; the lines traced out by changing spacing at a smaller number of elements are roughly parallel to the lines traced out by changing spacing at a larger number of elements.

6.2.1 No interaction between element number and spacing

I checked whether there was an interaction between spacing and element number using a logistic regression. Considering only the data from Experiment 2, the data may be empirically fit by a logistic regression; for fixed values of carrier and envelope motion, a simple regression model is

$$\Pr(\text{clockwise}) = \text{logit}^{-1}\left(\beta_N CN + \beta_S CS + \beta_E CNS + \beta_0 C + I\right),$$

where, β_N controls the change in motion sensitivity as a function of element number, β_S the sensitivity as a function of spacing, β_E the interaction term due to the stimulus extent. an interaction term. β_0 and I are intercept and bias terms. Note that each term includes a factor of C, whose sign randomly alternates from trial to trial; the regression is modeling the response to carrier motion strength in terms of the number of elements and the spacing. (The spatial displacement is disregarded for this regression, because it always has the same sign relation to carrier motion in this experiment.)

The quality of fit for β_N and β_S are good, achieving R_L^2 scores of .87 and .87, respectively, aggregated over all observers (as described in , these measures compare the given model against a null model with constant effect and a full model saturated over each value of the given variable.) In the absence of an interaction term, β_S was found significantly different from zero at the $p < 0.05$ level for 6/8 observers, and β_N significantly differed from zero for 6/8 observers. Thus the response

rates depend on both spacing and number. The support for an interaction term β_E is weaker. When models included the interaction term, the resulting coefficients varied in sign, and aggregated over all observers only obtained a R^2_L score of .25. Thus it appears to be a satisfactory qualitative description of the data to say that motion direction judgements covary with spacing and element number, without much interaction. In the next section I will evaluate whether a single model fit may account for data from both this experiment and Experiment 1.

The lack of interaction can be predicted from the model sketched in Section 4. This model predicts that there will be a progressive change in sensitivity to envelope motion as a function of spacing (or number) and there will be a change in sensitivity to carrier motion based on changes in the number or elements (or their spacing). Thus, as either spacing or number changes, the proportion of responses clockwise will progressively change, with the amount of change dependent on the observer's particular sensitivity to envelope and carrier motion and the particular stimulus parameters. Thus, the model of Section 4 would not predict much interaction between spacing and element number. Note that a lack of interaction also implies that there is not a limited spatial range of summation coming into play; that is, if element number determines carrier sensitivity, an element far away from the locus of attention adds as much as an element nearby. If carrier motion were integrated over a spatial scale within the range tested by this experiment, we would see summation trail off for stimuli with larger spatial extents, which would have produced an interaction in this data.

6.2.2 Extending model predictions from Experiment 1

I extended the model from Section 4 to the data from Experiment 2 and fit it to data from both experiments. There are four general scenarios under which the model may be extended to these stimuli, based on whether the sensitivity to envelope motion was determined by spacing (envelope local) or element number (envelope § 6.2.2global,) and by whether the sensitivity to carrier motion was determined by spacing (carrier local) or by element number (carrier global.) These four

models make identical predictions for the data from Experiment 1, but differ in their predictions for Experiment 2.

The "global" models calculated the sensitivities to motion as a function of the number of elements falling within a hemifield. That is, the trials from Experiment 1 are considered to have an N equal to half the number of elements that were actually displayed, while trials from Experiment 2 use the full count. This appeared to fit better than using the complete element count for both trial types, and is consistent with the observation that the effect of crowding does not cross the vertical meridian (Liu et al., 2009).

For some observers, the responses appeared to differ between left and right hemifields; this is consistent with the observation that the critical spacing of crowding is not uniform across the visual field (Petrov and Meleshkevich, 2011). Another confound may be the influence of the stationary flankers located on either end of the array of objects. The intention behind including these flankers was to avoid giving away the envelope motion by the motion of the outermost elements, since effective crowding requires flankers on either side of a target (Toet and Levi, 1992; Pelli et al., 2004), and is weaker for targets closer to the ends of an array (Felisbert et al., 2005). While the flankers prevented the envelope motion from becoming uncrowded, they may have induced other side effects, since being positioned at the ends of the array makes them more salient than the moving elements and their lack of carrier or envelope motion is likely to have weakened both types of motion signal.

I added two parameters to account for possible effect of endpoints and for differences in carrier motion sensitivity between hemifields, making the substitution

$$\beta_S \rightarrow (1 + \delta_e e + \delta_h h)\,\beta_S,$$

where e indicates whether endpoint flankers are present, and h takes on values of -1, 0, or 1 based on which hemifield the stimulus is shown in. Note that this adjustment was the same for all four models considered here. The ranking of local and global scenarios was similar with or without this

adjustment.

Example results are shown in Figure 6.5. These show the model predictions corresponding to four scenarios (labeled on the right side.) For comparison the observed data is shown in the top row. Visually, these predictions confirm that both the entirely-local (row C) and entirely-global scenarios (row D) cannot capture the behavior of every observer. When both carrier and envelope processing depends on global element number, there is no change in response rate with spacing (row D), and when both carrier and envelope motion sensitivity depend on local spacing, the change in response rate with element number is not captured (row C).

The two remaining alternatives are carrier global, envelope local (row B) and carrier global, envelope local (row E). Between these alternatives, carrier global, envelope local appears to fit the data better. Aggregated across observers, it fits with the highest likelihood out of the four models, with a log-likelihood ratio of 407 over the next best fit. However, the comparison in likelihoods does not hold for every observer. Given local envelope motion, global carrier motion gave a better fit, in terms of likelihood, for 7 out of 8 observers. Results for envelope motion were more equivocal; given global carrier motion, local envelope motion fit better for 4 out of 8 observers. However as mentioned earlier, unknown effects of the flankers may be present which would tend to make strict likelihood comparisons unreliable. Visually comparing the complete set of model predictions (Figure 8.26) I find that carrier global, envelope local (column E) does the best job at capturing the directions of effect; models with global envelope motion often have the wrong direction of effect for changes in element number (see observers JE, MC, ML.) It is possible that a mixture of local and global effects determines envelope motion visibility.

The model fits to the data from this experiment for all the observers tested are shown in Figure 6.3. In summary, as discussed in more detail below, results from Experiment 2 suggest that the summation of carrier motion is determined over a large spatial scale, large enough to encompass several targets, while the decline in sensitivity to envelope motion might be determined within a smaller spatial scale (though this point needs additional confirmation.)

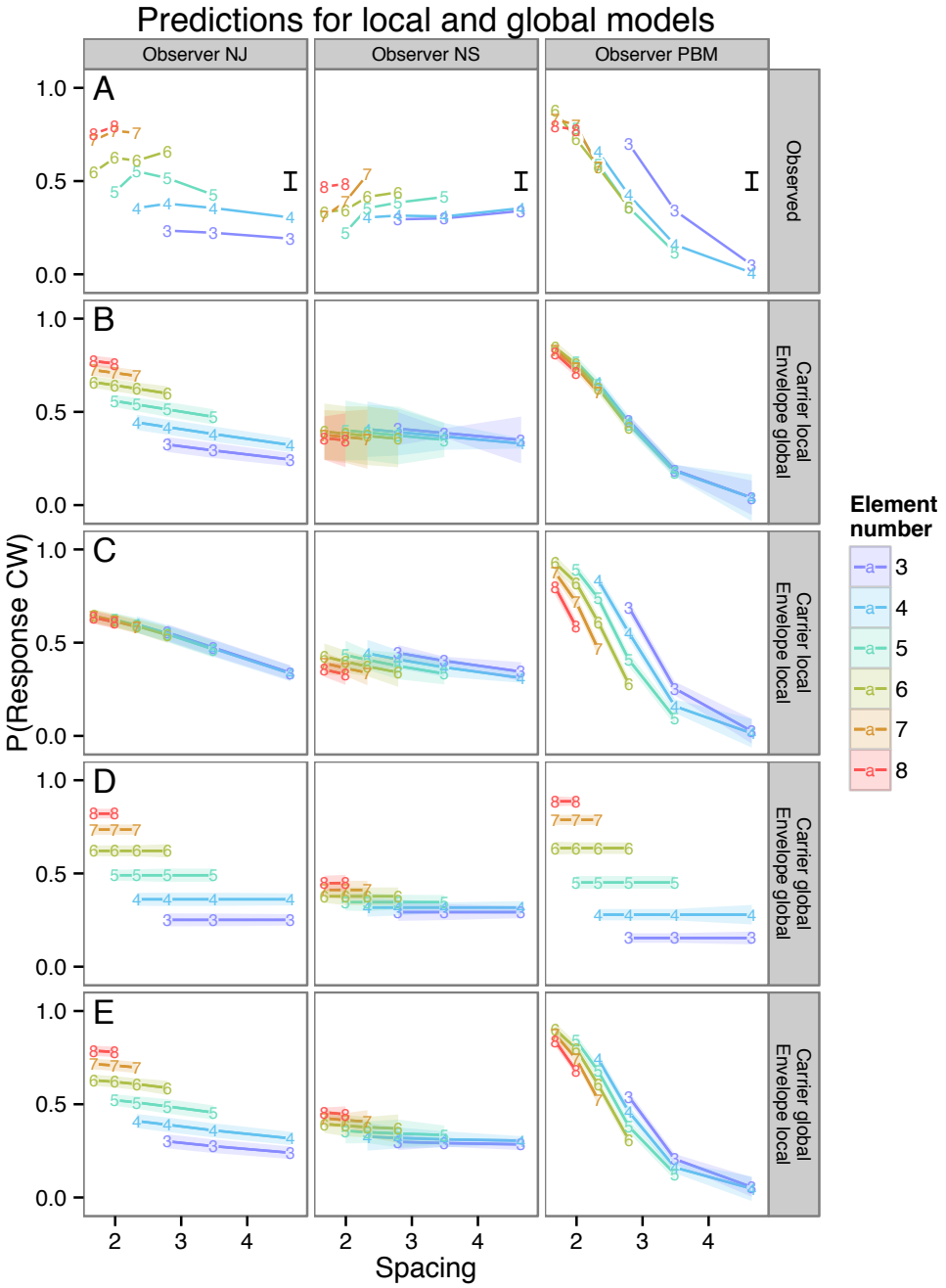

Figure 6.5: Alternate predictions for Experiment 2. Data for three observers are shown, one in each column. The top row shows observed data. Each of the subsequent rows shows the model prediction under a particular interpretation of envelope and carrier motion processing: either local or global, so four combinations in all. Width of shaded region in predictions shows ± standard error of fit; error bar in top row shows ± standard error of observed response rates.

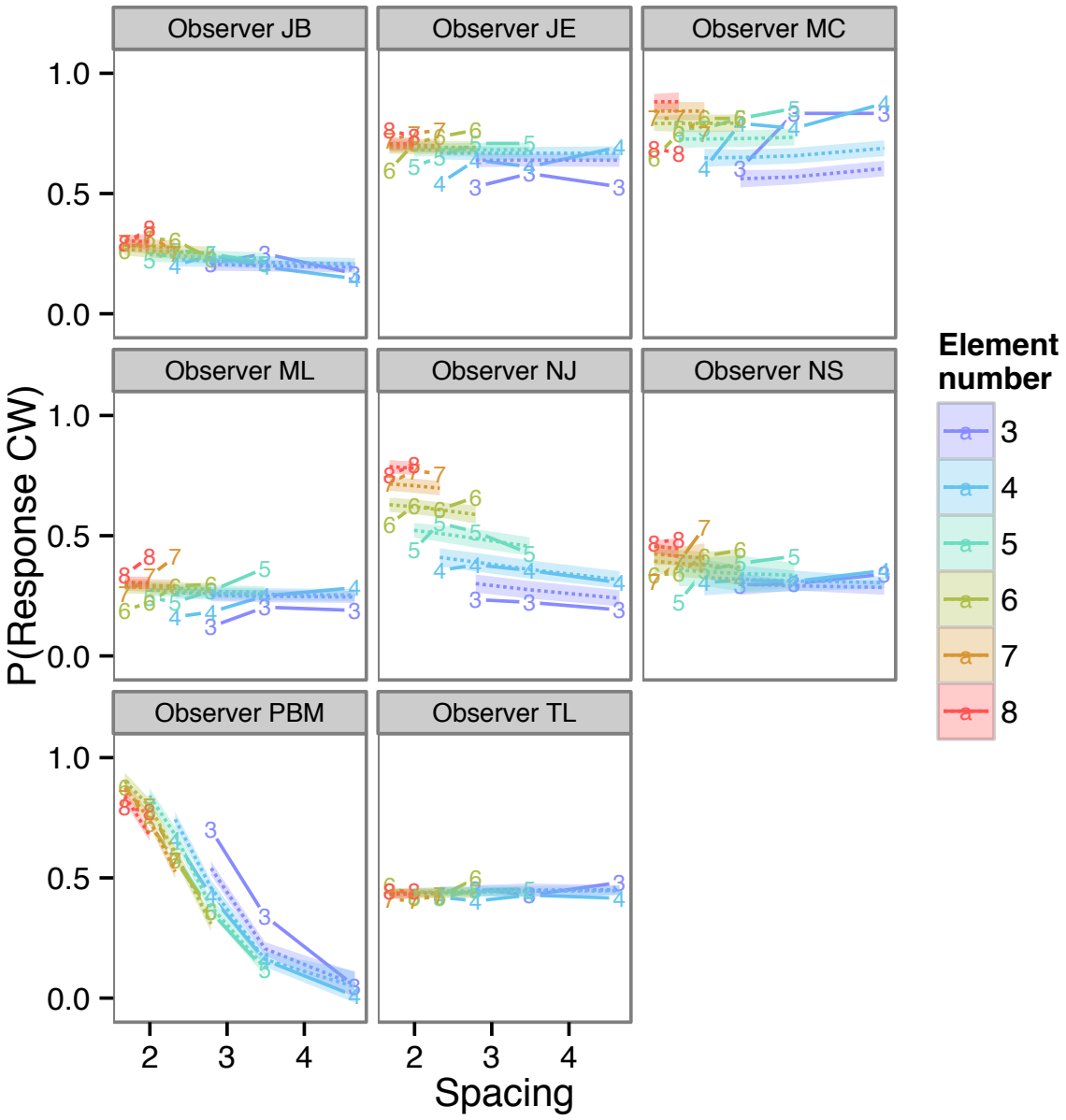

Figure 6.6: Model fits using the carrier-global, envelope-local model, plotted under data from Experiment 2. Connected lines with symbols show observed data, while shaded lines are model predictions.

7 Discussion

Physical motion can be defined simply as the change in position of an object over time. Visual motion is more challenging to define. Different classes of motion stimuli can be defined, such as first-order or position-defined motion. However, the mechanisms underlying position-defined motion, and how it combines with first-order motion are not well understood. Here I describe a series of experiments and a model of how first-order and position-defined motion might contribute to the appearance of visual motion. Giving conflicting component motions to multiple moving elements produced the novel effect that the appearance of motion favors its first-order or position-defined components as a function of the spacing between elements. This is a result of two complementary effects. First-order motion exhibits summation over large areas: the more elements contribute first-order motion, the stronger the influence of first-order motion. In contrast, position-defined motion exhibits spatial interference: the more closely spaced the motion elements the weaker the positional information. The two signals are combined with a subtractive interaction, which, as described below, may help to dissociate moving objects from the background.

7.1 First order motion exhibits summation over large areas

My finding that first-order motion integrates over large areas is consistent with the previous literature. When observers are asked to detect weak broadband motion signals in noise, they can integrate localized motion signals over relatively large regions (Williams and Sekuler, 1984; Downing and Movshon, 1989; Fredericksen et al., 1994); this has been modeled in terms of summation of first-order motion mechanisms. In the case of optic flow stimuli, which may include the rotational carrier motion stimuli used in my experiments, summation can take place over much of the visual field (Morrone et al., 1995; Burr et al., 1998).

However these previous results took measurements of detection or direction discrimination at threshold and not of suprathreshold appearance. In the present experiments it appears that the large-scale summation of first-order motion extends to appearance as well as detection. Under a

wide range of conditions motion judgements are influenced by first-order motion in proportion to the density of elements multiplied by the strength of the motion signal.

With the aim of discovering the extent of this spatial summation I controlled the circumferential extent of stimuli in Experiment 2. A limited extent of spatial summation ought to have resulted in saturation with stimuli of larger extents which would have resulted in either a significant interaction between number and spacing or a better fit of carrier motion responses to element spacing rather than number. However, linear summation and dependence on first order motion to number still gave a good account of observers' behavior in this experiment. While the coefficient of linearity for stimuli in a single hemifield differed from that needed to account for stimuli spanning both hemifields (as in Experiment 1), unrestricted linear summation within each hemifield still provided the best account of sensitivity to carrier motion for stimuli subtending up to 160 degrees of arc.

Note that the extent of this spatial summation is larger than that of the effective receptive field size for motion detecting units in V1 or even MT (Mikami et al., 1986; Livingstone et al., 2001), and appears to be larger than the objects that we have experience in tracking in peripheral vision. One might then wonder why large-scale summation would be part of a mechanism that parses the motion of objects from a possibly cluttered environment containing multiple moving objects. It seems significant that in the present study, all carrier motions had the same rotational direction (a rotation around a central point) within each trial. This might selectively activate global flow mechanisms which integrate over the whole scene (Snowden and Milne, 1997; Price et al., 2004). If this is the case masking optic flow integration by adding iso-eccentric noise (Maruya et al., 2013) might result in reduced summation. This explanation would imply that optic flow mechanisms process first-order motion only, or independently of other types of motion, for which there is some evidence (Aaen-Stockdale et al., 2007). An optic flow contribution could also be tested by varying the direction of first-order motion in my stimuli so as to be incompatible with optic flow mechanisms.

Another possibility is that first-order motion in my stimuli were integrated across space in a

kind of contour integration. Detection of a motion element is facilitated when it aligns in direction and position with another moving element (Verghese et al., 2000; Verghese and McKee, 2002); when extended to contours formed of image motion, this effect increases with the number of elements in a path (Ledgeway and Hess, 2002). If motion-defined contour integration is selective for first-order motion, that might have explained the large extent of summation I observed in my experiments. This would require that contour integration take place at an earlier or parallel stage to mechanisms responding to changes in position, since the strength of summation did not depend on the degree to which first-order motion conflicted with position-defined motion. However, I also observed summation at larger inter-element separations than has been found for detection of motion-defined contours in noise (Watt et al., 2008). To test if contour integration accounts for first-order motion summation in these stimuli, one might adjust the stimulus or task to promote segmenting the stimulus into multiple pieces (Verghese and Stone, 1997; Burr et al., 2009).

7.2 Position-defined motion does not pool across objects

The previous literature is unclear about whether we might or might not have expected global summation for position-defined motion. Second-order motion does not appear to define contours (Hess et al., 2000), and evidence for any processing of second-order optic flow stimuli is mixed at best (Cassanello et al., 2011; Allard and Faubert, 2013). Even without either of these mechanisms, one might expect observers to be able to pool position-defined motion from multiple identically moving elements, simply due to probabilistic cue combination of multiple cues within a single modality. So it is reasonable to expect at least some improvement of sensitivity to position-defined motion when the number of elements is increased. However I did not find this. The highest sensitivities to envelope motion were achieved when the fewest elements were on screen. Even when elements were separated by more than their retinal eccentricity, so that crowding should not be an issue, there was no improvement in sensitivity to envelope motion when extra elements were added. Instead, sensitivity to envelope motion remained constant for larger separations between

elements, and declined as element separation decreased further.

Since each element also carried some carrier motion, adding more elements to the stimulus adds more first-order motion. Some studies find that first-order noise interferes with detection of second-order stimuli (Edwards and Badcock, 1995; Aaen-Stockdale et al., 2012). These studies found that the interference between first- and second- order stimuli scaled with the modulation strength of the first-order stimuli. However, the first-order component in the stimuli I used was not noise. Rather all elements carried identical signals; moreover first-order motion was co-located with the position-defined motion, so that there was no spatial interference between signal and noise elements as in previous studies. I found that varying the strength of the first-order motion signal leads to no changes in the sensitivity to position-defined motion, only a change in bias. In my stimulus, position-defined motion processing does not seem to be subject to interference from first order motion.

It may be surprising that envelope motion becomes less, rather than more visible when "flankers" are added which in fact carry identical information. This may represent a constraint on how position-defined motion is processed. It may be due a limitation of spatial attention, which multiple-object-tracking studies have shown is limited to approximately two moving elements per hemifield (Pylyshyn and Storm, 1988; Alvarez and Cavanagh, 2005; Cavanagh and Alvarez, 2005, review). However, note that since all elements are identical, it is not necessary to distinguish target from non-target, as in the MOT task, unless attentional tracking is in fact necessary to extract position-defined motion. It may also be the case that mechanisms capable of integrating motion among objects require more time than the 500 ms stimulus duration I used.

7.3 Sensitivity to position-defined motion is limited by crowding

A possible explanation of a loss in sensitivity to envelope motion is that it is a loss in sensitivity to position itself (and thereby to changes in position.) Some studies have found that localization or form perception of second-order motion stimuli is much poorer than for first-order stimuli (Zanker,

1997; Allen et al., 2004). On the other hand, other studies find very good spatial precision for second-order motion stimuli (Banton and Levi, 1993; Volz and Zanker, 1996). My experiments resolve this apparent difference by showing that the sensitivity to position-defined movement is limited by spatial interference from neighboring features. In the studies mentioned above, poor resolution was found for motion stimuli embedded in noise, while good performance was found for stimuli that were defined by local contrast.

In my experiments I determined that the sensitivity to envelope motion was controlled by the spacing between each element and its nearest neighbors. This finding is typical of the visual phenomenon of crowding (see Pelli and Tillman, 2008; Whitney and Levi, 2011for reviews). In crowding the discrimination or identification of a feature suffers when surrounded by flankers. One can define a "critical distance" as the target-flanker separation which achieves some set elevation of threshold for discrimination or recognition, analogous to how parameter *cs* operates in the model in Section 4. A typical finding has critical spacing approximately half the retinal eccentricity, which is in line with my findings for envelope motion. However, since Experiment 1 did not distinguish between element spacing and element number as the explanatory variable, I constructed Experiment 2 to compare these possibilities. The results appear to favor element spacing, though the sensitivity of this check was less than desired.

To my knowledge these experiments are the first to establish crowding as the bottleneck limiting sensitivity to position-defined motion. Previously, Bex and Dakin (2005) showed that crowding affects perception of first-order motion in the near periphery. However, there is an important difference between the first-order case and the position-defined case; for first-order motion, the perceived motion is affected by the motion carried by the flanker, showing "compulsory averaging," which was consistent with what I found for first-order motion. But for position-defined motion I found there was no summation. In the literature it seems that there are two manifestations of the crowding effect, depending on the task: object-level and feature-level. At the feature level, discrimination of elementary features like orientation, motion direction, spatial frequency, hue, and contrast is

impaired in the presence of flankers, and there is compulsory averaging (Parkes et al., 2001): the perceived feature is some mixture of the target and flanker features. At object level, stimuli such as letters, objects, and faces, being juxtapositions of multiple features, cannot be recognized in the presence of flankers, but pooling is less obvious; phenomenally the disparate features are mixed into a "jumble" (Zigler et al., 1930). For envelope motion to show no summation suggests that the process subserving envelope motion detection in the visual system does not detect changes in position prior to the crowding bottleneck, but afterwards. Thus position-defined motion is not an elementary feature in the way that first-order motion is. Instead it can be considered at the object level as a juxtaposition of multiple features, if we allow the multiple features to be arranged over time as well as space. In other words the detection of envelope motion rests on an encoding and comparison of successive positions, rather than a lower-level encoding of movement *per se.*

A recent hypothesis for the mechanism of visual crowding is that outside the fovea, the visual system computes a sort of reduced or "summary statistic" representation of the visual content of regions (Balas et al., 2009; Freeman and Simoncelli, 2011); this summary encodes the density and variance of basic features (e.g. orientation and first-order motion) as well as some second-order interactions between features like collinearity and curvature. This summary-statistic model is derived from models of texture perception, which effectively makes the claim that crowding and texture are the same thing (or, as Parkes et al. put it, "'crowding' is simply the name we give to texture perception when we do not wish it to occur.") Crucially, a summary-statistic representation fails to preserve the relative position of features when more than one object occupies a given region. For example, when targets consist of two crossed bars, their relative position (which distinguishes a "+" from a "T") is lost or averaged with the flanker (Greenwood et al., 2009; Dakin et al., 2010; Greenwood et al., 2012). Recognition of objects composed of juxtaposed features, such as letters, are thus more difficult under crowded conditions. An account of crowding as a loss of position information is a natural fit for what I found in position-defined motion; since position information becomes less precise under crowding, so does the motion signal computed from successive

positions.

7.4 Local and global motion (a note on terminology)

When different stimuli or processes in spatial vision are investigated they are often framed as "local" versus "global." Usually this refers to a difference in spatial scale, either between two aspects of the stimulus used or between the mechanisms that are proposed to respond to them. (Braddick, 1974, 1997; Majaj et al., 2007; Bex and Dakin, 2002) Another usage of "global" describes stimuli that are in some way coherent across the entire visual field (Edwards and Badcock, 1995; Cassanello et al., 2011; Anstis and Kim, 2011), such as optic flow stimuli or rigid-body motions of large objects. Yet another usage is when "global" refers to motion mechanisms that pool or integrate many locally defined signals into a coherent whole (Cropper, 2001), such as combining several local orientation-specific motion signals to compute overall pattern motion (Movshon and Newsome, 1996; Majaj et al., 2007), or in combining several small, noisy displacement signals across a larger area in order to detect random dot motion (Braddick, 1974; Williams and Sekuler, 1984; Newsome et al., 1989). Each of these usages shares the theme that a "global" mechanism is one that can combine information over a relatively large area.

For stimuli that resemble those used in my experiment, which put a first-order, textural motion into conflict with a position-defined motion, the tendency has been to use "local" to refer to the first-order component and "global" to the position. (Tse and Hsieh, 2006; Shapiro et al., 2010, 2011; Hedges et al., 2011; but note Butzer et al., 1997 make the opposite assignment). This may be reasonable from the point of view of constructing the stimulus; first order motion can be constructed in a large field by displacing dots one at a time independently, while producing position-defined motion for a larger object involves coordinating changes over many display pixels in concert. First-order motion may also be defined within a small window, while position-defined motion (by definition) must cross multiple locations. Calling position-defined motion "global" also aligns with the intuition that some process must be able to integrate changes in position over

a path that crosses several local receptive fields; otherwise how could a moving object appear to be the same object after it has moved? Nonetheless, care should be taken to avoid identifying the properties of the stimulus construction with those of the mechanism it probes (Cavanagh, 1991; Boulton and Baker, 1993).

In the case of my experiments, neither the carrier or envelope motion, in terms of the stimulus, is constructed to be more local or global than the other. For instance, the spatial scale of the step sizeΔx that defines the envelope motion is similar to (and in uncrowded conditions, much smaller than) the size of the envelope as well as the spatial scale of the oscillation in luminance $\frac{1}{f}$ that defines the carrier motion. Both components are local, in that they are defined within small areas of the stimulus, so it is possible to extract both the carrier and envelope motion from the stimulus by considering only a small region of the scene (somewhat larger than the envelope). At the same time, both components are global, both (independently) being consistent with a single rotating ring of elements. From this point of view a global motion mechanism would be one that can make use of the entire stimulus, while a local mechanism is one that is limited to using only a small portion.

As it turns out, the first-order motion mechanism is able to do this pooling over a wide area, while the position-defined motion mechanism cannot. Moreover, the first-order mechanism does not appear to particularly care about the *location* of its input, while *location* is the primary thing the position-defined mechanism uses (so disrupting information about location by crowding disrupts the position-defined motion mechanism.) So in terms of the mechanism revealed by my experiments, I would have to say that first-order motion mechanism functions globally, while the position-defined mechanism functions locally. However, perhaps these terms should be better avoided, as they produce conflicting intuitions in different readers.

7.5 First-order and position-defined motion have a subtractive interaction

One curious feature of these experiments is that for stimuli with zero envelope motion, and weak carrier motion to the left, some but not all observers consistently saw the stimuli as moving right-

wards. However, individual differences in motion perception have been seen previously when two types of motion are put into conflict.Fraser and Wilcox (1979) showed a drifting motion illusion which some people see as clockwise and others counterclockwise. Wilmer and Nakayama (2007) exploited individual differences to investigate how first-order and position-defined motion each contribute to the production of oculomotor pursuit. However it was still a puzzle why these individual differences should occur for a stimulus that only contained carrier motion.

This was eventually explained by collecting data which varied carrier and envelope motion along with spacing and constructing a model in those terms This model resolved the individual differences into a model of motion response that was qualitatively similar for each observer, but for which the proportions of contributions of each mechanism differed. This revealed that in fact most observers (all but CJ in this sample) do show repulsion from carrier motion, at weak carrier motion and larger spacings; using a weak counterclockwise envelope motion biased most observers' responses clockwise. I incorporated this into the model as a repulsion parameter β_I.

In the model, this repulsion effect has a nonlinearity, where perceived direction is a nonmonotonic function of carrier strength; at weak carrier strengths there is repulsion, but at stronger carrier strengths repulsion ceased and reversed. This nonlinearity was necessary because the effect of an increment in carrier motion changed depending on the strength of the original carrier motion: an increment of carrier motion strength applied to pure counterphase flicker led to observers' reporting apparent motion in the opposite direction to that of the increment, while the same increment added to a strong carrier motion produced a stronger perception of motion in the same direction of the increment.

The strength of the repulsion effect and its nonlinearity did not appear to vary with the number of elements; the same magnitude of repulsion appeared to apply to stimuli with two elements as with four or six. As a result, when more elements are present, repulsion is typically overwhelmed by global summation of carrier motion, for most but not all observers (in this sample, observers MC and JB have particularly strong repulsion in comparison to summation.) It should be noted

that although I modeled the response to carrier motion by separating the response due to carrier motion into two components, one that depends on element number (global summation) and a second nonlinear component that is not affected by global summation, the model fit might not reflect the mechanisms involved; it is possible that the nonlinearity is a component of global summation, or that it is related to the stimulus construction which mixes opposing motion directions to vary motion strength.

The repulsion effect may be related to some of the phenomena known as induced motion, or the Duncker illusion (Duncker, 1938; Reinhardt-Rutland, 1988, review), in which conflict between two component motions leads to an incorrect attribution of motion to each component. A familiar example of induced motion occurs when the moon is visible between low-lying clouds. When the clouds move with the wind, it gives rise to an illusion of the moon appearing to move in the opposite direction, while the clouds appear to be stationary. The general pattern is that induced motion arises when there is a difference between the motion of a larger field (the clouds in this case) and that of a smaller object (the moon.) The tendency is to view the field as stationary and attribute the difference in motion to the object; this results in a perception of object motion opposite the actual field motion. A normative explanation for why induced motion exists may be that large-scale motions are more likely to be due to the observer's motion (from motion in environment or eye movements) than isolated motion, so in most situations a subtractive interaction would result in a more accurate perception of object motion.

In my stimulus there is not a large field moving distinctly from a small object, but a set of identical objects with identical motion. But as discussed above, the spatial scale for integration of first-order motion appears to be larger than that for position-defined motion, and there is by design a conflict between the two. So the ingredients for a conflict between field motion and object motion are present, depending on which motion systems contribute to each.

Some properties that have been seen for induced motion are similar to what I found for repulsion: there is considerable intersubject variability in the strength of the illusion (Murakami and

Shimojo, 1993; Zivotofsky, 2004), and the strength of the illusion is a nonmonotonic function of the motion strength and/or target contrast (Murakami and Shimojo, 1993; Serrano-Pedraza and Derrington, 2010). Induced motion is often explained in terms of antagonism between center and surround when integrating motion over space. This cannot explain repulsion in my stimuli because its position-defined and first-order motion components share the same physical locations. However, many of the stimuli used in induced motion experiments can also be described as a textural or first-order background motion which conflicts with the motion of a salient object, and my stimuli can also be described this way. Thus there may be a common mechanism of a subtractive interaction between first-order and positional motion mechanisms, rather than a center-surround interaction. Still it is likely that "induced motion" encompasses several different effects; there are also variants of induced motion whose stimuli are not clearly position-defined (Murakami and Shimojo, 1996; Serrano-Pedraza et al., 2007), or for that matter neither position-defined nor center-surround (Derrington and Henning, 1987; Serrano-Pedraza et al., 2007). I modeled the repulsion effect as a subtractive interaction between position-defined and first-order motion in Figure 4.1, but this is only one of many possible instantiations.

7.6 Conflicts between first-order and position-defined motion

In most cases, the first order motion and higher order motion of a moving object will agree; however, when they conflict, the manner in which conflicts are resolved may reveal an interaction between the two systems. Previous work has also put suprathreshold first-order and position-defined motion in conflict, which I will review.

Reverse phi motion Reverse-phi motion combines a spatial displacement with a contrast inversion; following Fourier analysis, the motion energy is directed opposite the displacement. (Anstis, 1970; Anstis and Rogers, 1975). Most investigations of reversed phi use conditions where the first order component is dominant, but when stimulus features are salient enough, the displacement can

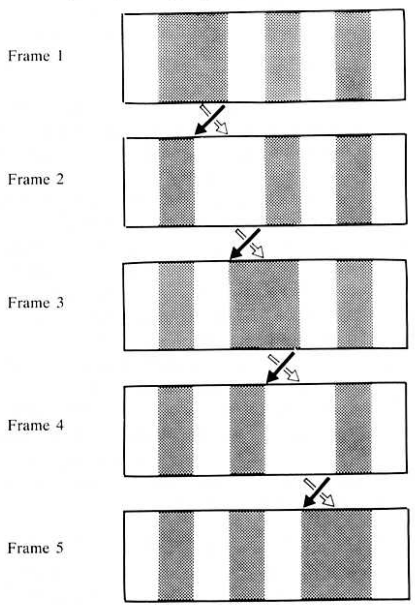

Figure 7.1: The stimulus used by Mather et al. (1985). A sequence of frames in illustrated. The first-order, luminance defined motion is to the left, and position-defined motion is to the right.

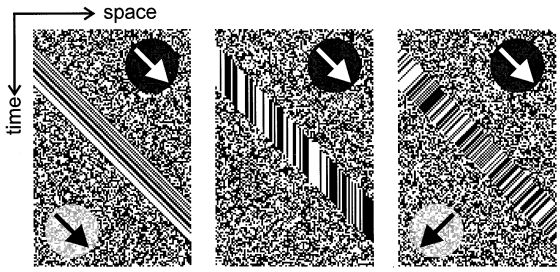

Figure 7.2: Motion stimuli devised by Zanker (1990). Three *xt*-plots of motion stimuli are shown. These stimuli comprised a random-dot kinematogram (RDK) within a moving window, against a backdrop of either dynamic or static noise. The window moves from left to right in all three examples, while the pattern within is independent. From left to right are "Fourier" motion, "drift balanced" motion, and "theta" motion. Figure is from Lindner and Ilg (2000).

be seen opposing the motion. For example, if there is only one luminance edge, apparent motion follows the movement of the edge and not the motion energy (Anstis and Cavanagh, 1981). Mather et al. (1985) used a display with a single moving "wide" bar that moved while reversing the contrast of its background, as illustrated in Figure 7.1. The motion that was seen in this display depended on the size of the bar and the retinal eccentricity at which the stimulus was viewed; in central vision, the position-defined motion (rightward in Figure 7.1) was seen at moderate to large bar sizes. However, at a retinal eccentricity of 5 degrees, only the first-order motion component (leftward) was seen. Similarly Chubb and Sperling (1989) used a reverse phi grating with widely spaced bars, and observed that the direction of apparent motion reversed depending on viewing distance, with the apparent motion agreeing with the step direction when viewed from near distances in central vision, but agreeing with first-order motion when viewed from farther distances, or near distances in peripheral vision. In both cases motion after-effects were always opposite first order motion regardless of the apparent motion seen.

As described above, in my experiments I saw similar effects of retinal eccentricity and feature separation as those seen in these studies. Chubb and Sperling proposed a second-order mechanism (i.e. a motion-energy detector with a rectifying input nonlinearity) where the reversal would be explained by a lower limit on spatial frequency sensitivity for the second-order channel. However, this would require spatial frequency selectivity for second order motion in the periphery to drop off faster than for first-order motion. An alternate explanation may be that the position-defined motion system is responsible for detecting these features in the fovea, but crowding between the object and the high-contrast background prevents this in the periphery.

Theta motion Zanker (1990; 1993) constructed stimuli consisting of a windowed random-dot kinematogram, where the object motion (defined by the boundaries of the window) and windowed texture were allowed to take different directions of motion. Since the target and background are only distinguishable by the difference in motion, this has been called "motion-defined motion" (Zanker, 1997). Example xt-plots of these stimuli are shown in Figure 7.2, illustrating three condi-

tions of agreement between the motions of the object texture and window. The condition in which texture motion disagreed with the window was called "theta" motion. Zanker (1993) found that the direction of window motion was readily perceived in central vision but only the texture motion was visible in peripheral vision. To compare the sensitivity to each component, Zanker (1997) oriented texture motion at right angles to window motion; detection of window motion was particularly impaired in the near periphery.

In contrast I found that position-defined (envelope) motion was perfectly visible in the periphery, and even tends to be more salient and precise than the carrier motion, as long as the moving object is not crowded by flanking objects. How can we reconcile these results? There is a difference in how the stimuli are constructed: Zanker's experiments had the motion stimulus shown against a noise background, so that the first order motion or flicker was the only cue by which the object could be located. In my stimuli the object stands against a flat background, so that it is locatable by the local contrast. Under these conditions the direction of object motion is clearly visible.

Thus, one hypothesis that could reconcile Zanker's results with our own is that the features available to track the position of the window or envelope do not include first order motion itself. To be more specific, the *location* of first order motion may not be readily available to a feature tracking mechanism, while the location of other features (such a localized orientation and contrast) is. Thus, my stimuli were easily visible to the feature tracking mechanism, whereas Zanker's stimuli were far less visible. In central vision, even imprecise localization in the scale of an MT receptive field would be enough to be able to track a shift in location. Alternately, motion might be bound together with other features at a stage earlier than that at which feature tracking operates. In Zanker's stimulus there is no distinct feature to bind motion to in the periphery. Either alternative would explain why observers have no difficulty with detecting isolated motion in the periphery even when carrier motion conflicts, so long as flankers are distant.

Windowed texture or carrier/envelope stimuli Another way to construct a stimulus that opposes first-order and higher order motion is to have a moving window define the higher order motion, while the moving window modulates the contrast of an underlying moving texture. My stimuli fall into this class, as well as some others.

Several striking illusions have been constructed in this fashion. Tse (2006) presented an illusion which combined vertical translation of Gabor-like envelopes with a horizontal motion of the carrier. A similar illusion was presented by Shapiro (2008); Shapiro et al. (2009). When viewed in the periphery, the motion appears distinctly diagonal, and its perceived position seems to drift far from its true position (though whether the apparent position shift is reflected in position judgements has not been well tested.) Additionally the appearance shifts markedly between central and peripheral vision, with the envelope motion being more clearly visible in central vision. Similarly, we noticed that the perceived direction of motion could be affected by the retinal eccentricity, but we also showed that proximity of the target to adjacent flankers controls appearance (Meilstrup and Shadlen 2008; 2010).

Hedges et al. (2011) asked observers to judge the carrier motion of a single test pulse in a sequence of pulsed envelope motion. Only the test pulse had carrier motion; the other pulses had only flicker. This task was found to be very difficult; when envelope motion is available it "captured" the carrier motion, that is, envelope motion biased judgements toward the envelope motion and decreased the sensitivity to carrier motion. Note that these results differ from mine: while carrier and envelope motion both contributed a bias, I did not find the sensitivity to carrier motion to change as a function of envelope motion. This may be due to differences in stimulus parameters explored; I used slower envelope motion and faster carrier motion. There was also a difference in tasks; I asked observers for an overall report of motion appearance rather than to discriminate the carrier motion. However, it would not make much sense for a judgement of overall appearance to have unchanged sensitivity to carrier motion but for a judgement of carrier motion itself to have impaired sensitivity.

Alternately, the difference may be due to different ways in which the stimuli were modulated. I controlled envelope motion by varying the spatial step size. In contrast, Hedges et al. controlled envelope motion by varying the temporal interval between pulses. As a result, when faster envelope motion was employed, i.e. a smaller temporal interval between pulses was used, the pulses overlapped in time so that there were more flickering elements on the screen simultaneously. The faster the motion, the more flicker existed simultaneously with the test pulse. If the task is to detect first-order motion, and the first-order motion system sums over large areas, it is possible that the elevation of threshold for detecting the test pulse may be due to the increased counterphase flicker, which is known to mask motion signals (Anderson and Burr, 1989). It would be interesting to see if the capture of motion perception by position-defined motion were also present for other manipulations.

Pursuit eye movements to conflicting motion stimuli Response measures other than appearance or detection judgements can also be used to investigate motion processing; pursuit eye movements are one promising avenue. Butzer et al. (1997) recorded pursuit eye movements made to theta motion stimuli. Observers could initiate pursuit, in agreement with object motion, to targets whose object motion disagreed with their Fourier motion, but the initial velocity of the pursuit was slower for the first couple of hundred milliseconds. Hawken and Gegenfurtner (2001) used a windowed texture stimulus and found that the carrier motion condition (agreeing, disagreeing, or neutral with respect to the envelope motion) affected the initial pursuit velocity for targets with slow envelope motion ($1^{\circ}s^{-1}$.) For faster ($6^{\circ}s^{-1}$) envelope motions, they reported that the effect of carrier motion velocity on initial pursuit velocity was a smaller proportion of the envelope motion; however examination of their data suggests that the effect of carrier motion velocity actually appears to have a similar absolute value in both conditions, which tends to agree with our finding that carrier and envelope motion appear to contribute independently to the judgement of motion direction.

It has been found that different aspects of visual motion affect different phases of oculomotor

pursuit; the earliest phases depend on target velocity with little effect of target position, while later phases show an effect of target position (Lisberger et al., 1987). Additionally, when there is a catch-up saccade, pursuit velocity following the saccade is more precise than preceding the saccade (Lisberger, 1998). Using between-subjects comparisons, Wilmer and Nakayama (2007) found that observer's measured sensitivities on two psychophysical motion-discrimination tasks (using first-order and position-defined stimuli) correlated to the precision of the same subjects' pursuit velocity before and after a catch-up saccade.

We have presented pilot data (Meilstrup and Shadlen, 2008) on oculomotor saccade and pursuit responses to carrier/envelope motion stimuli. Observers made saccades towards a target moving on a circle of constant eccentricity, after which they followed the target in smooth pursuit. For human observers, it was found that observers readily initiated pursuit in the same direction as the envelope rather than carrier motion; however both the position of the initial saccade endpoint and the postsaccadic pursuit velocity were biased by the carrier motion. This is consistent with the psychophysics on uncrowded stimuli we saw here. We trained a rhesus macaque on the same task and found that the monkey could also generate pursuit in agreement with envelope motion (but this required some training; pursuit velocities captured by carrier motion were more prevalent than for human observers.) It also appeared that the precision of saccadic endpoints and pursuit velocities was affected by target-flanker spacing, in agreement with the psychophysical results in this thesis relating position motion detection to crowding effects.

7.7 Possible neurophysiology of position-defined motion

Much work on the neurophysiology underlying motion perception has focused on cortical areas V1, MT, and MST. Area MT takes input from V1 and integrates it over a larger area, resolving one-dimensional motion signals into two-dimensional texture motion (Movshon et al., 1985; Simoncelli and Heeger, 1998; Rust et al., 2006). Because MT has a much larger receptive field size than V1, MT cells can gather information from an object that changes position to pass through several V1

receptive fields, so it has been suggested that MT activity has an effect on the perceived position of moving objects (Nishida and Johnston, 1999; McGraw et al., 2004; Mather and Pavan, 2009). However, increasing evidence indicates that position-defined motion itself has no representation in MT and probably not in MST (Livingstone et al., 2001; Ilg and Churan, 2004; Hedges et al., 2011). Although position-based feature tracking appears to be a primary driver of motion appearance, often overriding first-order motion, how exactly it is implemented remains an open question.

Viewing position-defined motion as a feature integration problem, analogous to letter recognition, may be useful. In this thesis I have found that position-defined motion suffers crowding in the same way that object recognition does (and unlike the spatial summation that first-order motion exhibits). Perhaps position-defined motion processing may use similar mechanisms as feature integration; detecting a change in position of a feature over time may be analogous to detecting multiple features in a particular relative arrangement, as is done in object recognition. This suggests an interesting hypothesis: the appearance of object motion may be determined in the ventral stream, while most work has focused on the dorsal stream. Consistent with this, there is some evidence for processing of long-range apparent motion in the ventral stream (Vaina and Soloviev, 2004; Zhuo et al., 2003).

Unfortunately, the neural mechanisms responsible for crowding remain as mysterious as those for object motion. The spatial interference in crowding is roughly scaled the same as a receptive field in V4, which has made V4 one suggestion for a locus of crowding (Motter, 2002, 2006; Liu et al., 2009). As it happens, some effects relating to the integration of visual motion and position also have correlates in V4. (Sundberg et al., 2006; Fischer et al., 2011)

7.8 Motion processing systems may complement each others' limitations

The motion stimuli an organism must interpret in its natural environment are in many ways much more complicated than the stimuli we construct in an artificial experimental setting. However, in this thesis I have identified two ways in which motion perception appears to be profoundly limited,

both of which would appear to only become worse as a scene becomes more complicated. The first order mechanism which detects carrier motion in our experiment is known to be sensitive to very small amounts of motion spread among noise, but has little idea of the position of the objects producing that motion. In the other hand, the position-defined motion system is confounded by clutter, takes several hundred milliseconds to detect a change in position of an object, and is not as good at determining precise velocities needed for pursuit.

How, then, can the visual system make sense of typical, cluttered visual scene? The stimuli I use are artificial, with the first-order designed to provide no information about the position-defined component and vice versa. In most natural situations cases, the two components will be mutually informative. In that case, the different sensitivities and bottlenecks of the two systems may complement each other. Large scale image motion detected by the first order system is typically generated by the movement of the organism through the environment, and should be discounted when searching for moving objects. The subtractive interactions I observed between first-order and position-defined motion may play this part, helping to boost the visibility of isolated features so that they can be tracked. There is evidence that localized first-order motion, when it can be bound to a feature, boosts the visibility of that feature allowing it to be detected in clutter (Watamaniuk et al., 1995; Verghese et al., 1999; Verghese and McKee, 2002). While the first-order system is by far more understood in terms of its mechanism, the position-tracking system may be the more important for understanding the phenomenal experience of visual motion. It seems likely that many aspects of motion vision may be explained by by the same processes that underlie phenomena of spatial interference, texture perception, and object recognition.

7.9 Acknowledgements

The pulsed apparent-motion stimuli I used in these experiments were originally devised by Michael Shadlen. I performed the experiments in his laboratory with his gracious support and advisement. Ione Fine assisted greatly with the preparation and editing of this manuscript and served as a second

advisor and very effective manager in the later stages of this project. Thanks are also due to John Palmer, Geoff Boynton, and Tony Movshon for exchanging ideas and for crucial pieces of advice regarding psychophysical measurement and modeling.

8 Appendix: Model fits and data for all observers

In this section I show the complete collection of model and diagnostic plots for all observers.

8.1 Model fits in perspective and contour plots

The following figures illustrate the main effects of the motion model described in Section 4 as fitted to each observer's data. They are formatted identically to Figure 5.3 and Figure 5.4, as described in § 5.3.

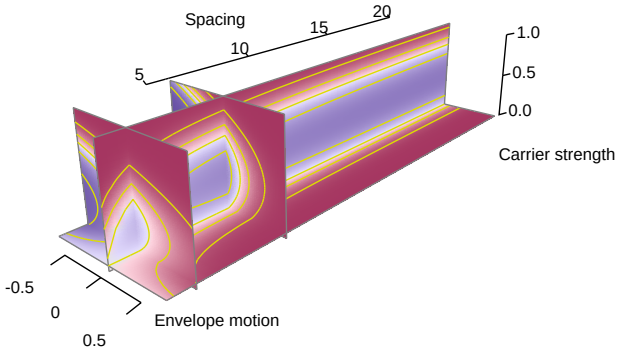

Figure 8.1: Perspective view of fitted model for observer AS. The format of the plot is the same as Figure 5.3.

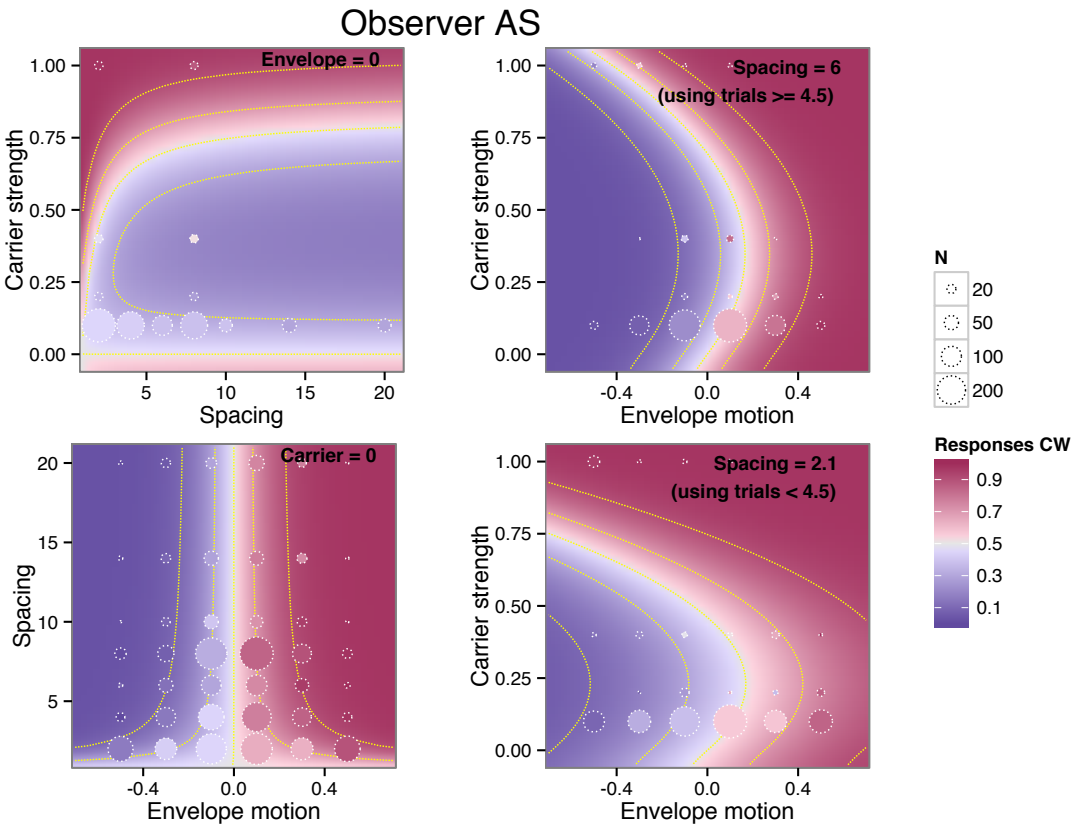

Figure 8.2: Model fits and summary of data for observer AS. The format of the plot is the same as Figure 5.4.

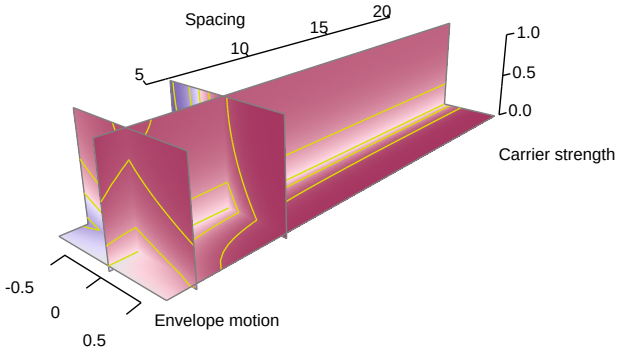

Figure 8.3: Perspective view of fitted model for observer CJ. The format of the plot is the same as Figure 5.3.

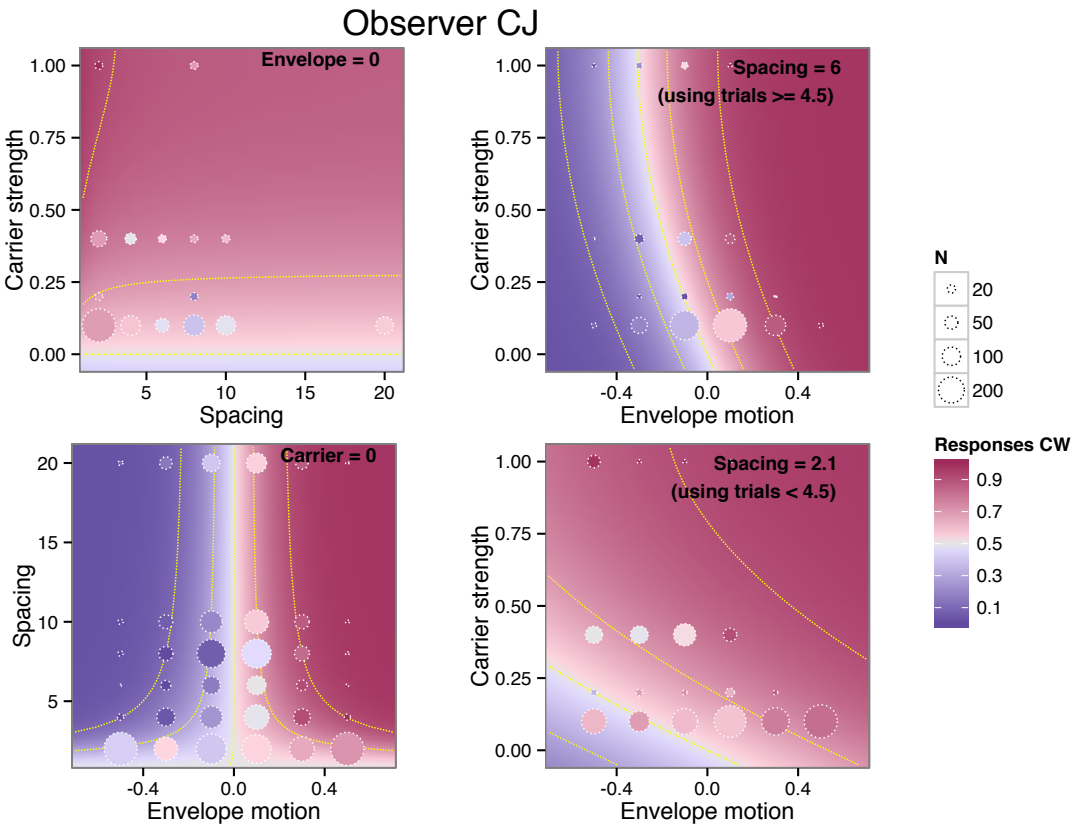

Figure 8.4: Model fits and summary of data for observer CJ. The format of the plot is the same as Figure 5.4.

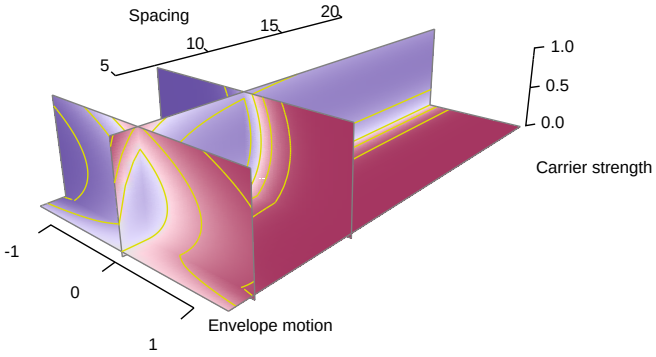

Figure 8.5: Perspective view of fitted model for observer JB. The format of the plot is the same as Figure 5.3.

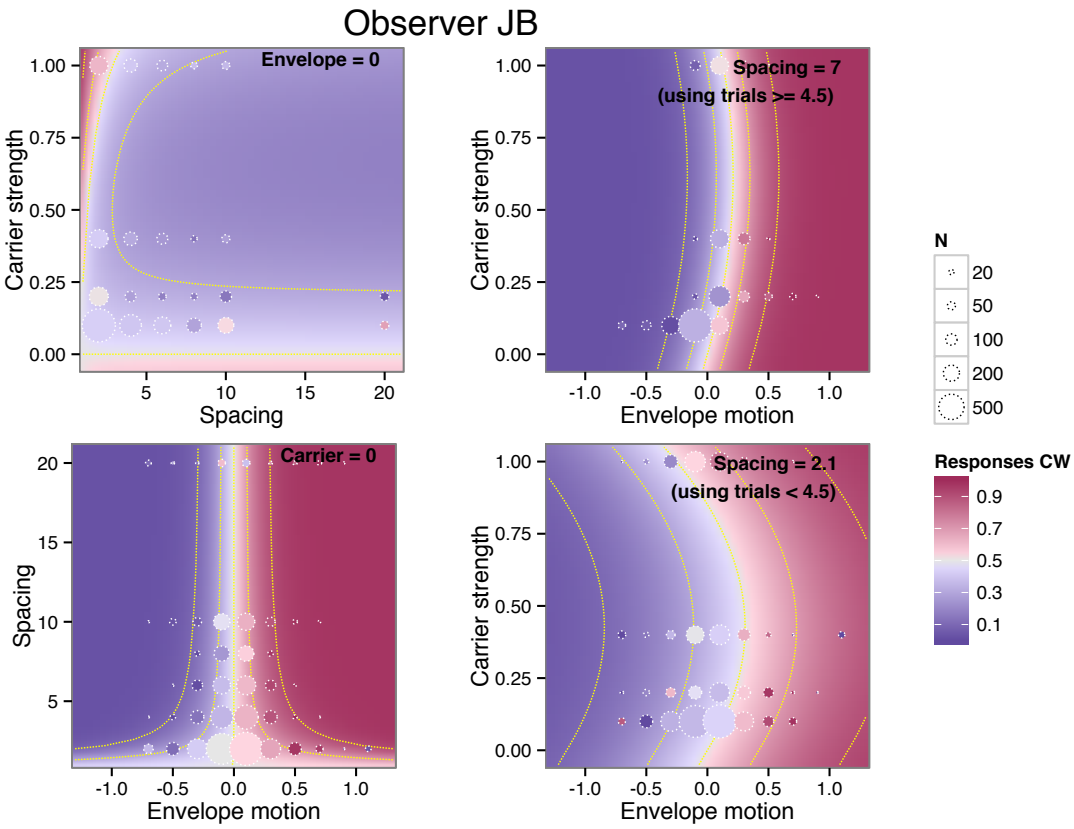

Figure 8.6: Model fits and summary of data for observer JB. The format of the plot is the same as Figure 5.4.

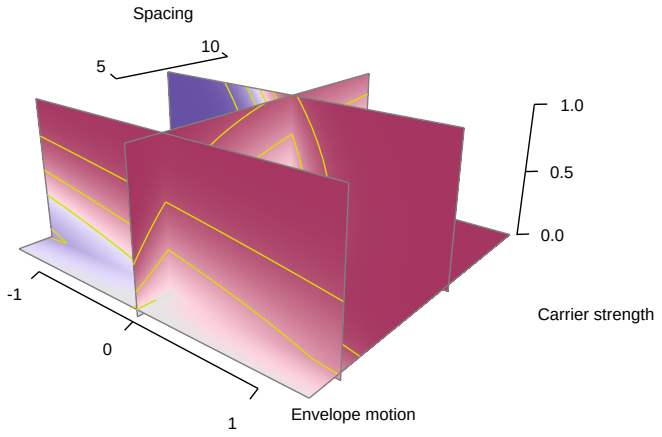

Figure 8.7: Perspective view of fitted model for observer JE. The format of the plot is the same as Figure 5.3.

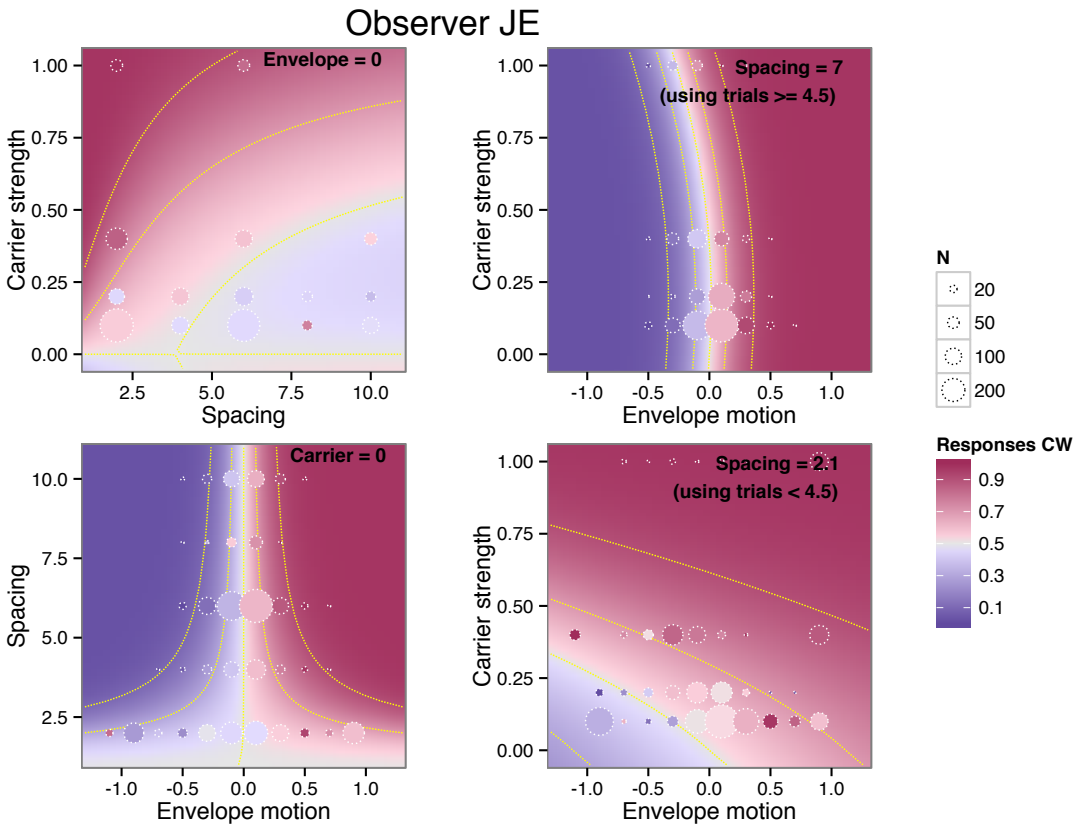

Figure 8.8: Model fits and summary of data for observer JE. The format of the plot is the same as Figure 5.4.

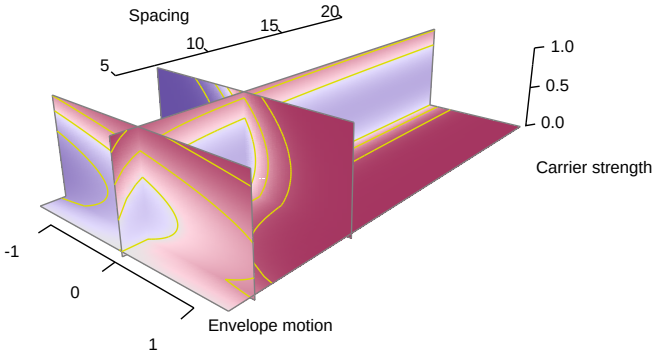

Figure 8.9: Perspective view of fitted model for observer KO. The format of the plot is the same as Figure 5.3.

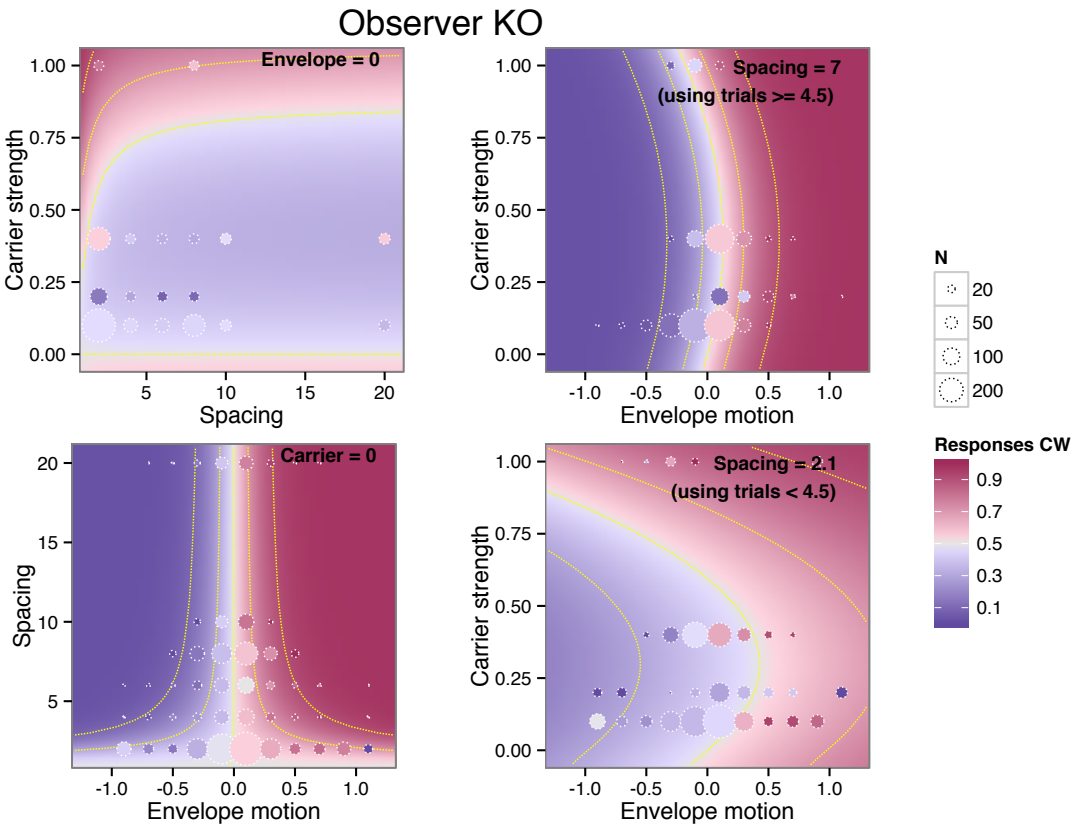

Figure 8.10: Model fits and summary of data for observer KO. The format of the plot is the same as Figure 5.4.

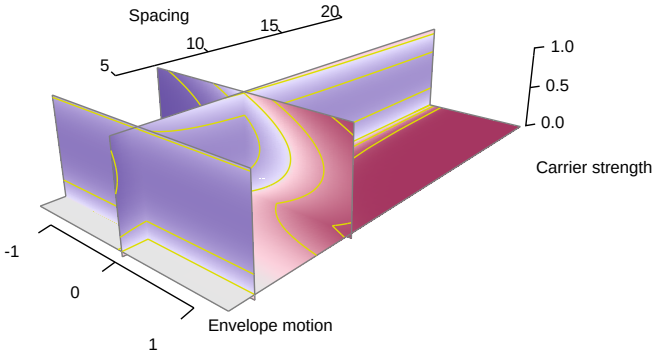

Figure 8.11: Perspective view of fitted model for observer MC. The format of the plot is the same as Figure 5.3.

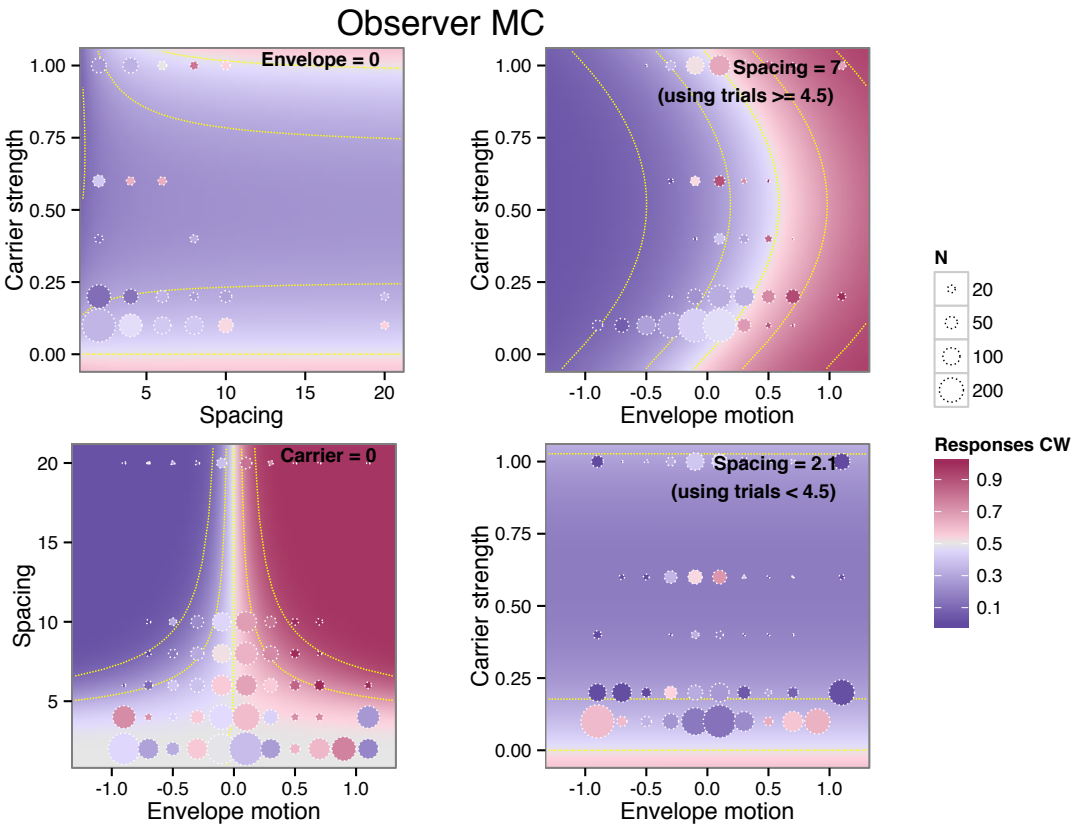

Figure 8.12: Model fits and summary of data for observer MC. The format of the plot is the same as Figure 5.4.

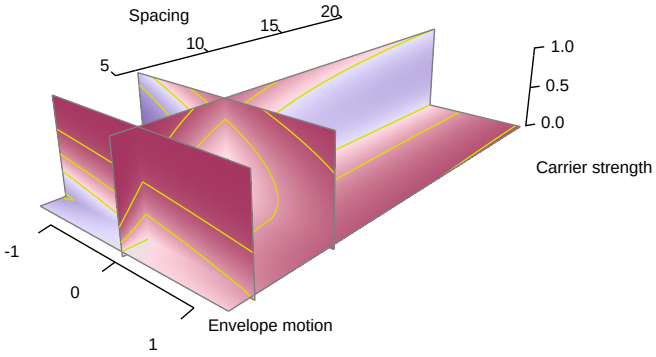

Figure 8.13: Perspective view of fitted model for observer ML. The format of the plot is the same as Figure 5.3.

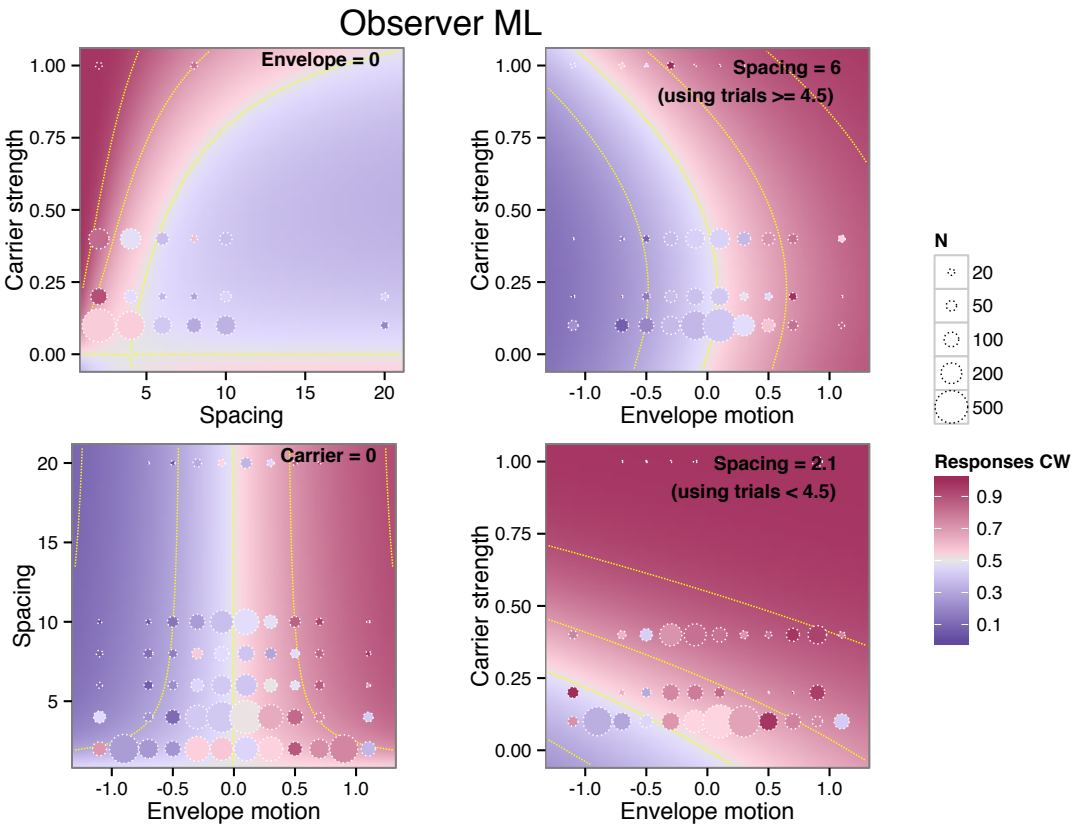

Figure 8.14: Model fits and summary of data for observer ML. The format of the plot is the same as Figure 5.4.

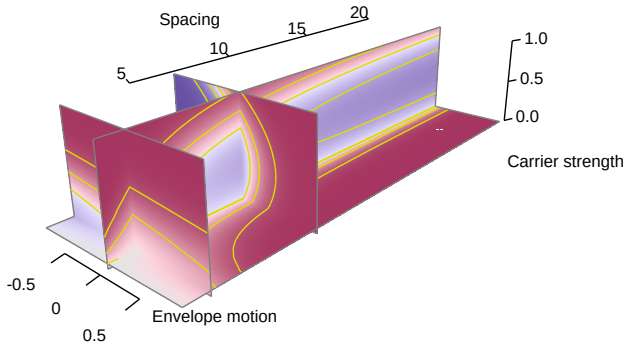

Figure 8.15: Perspective view of fitted model for observer NJ. The format of the plot is the same as Figure 5.3.

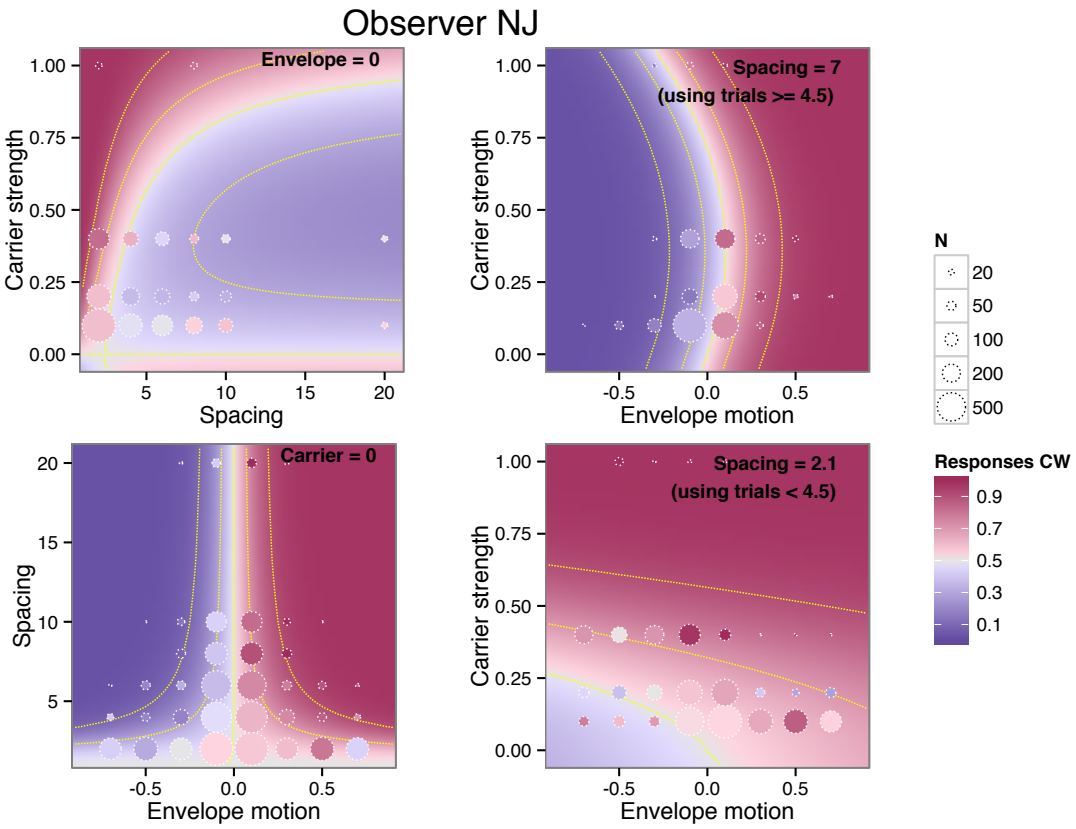

Figure 8.16: Model fits and summary of data for observer NJ. The format of the plot is the same as Figure 5.4.

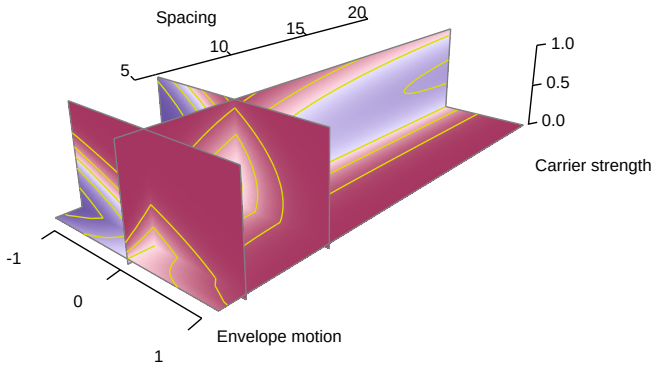

Figure 8.17: Perspective view of fitted model for observer NS. The format of the plot is the same as Figure 5.3.

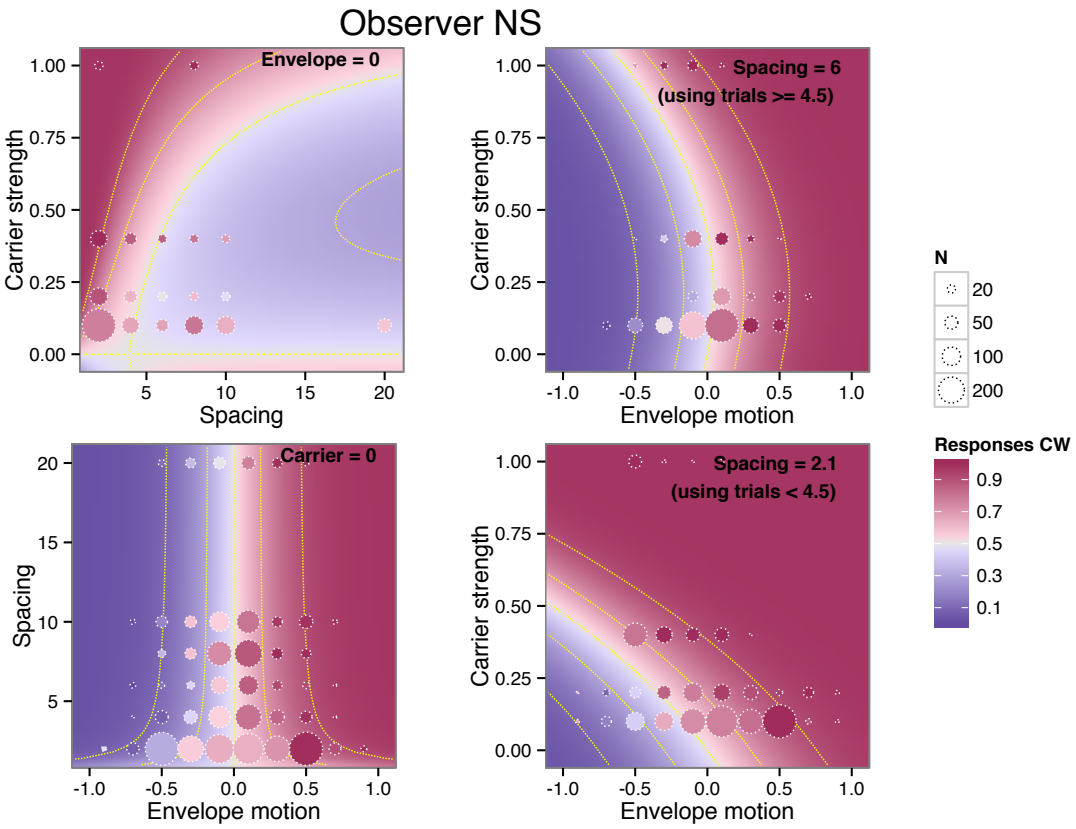

Figure 8.18: Model fits and summary of data for observer NS. The format of the plot is the same as Figure 5.4.

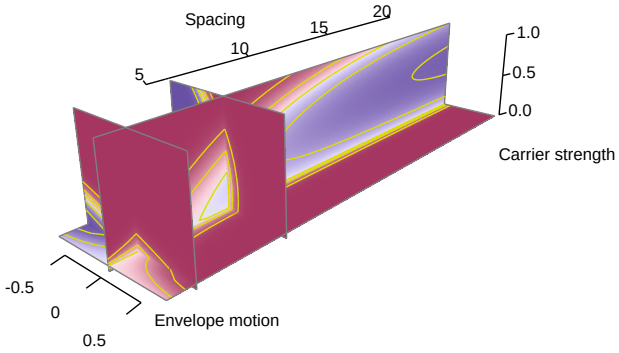

Figure 8.19: Perspective view of fitted model for observer PBM. The format of the plot is the same as Figure 5.3.

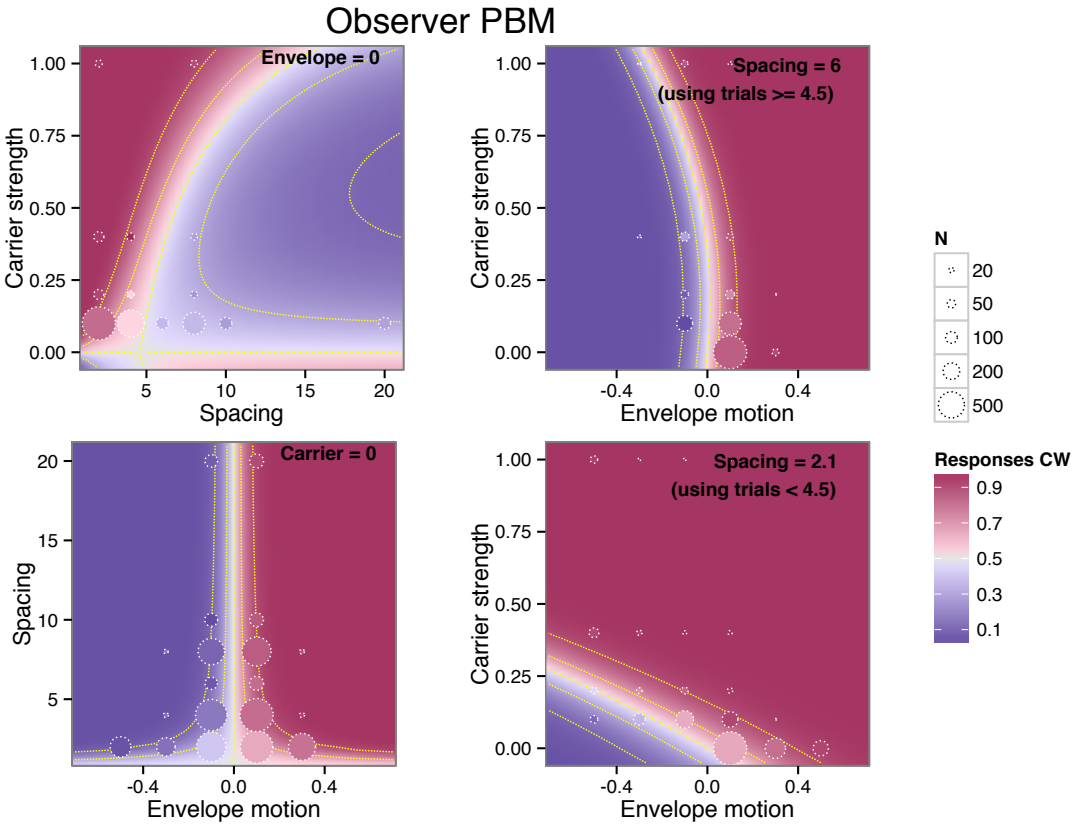

Figure 8.20: Model fits and summary of data for observer PBM. The format of the plot is the same as Figure 5.4.

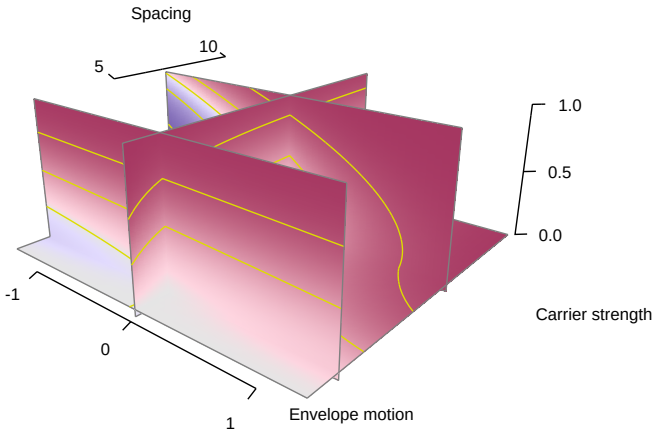

Figure 8.21: Perspective view of fitted model for observer TL. The format of the plot is the same as Figure 5.3.

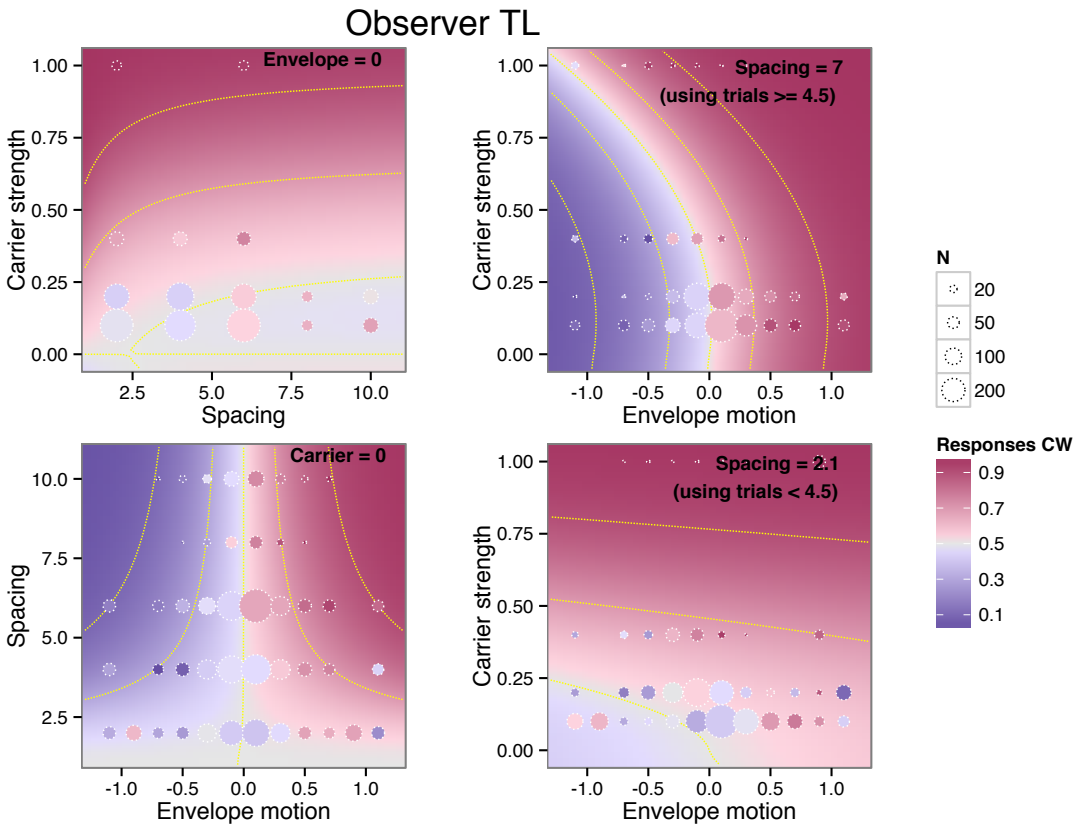

Figure 8.22: Model fits and summary of data for observer TL. The format of the plot is the same as Figure 5.4.

8.2 Sensitivity to envelope displacement

Figure 8.23 depicts the sensitivity measure $\beta_{\Delta x}(s)$ as a function of spacing. The construction of the measure and the figure is the same as described in § 5.4.3.

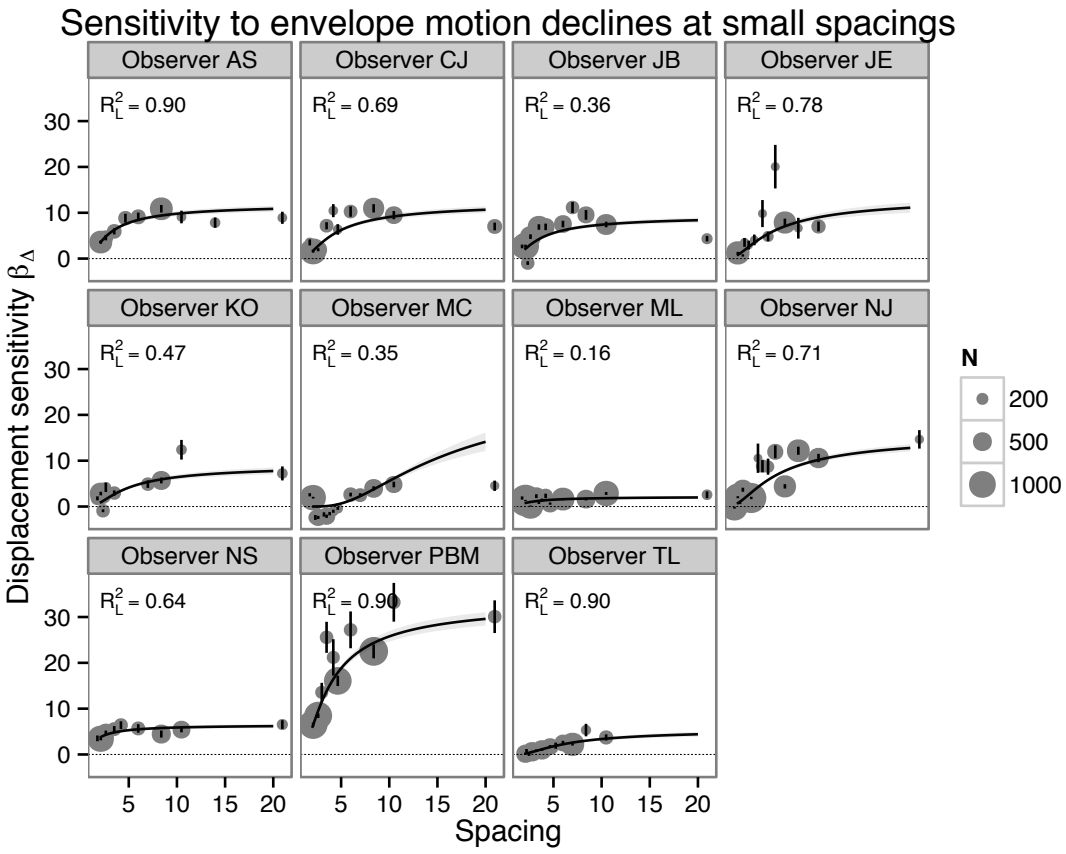

Figure 8.23: Sensitivity to envelope motion as a function of element spacing. This is a complete version of Figure 5.5 showing all observers, and is otherwise formatted identically.

8.3 Sensitivity to carrier motion

Figure 8.24 measures the spacing-dependent summation of carrier motion, denoted in the model as M_S for all observers who participated in the experiment. The construction is described in § 5.2.2.

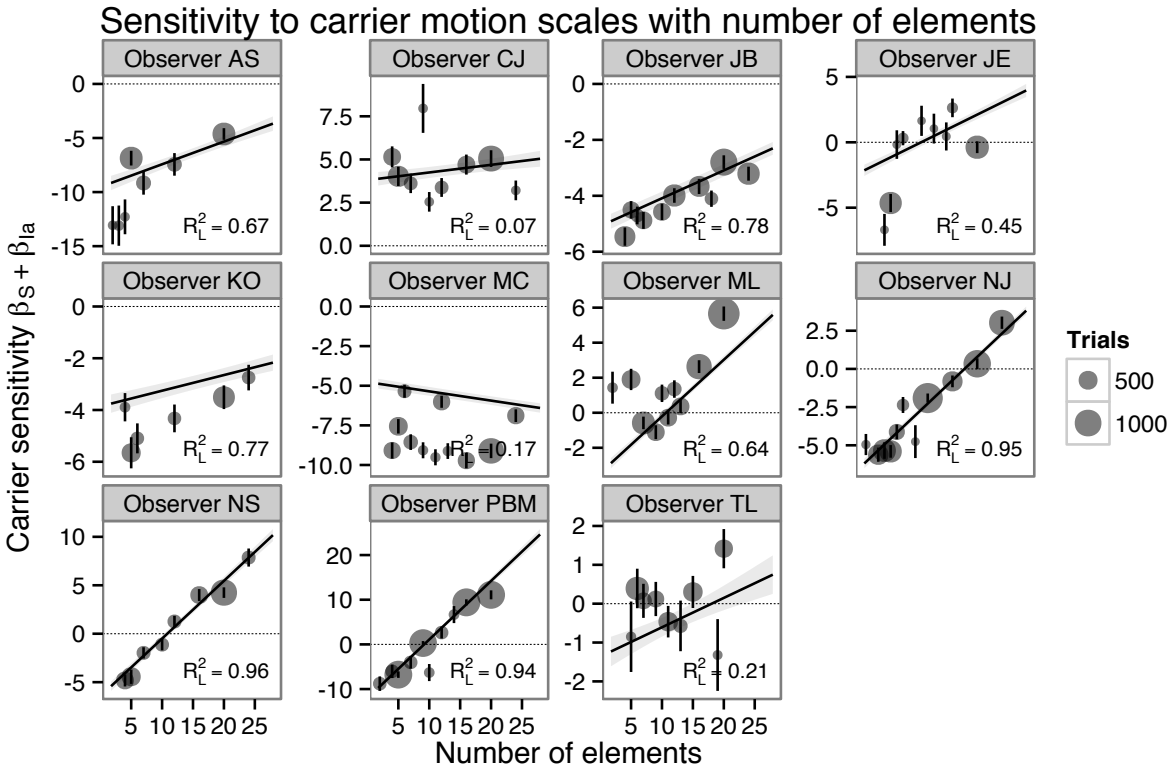

Figure 8.24: Sensitivity to carrier motion as a function of spacing. This is a complete version of Figure 5.6 showing all observers; see § 5.2.2 for details on construction.

8.4 Carrier repulsion

Figure 8.25 depicts the repulsion to carrier motion M_I for all observers who participated in the experiment. The construction is described in § 5.4.6.

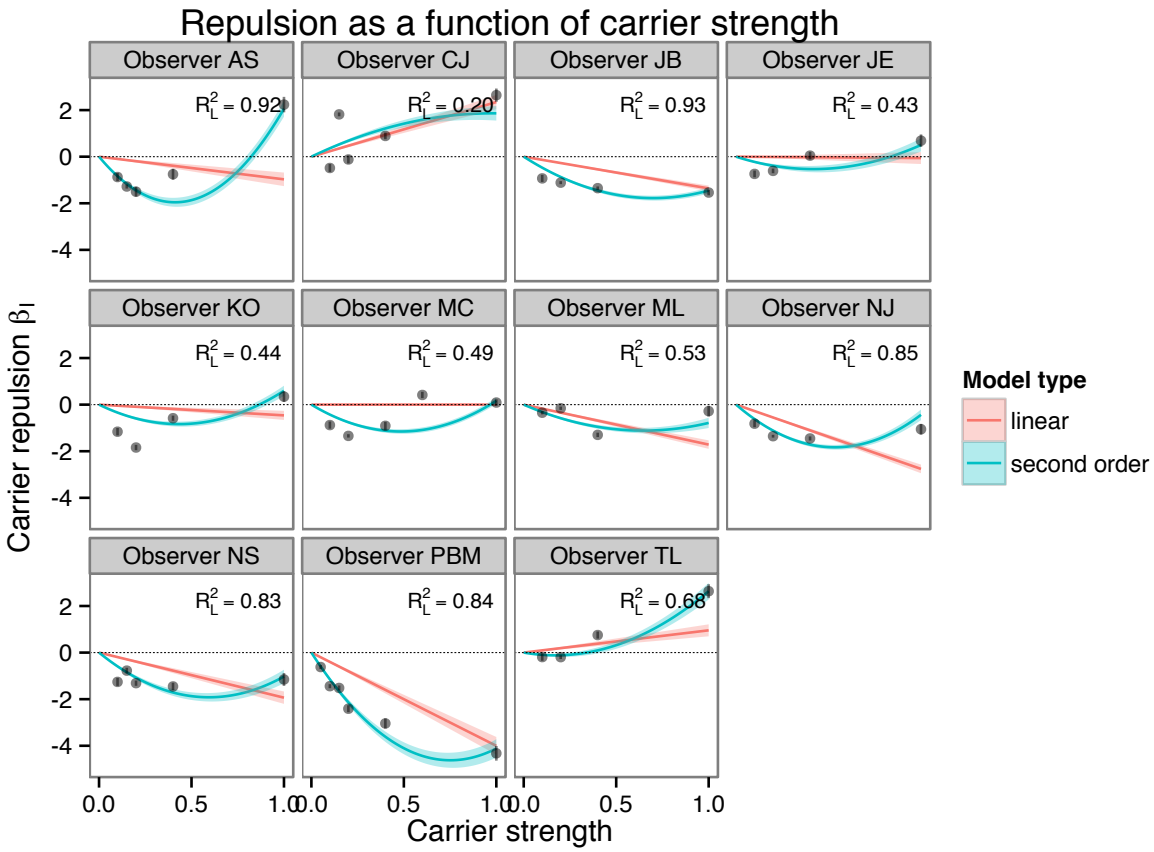

Figure 8.25: The strength of the repulsion effect as a function of carrier strength. This is a version of Figure 5.7 showing all observers; see § 5.4.6 for details on construction.

8.5 Number and spacing

Figure 8.26 compares four model predictions for data from Experiment 2, as described in § 6.2.2.

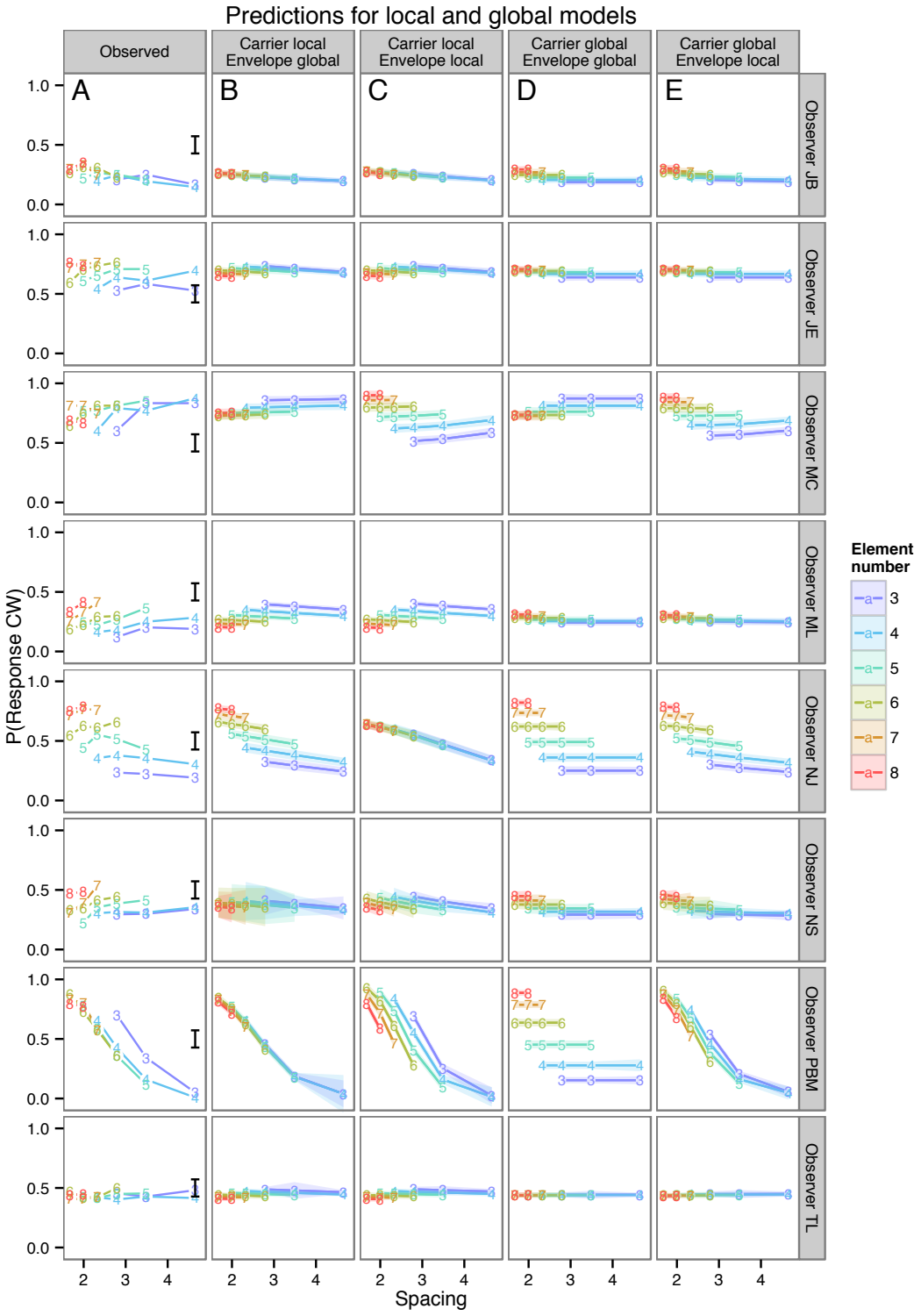

Figure 8.26: Predictions for four models compared to data from Section 6, after Figure 6.4. Vertical axis measures the proportion of responding "clockwise" to a stimulus, while the horizontal axis measures inter-element spacing; colors and labels show the number of moving elements shown. See § 6.1 for details.

References

Aaen-Stockdale, C., Ledgeway, T., and Hess, R. F. (2007). Second-order optic flow processing. *Vision Res*, 47(13):1798–808, doi:10.1016/j.visres.2007.02.022.

Aaen-Stockdale, C., Ledgeway, T., McGraw, P., and Hess, R. F. (2012). Interaction of first- and second-order signals in the extraction of global-motion and optic-flow. *Vision Res*, 68:28–39, doi:10.1016/j.visres.2012.07.004.

Adelson, E. H. and Bergen, J. R. (1985). Spatiotemporal energy models for the perception of motion. *J Opt Soc Am A*, 2(2):284–299, PMID 3973762.

Adelson, E. H. and Movshon, J. A. (1982). Phenomenal coherence of moving visual patterns. *Nature*, 300(5892):523–525, PMID 7144903.

Adler, D. and Murdoch, D. (2013). *rgl: 3D visualization device system (OpenGL)*. http://CRAN.R-project.org/package=rgl, R package version 0.93.935.

Akaike, H. (1974). A new look at the statistical model identification. *IEEE Trans Automatic Control*, 19(6):716–723.

Allard, R. and Faubert, J. (2013). No dedicated second-order motion system. *J Vis*, 13(11), doi:10.1167/13.11.2.

Allen, H. A., Ledgeway, T., and Hess, R. F. (2004). Poor encoding of position by contrast-defined motion. *Vision Res*, 44(17):1985–99, doi:10.1016/j.visres.2004.03.025.

Alvarez, G. A. and Cavanagh, P. (2005). Independent resources for attentional tracking in the left and right visual hemifields. *Psychol Sci*, 16(8):637–43, doi:10.1111/j.1467-9280.2005.01587.x.

Anderson, S. J. and Burr, D. C. (1987). Receptive field size of human motion detection units. *Vision Res*, 27(4):621–35, PMID 3660623.

Anderson, S. J. and Burr, D. C. (1989). Receptive field properties of human motion detector units inferred from spatial frequency masking. *Vision Res*, 29(10):1343–58, PMID 2635464.

Anderson, S. J., Burr, D. C., and Morrone, M. C. (1991). Two-dimensional spatial and spatial-frequency selectivity of motion-sensitive mechanisms in human vision. *J Opt Soc Am A*, 8(8):1340–51, PMID 1919837.

Anstis, S. and Kim, J. (2011). Local versus global perception of ambiguous motion displays. *J Vis*, 11(3):13, doi:10.1167/11.3.13.

Anstis, S. M. (1970). Phi movement as a subtraction process. *Vision Res*, 10(12):1411–30, PMID 5516541.

Anstis, S. M. and Cavanagh, P. (1981). What goes up need not come down: Moving flickering edges give positive motion aftereffects. In Long, J. B. and Baddeley, A. D., editors, *Attention and performance IX*, chapter 4, pages 63–78. L. Erlbaum Associates.

Anstis, S. M. and Rogers, B. J. (1975). Illusory reversal of visual depth and movement during changes of contrast. *Vision Res*, 15:957–61, PMID 1166630.

Archer, K. J., Lemeshow, S., and Hosmer, D. W. (2007). Goodness-of-fit tests for logistic regression models when data are collected using a complex sampling design. *Computational Statistics & Data Analysis*, 51(9):4450–4464.

Balas, B., Nakano, L., and Rosenholtz, R. (2009). A summary-statistic representation in peripheral vision explains visual crowding. *J Vis*, 9(12):13.1–18, doi:10.1167/9.12.13.

Banks, M. S., Sekuler, A. B., and Anderson, S. J. (1991). Peripheral spatial vision: limits imposed by optics, photoreceptors, and receptor pooling. *J Opt Soc Am A*, 8(11):1775–87, PMID 1744774.

Banton, T. and Levi, D. M. (1993). Spatial localization of motion-defined and luminance-defined contours. *Vision Res*, 33(16):2225–37, PMID 8273289.

Bex, P. J. and Dakin, S. C. (2002). Comparison of the spatial-frequency selectivity of local and global motion detectors. *J Opt Soc Am A Opt Image Sci Vis*, 19(4):670–7, PMID 11934159.

Bex, P. J. and Dakin, S. C. (2005). Spatial interference among moving targets. *Vision Res*, 45(11):1385–1398, doi:10.1016/j.visres.2004.12.001.

Boi, M., Öğmen, H., Krummenacher, J., Otto, T. U., and Herzog, M. H. (2009). A (fascinating) litmus test for human retino- vs. non-retinotopic processing. *J. Vis.*, 9(13):1–11. http://journalofvision.org/9/13/5/.

Boulton, J. C. and Baker, C. L. J. (1993). Different parameters control motion perception above and below a critical density. *Vision Res*, 33(13):1803–11, PMID 8266636.

Braddick, O. (1974). A short-range process in apparent motion. *Vision Res*, 14(7):519–27, PMID 4423193.

Braddick, O. (1997). Local and global representations of velocity: transparency, opponency, and global direction perception. *Perception*, 26(8):995–1010, PMID 9509159.

Brainard, D. (1997). The psychophysics toolbox. *Spatial Vision*, 10(4):433–436.

Burr, D. C., Baldassi, S., Morrone, M. C., and Verghese, P. (2009). Pooling and segmenting motion signals. *Vision Res*, 49(10):1065–72, doi:10.1016/j.visres.2008.10.024.

Burr, D. C., Morrone, M. C., and Vaina, L. M. (1998). Large receptive fields for optic flow detection in humans. *Vision Res*, 38(12):1731–43, PMID 9797952.

Butzer, F., Ilg, U. J., and Zanker, J. M. (1997). Smooth-pursuit eye movements elicited by first-order and second-order motion. *Exp Brain Res*, 115(1):61–70, PMID 9224834.

Cassanello, C. R., Edwards, M., Badcock, D. R., and Nishida, S. (2011). No interaction of first- and second-order signals in the extraction of global-motion and optic-flow. *Vision Res*, 51(3):352–61, doi:10.1016/j.visres.2010.11.012.

Cavanagh, P. (1991). Short-range vs long-range motion: not a valid distinction. *Spat Vis*, 5(4):303–9, PMID 1751430.

Cavanagh, P. and Alvarez, G. A. (2005). Tracking multiple targets with multifocal attention. *Trends Cogn Sci*, 9(7):349–54, doi:10.1016/j.tics.2005.05.009.

Chen, X., Han, F., Poo, M.-M., and Dan, Y. (2007). Excitatory and suppressive receptive field subunits in awake monkey primary visual cortex (v1). *Proc Natl Acad Sci U S A*, 104(48):19120–5, doi:10.1073/pnas.0706938104.

Chubb, C. and Sperling, G. (1988). Drift-balanced random stimuli: a general basis for studying non-fourier motion perception. *J Opt Soc Am A*, 5(11):1986–2007, PMID 3210090.

Chubb, C. and Sperling, G. (1989). Two motion perception mechanisms revealed through distance-driven reversal of apparent motion. *Proc Natl Acad Sci U S A*, 86(8):2985–2989, PMID 16594030.

Collett, D. (2003). *Modelling binary data*. Texts in statistical science. Chapman & Hall/CRC, Boca Raton, 2nd ed edition. http://www.loc.gov/catdir/enhancements/fy0646/2002073648-d.html.

Cornelissen, F. W., Peters, E. M., and Palmer, J. (2002). The eyelink toolbox: eye tracking with matlab and the psychophysics toolbox. *Behav Res Methods Instrum Comput*, 34(4):613–617, PMID 12564564.

Cropper, S. J. (2001). Local and global motion signals and their interaction in space and time. In Zanker, J. M. and Zeil, J., editors, *Motion Vision - Computational, Neural, and Ecological Constraints*. Springer Verlag, Berlin Heidelberg New York.

Dakin, S. C., Cass, J., Greenwood, J. A., and Bex, P. J. (2010). Probabilistic, positional averaging predicts object-level crowding effects with letter-like stimuli. *J Vis*, 10(10):14, doi:10.1167/10.10.14.

De Valois, R. L. and De Valois, K. K. (1991). Vernier acuity with stationary moving gabors. *Vision Res*, 31(9):1619–1626, PMID 1949630.

Derrington, A. M. and Badcock, D. R. (1985). Separate detectors for simple and complex grating patterns? *Vision Res*, 25(12):1869–78, PMID 3832611.

Derrington, A. M. and Henning, G. B. (1987). Errors in direction-of-motion discrimination with complex stimuli. *Vision Res*, 27(1):61–75, PMID 3617547.

Downing, C. J. and Movshon, J. A. (1989). Spatial and temporal summation in the detection of motion in stochastic random dot displays. *Invest-. Ophthalmol Vis Sci [Suppl]*, 30:72.

Duncker, K. (1938). Induced motion. In Ellis, W. D., editor, *A Source Book of Gestalt Psychology*, volume 2, chapter 11, pages 161–172. Taylor and Francis.

Edwards, M. and Badcock, D. R. (1995). Global motion perception: no interaction between the first- and second-order motion pathways. *Vision Res*, 35(18):2589–602, PMID 7483303.

Felisbert, F. M., Solomon, J. A., and Morgan, M. J. (2005). The role of target salience in crowding. *Perception*, 34(7):823–33, PMID 16124268.

Fischer, J., Spotswood, N., and Whitney, D. (2011). The emergence of perceived position in the visual system. *J Cogn Neurosci*, 23(1):119–36, doi:10.1162/jocn.2010.21417.

Fraser, A. and Wilcox, K. J. (1979). Perception of illusory movement. *Nature*, 281(5732):565–6, PMID 573864.

Fredericksen, R. E., Verstraten, F. A. J., and Van De Grind, W. A. (1994). Spatial summation and its interaction with the temporal integration mechanism in human motion perception. *Vision Res*, 34(23):3171–3188. http://www.sciencedirect.com/science/article/B6T0W-4846YPV-5K/2/71b01216886ba102ff37cc9bf4e8e10b.

Freeman, J. and Simoncelli, E. P. (2011). Metamers of the ventral stream. *Nat Neurosci*, 14(9):1195–201, doi:10.1038/nn.2889.

Graham, N. V. (2011). Beyond multiple pattern analyzers modeled as linear filters (as classical v1 simple cells): useful additions of the last 25 years. *Vision Res*, 51(13):1397–430, doi:10.1016/j.visres.2011.02.007.

Greenwood, J. A., Bex, P. J., and Dakin, S. C. (2009). Positional averaging explains crowding with letter-like stimuli. *Proc Natl Acad Sci U S A*, 106(31):13130–5, doi:10.1073/pnas.0901352106.

Greenwood, J. A., Bex, P. J., and Dakin, S. C. (2012). Crowding follows the binding of relative position and orientation. *J Vis*, 12(3), doi:10.1167/12.3.18.

Hawken, M. J. and Gegenfurtner, K. R. (2001). Pursuit eye movements to second-order motion targets. *J Opt Soc Am A Opt Image Sci Vis*, 18(9):2282–2296, PMID 11551063.

Hedges, J. H., Gartshteyn, Y., Kohn, A., Rust, N. C., Shadlen, M. N., Newsome, W. T., and Movshon, J. A. (2011). Dissociation of neuronal and psychophysical responses to local and global motion. *Curr Biol*, 21(23):2023–8, doi:10.1016/j.cub.2011.10.049.

Hess, R. F., Ledgeway, T., and Dakin, S. (2000). Impoverished second-order input to global linking in human vision. *Vision Res*, 40(24):3309–18, PMID 11058730.

Hosmer, D. W., Lemeshow, S., and Sturdivant, R. X. (2013). *Applied logistic regression*. Wiley series in probability and statistics. Hoboken, NJ: Wiley, third edition.

Ilg, U. J. and Churan, J. (2004). Motion perception without explicit activity in areas MT and MST. *J Neurophysiol*, 92(3):1512–1523, doi:10.1152/jn.01174.2003.

Ilildreth, E. C. and Ullman, S. (1982). The measurement of visual motion. Technical report, Massachusetts Institute of Technology. A.I. Memo No. 699.

Klein, S. A. and Levi, D. M. (1985). Hyperacuity thresholds of 1 sec: theoretical predictions and empirical validation. *J Opt Soc Am A*, 2(7):1170–1190, PMID 4020514.

Ledgeway, T. and Hess, R. F. (2002). Rules for combining the outputs of local motion detectors to define simple contours. *Vision Res*, 42(5):653–9, PMID 11853781.

Levi, D. M. (2008). Crowding–an essential bottleneck for object recognition: a mini-review. *Vision Res*, 48(5):635–654, doi:10.1016/j.visres.2007.12.009.

Levi, D. M., Klein, S. A., and Hariharan, S. (2002). Suppressive and facilitatory spatial interactions in foveal vision: foveal crowding is simple contrast masking. *J Vis*, 2(2):140–166, doi:10:1167/2.2.2.

Lindner, A. and Ilg, U. J. (2000). Initiation of smooth-pursuit eye movements to first-order and second-order motion stimuli. *Exp Brain Res*, 133(4):450–6, PMID 10985680.

Lisberger, S. G. (1998). Postsaccadic enhancement of initiation of smooth pursuit eye movements in monkeys. *J Neurophysiol*, 79(4):1918–1930, PMID 9535958.

Lisberger, S. G., Morris, E. J., and Tychsen, L. (1987). Visual motion processing and sensory-motor integration for smooth pursuit eye movements. *Annual Reviews in Neuroscience*, 10:97–129, doi:10.1146/annurev.ne.10.030187.000525.

Liu, T., Jiang, Y., Sun, X., and He, S. (2009). Reduction of the crowding effect in spatially adjacent but cortically remote visual stimuli. *Curr Biol*, 19(2):127–32, doi:10.1016/j.cub.2008.11.065.

Livingstone, M. S., Pack, C. C., and Born, R. T. (2001). Two-dimensional substructure of mt receptive fields. *Neuron*, 30(3):781–93, PMID 11430811.

Lu, Z. L. and Sperling, G. (1995). The functional architecture of human visual motion perception. *Vision Res*, 35(19):2697–2722, PMID 7483311.

Lu, Z. L. and Sperling, G. (2001). Three-systems theory of human visual motion perception: review and update. *J Opt Soc Am A Opt Image Sci Vis*, 18(9):2331–2370, PMID 11551067.

Majaj, N. J., Carandini, M., and Movshon, J. A. (2007). Motion integration by neurons in macaque MT is local, not global. *J Neurosci*, 27(2):366–70, doi:10.1523/JNEUROSCI.3183-06.2007.

Maruya, K., Holcombe, A. O., and Nishida, S. (2013). Rapid encoding of relationships between spatially remote motion signals. *J Vis*, 13(2):4, doi:10.1167/13.2.4.

Mather, G., Cavanagh, P., and Anstis, S. M. (1985). A moving display which opposes short-range and long-range signals. *Perception*, 14(2):163–166, PMID 4069946.

Mather, G. and Pavan, A. (2009). Motion-induced position shifts occur after motion integration. *Vision Res*, 49(23):2741–6, doi:10.1016/j.visres.2009.07.016.

McGraw, P. V., Walsh, V., and Barrett, B. T. (2004). Motion-sensitive neurones in V5/MT modulate perceived spatial position. *Curr Biol*, 14(12):1090–3, doi:10.1016/j.cub.2004.06.028.

Meilstrup, P. B. and Shadlen, M. N. (2008). Integration of local and global visual motion revealed by localization judgments. Program No. 460.11/GG3. In *2008 Neuroscience Meeting Planner*. Washington, DC: Society for Neuroscience. Online.

Meilstrup, P. B. and Shadlen, M. N. (2010). The steerable spiral. In *Best Illusion of the Year Contest*. Neural Correlate Society. http://illusionoftheyear.com/2010/the-steerable-spiral/.

Mikami, A., Newsome, W. T., and Wurtz, R. H. (1986). Motion selectivity in macaque visual cortex. ii. spatiotemporal range of directional interactions in mt and v1. *J Neurophysiol*, 55(6):1328–39, PMID 3734858.

Morrone, M. C., Burr, D. C., and Vaina, L. M. (1995). Two stages of visual processing for radial and circular motion. *Nature*, 376(6540):507–9, doi:10.1038/376507a0.

Motter, B. C. (2002). Crowding and object integration within the receptive field of v4 neurons. *Journal of Vision*, 2(7):274, doi:10.1167/2.7.274.

Motter, B. C. (2006). Modulation of transient and sustained response components of v4 neurons by temporal crowding in flashed stimulus sequences. *J Neurosci*, 26(38):9683–94, doi:10.1523/JNEUROSCI.5495-05.2006.

Movshon, J. A., Adelson, E. H., Gizzi, M. S., and Newsome, W. T. (1985). The analysis of moving visual patterns. In Chagas, C., Gattass, R., and Gross, C., editors, *Pattern Recognition Mechanisms*. Rome: Vatican Press.

Movshon, J. A. and Newsome, W. T. (1996). Visual response properties of striate cortical neurons projecting to area MT in macaque monkeys. *J Neurosci*, 16(23):7733–41, PMID 8922429.

Movshon, J. A., Thompson, I. D., and Tolhurst, D. J. (1978). Receptive field organization of complex cells in the cat's striate cortex. *J Physiol*, 283:79–99, PMID 722592.

Murakami, I. and Shimojo, S. (1993). Motion capture changes to induced motion at higher luminance contrasts, smaller eccentricities, and larger inducer sizes. *Vision Res*, 33(15):2091–107, PMID 8266651.

Murakami, I. and Shimojo, S. (1996). Assimilation-type and contrast-type bias of motion induced by the surround in a random-dot display: evidence for center-surround antagonism. *Vision Res*, 36(22):3629–39, PMID 8976993.

Newsome, W. T., Britten, K. H., and Movshon, J. A. (1989). Neuronal correlates of a perceptual decision. *Nature*, 341(6237):52–4, doi:10.1038/341052a0.

Nishida, S. (2011). Advancement of motion psychophysics: review 2001-2010. *J Vis*, 11(5):11, doi:10.1167/11.5.11.

Nishida, S. and Johnston, A. (1999). Influence of motion signals on the perceived position of spatial pattern. *Nature*, 397(6720):610–2, doi:10.1038/17600.

Nishida, S., Ledgeway, T., and Edwards, M. (1997). Dual multiple-scale processing for motion in the human visual system. *Vision Res*, 37(19):2685–98, PMID 9373668.

Nishida, S. and Sato, T. (1992). Positive motion after-effect induced by bandpass-filtered random-dot kinematograms. *Vision Res*, 32(9):1635–46, PMID 1455735.

Parkes, L., Lund, J., Angelucci, A., Solomon, J. A., and Morgan, M. (2001). Compulsory averaging of crowded orientation signals in human vision. *Nat Neurosci*, 4(7):739–44, doi:10.1038/89532.

Pelli, D. and Tillman, K. (2008). The uncrowded window of object recognition. *Nat Neurosci*, pages 1129–1135, doi:10.1038/nn.2187.

Pelli, D. G. (2008). Crowding: a cortical constraint on object recognition. *Curr Opin Neurobiol*, 18(4):445–451, doi:10.1016/j.conb.2008.09.008.

Pelli, D. G., Palomares, M., and Majaj, N. J. (2004). Crowding is unlike ordinary masking: distinguishing feature integration from detection. *J Vis*, 4(12):1136–69, doi:10:1167/4.12.12.

Petrov, Y. and Meleshkevich, O. (2011). Asymmetries and idiosyncratic hot spots in crowding. *Vision Res*, 51(10):1117–23, doi:10.1016/j.visres.2011.03.001.

Price, N. S. C., Greenwood, J. A., and Ibbotson, M. R. (2004). Tuning properties of radial phantom motion aftereffects. *Vision Res*, 44(17):1971–9, doi:10.1016/j.visres.2004.04.001.

Pylyshyn, Z. W. and Storm, R. W. (1988). Tracking multiple independent targets: evidence for a parallel tracking mechanism. *Spat Vis*, 3(3):179–97, PMID 3153671.

R Core Team (2013). *R: A Language and Environment for Statistical Computing*. R Foundation for Statistical Computing, Vienna, Austria. http://www.R-project.org/.

Ramachandran, V. S. and Anstis, S. M. (1990). Illusory displacement of equiluminous kinetic edges. *Perception*, 19(5):611–6, PMID 2102995.

Reinhardt-Rutland, A. H. (1988). Induced movement in the visual modality: an overview. *Psychol Bull*, 103(1):57–71, PMID 3279445.

Rust, N. C., Mante, V., Simoncelli, E. P., and Movshon, J. A. (2006). How MT cells analyze the motion of visual patterns. *Nature Neuroscience*, 9(11):1421–1431, doi:10.1038/nn1786.

Rust, N. C., Schwartz, O., Movshon, J. A., and Simoncelli, E. P. (2005). Spatiotemporal elements of macaque V1 receptive fields. *Neuron*, 46(6):945–956, doi:10.1016/j.neuron.2005.05.021.

Serrano-Pedraza, I. and Derrington, A. M. (2010). Antagonism between fine and coarse motion sensors depends on stimulus size and contrast. *J Vis*, 10(8):18, doi:10.1167/10.8.18.

Serrano-Pedraza, I., Goddard, P., and Derrington, A. M. (2007). Evidence for reciprocal antagonism between motion sensors tuned to coarse and fine features. *J Vis*, 7(12):8.1–14, doi:10.1167/7.12.8.

Shapiro, A., Lu, Z.-L., Huang, C.-B., Knight, E., and Ennis, R. (2010). Transitions between central and peripheral vision create spatial/temporal distortions: a hypothesis concerning the perceived break of the curveball. *PLoS One*, 5(10):e13296, doi:10.1371/journal.pone.0013296.

Shapiro, A., Lu, Z.-L., Knight, E., and Ennis, R. (2009). The break of the curveball. In *Best Illusion of the Year Contest*. Neural Correlate Society. http://illusionoftheyear.com/2009/the-break-of-the-curveball/.

Shapiro, A. G. (2008). Feature blur in peripheral vision. Program No. 811.3. In *2008 Neuroscience Meeting Planner*. Washington, DC: Society for Neuroscience. Online.

Shapiro, A. G., Knight, E. J., and Lu, Z.-L. (2011). A first- and second-order motion energy analysis of peripheral motion illusions leads to further evidence of "feature blur" in peripheral vision. *PLoS One*, 6(4):e18719, doi:10.1371/journal.pone.0018719.

Simoncelli, E. P. and Heeger, D. J. (1998). A model of neuronal responses in visual area MT. *Vision Res*, 38(5):743–761, PMID 9604103.

Snowden, R. J. and Milne, A. B. (1997). Phantom motion after effects–evidence of detectors for the analysis of optic flow. *Curr Biol*, 7(10):717–22, PMID 9368753.

Stan Development Team (2014). Stan: A c++ library for probability and sampling, version 2.2. http://mc-stan.org/.

Steinman, R. M., Pizlo, Z., and Pizlo, F. J. (2000). Phi is not beta, and why Wertheimer's discovery launched the gestalt revolution. *Vision Res*, 40(17):2257–2264. http://www.sciencedirect.com/science/article/B6T0W-40VT194-4/2/ccd5af03d347e42d9fb50131930ed666.

Sundberg, K. A., Fallah, M., and Reynolds, J. H. (2006). A motion-dependent distortion of retinotopy in area v4. *Neuron*, 49(3):447–457, doi:10.1016/j.neuron.2005.12.023.

Toet, A. and Levi, D. M. (1992). The two-dimensional shape of spatial interaction zones in the parafovea. *Vision Res*, 32(7):1349–1357, PMID 1455707.

Touryan, J., Felsen, G., and Dan, Y. (2005). Spatial structure of complex cell receptive fields measured with natural images. *Neuron*, 45(5):781–91, doi:10.1016/j.neuron.2005.01.029.

Tse, P. (2006). The infinite regress illusion. In *Best Illusion of the Year Contest*. Neural Correlate Society. http://illusionoftheyear.com/2006/infinite-regress-illusion/.

Tse, P. U. and Hsieh, P. J. (2006). The infinite regress illusion reveals faulty integration of local and global motion signals. *Vision Res*, 46(22):3881–3885. http://www.sciencedirect.com/science/article/B6T0W-4KJ5T3X-5/2/ef7fd1d77d18c40c9074c101edd1a11a.

Tsiatis, A. A. (1980). A note on a goodness-of-fit test for the logistic regression model. *Biometrika*, 67(1):250–251.

Turner, H. and Firth, D. (2012). *Generalized nonlinear models in R: An overview of the gnm package*. http://CRAN.R-project.org/package=gnm, R package version 1.0-6.

Vaina, L. M. and Cowey, A. (1996). Impairment of the perception of second order motion but not first order motion in a patient with unilateral focal brain damage. *Proc Biol Sci*, 263(1374):1225–1232, doi:10.1098/rspb.1996.0180.

Vaina, L. M. and Soloviev, S. (2004). First-order and second-order motion: neurological evidence for neuroanatomically distinct systems. *Prog Brain Res*, 144:197–212, PMID 14650850.

Verghese, P. and McKee, S. P. (2002). Predicting future motion. *J. Vis.*, 2(5):413–423. http://journalofvision.org/2/5/5/.

Verghese, P., McKee, S. P., and Grzywacz, N. M. (2000). Stimulus configuration determines the detectability of motion signals in noise. *J Opt Soc Am A Opt Image Sci Vis*, 17(9):1525–34, PMID 10975362.

Verghese, P. and Stone, L. S. (1997). Spatial layout affects speed discrimination. *Vision Res*, 37(4):397–406, PMID 9156171.

Verghese, P., Watamaniuk, S. N., McKee, S. P., and Grzywacz, N. M. (1999). Local motion detectors cannot account for the detectability of an extended trajectory in noise. *Vision Res*, 39(1):19–30, PMID 10211392.

Volz, H. and Zanker, J. M. (1996). Hyperacuity for spatial localization of contrast-modulated patterns. *Vision Res*, 36(9):1329–39, PMID 8711911.

Watamaniuk, S. N., McKee, S. P., and Grzywacz, N. M. (1995). Detecting a trajectory embedded in random-direction motion noise. *Vision Res*, 35(1):65–77, PMID 7839611.

Watson, A. B. and Ahumada, A. J. (1985). Model of human visual-motion sensing. *Optical Society of America, Journal, A: Optics and Image Science*, 2:322–342.

Watson, A. B. and Turano, K. (1995). The optimal motion stimulus. *Vision Res*, 35(3):325–336, PMID 7892728.

Watt, R., Ledgeway, T., and Dakin, S. C. (2008). Families of models for gabor paths demonstrate the importance of spatial adjacency. *J Vis*, 8(7):23.1–19, doi:10.1167/8.7.23.

Wertheimer, M. (1912). Experimentelle studien über das sehen von bewegung. *Zeitschrift für Psychologie und Physiologie der Sinnesorgane*, 61:161 – 265.

Wertheimer, M., Spillmann, L., Sarris, V., and Sekuler, R. (2012). *On perceived motion and figural organization*. MIT Press, Cambridge, Mass.

Whitney, D. and Levi, D. M. (2011). Visual crowding: a fundamental limit on conscious perception and object recognition. *Trends Cogn Sci*, 15(4):160–8, doi:10.1016/j.tics.2011.02.005.

Wichmann, F. A. and Hill, N. J. (2001). The psychometric function: I. fitting, sampling, and goodness of fit. *Percept Psychophys*, 63(8):1293–313, PMID 11800458.

Wickham, H. (2009). *Ggplot2: elegant graphics for data analysis*. Use R! Springer, New York, 1st edition. http://had.co.nz/ggplot2/book.

Williams, D. W. and Sekuler, R. (1984). Coherent global motion percepts from stochastic local motions. *Vision Res*, 24(1):55–62, PMID 6695508.

Wilmer, J. B. and Nakayama, K. (2007). Two distinct visual motion mechanisms for smooth pursuit: evidence from individual differences. *Neuron*, 54(6):987–1000, doi:10.1016/j.neuron.2007.06.007.

Zanker, J. M. (1990). Theta motion: a new psychophysical paradigm indicating two levels of visual motion perception. *Naturwissenschaften*, 77(5):243–6, PMID 2377238.

Zanker, J. M. (1993). Theta motion: a paradoxical stimulus to explore higher order motion extraction. *Vision Res*, 33(4):553–69, PMID 8503201.

Zanker, J. M. (1997). Second-order motion perception in the peripheral visual field. *J Opt Soc Am A Opt Image Sci Vis*, 14(7):1385–92, PMID 9203393.

Zhuo, Y., Zhou, T. G., Rao, H. Y., Wang, J. J., Meng, M., Chen, M., Zhou, C., and Chen, L. (2003). Contributions of the visual ventral pathway to long-range apparent motion. *Science*, 299(5605):417–20, doi:10.1126/science.1077091.

Zigler, M. J., Cook, B., Miller, D., and Wemple, L. (1930). The perception of form in peripheral vision. *The American Journal of Psychology*, 42(2):pp. 246–259. http://www.jstor.org/stable/1415274.

Zivotofsky, A. Z. (2004). The Duncker illusion: intersubject variability, brief exposure, and the role of eye movements in its generation. *Invest Ophthalmol Vis Sci*, 45(8):2867–72, doi:10.1167/iovs.04-0031.